Linköping Studies in Science and Technology
Thesis No. 1131

On Multivariable and Nonlinear Identification of Industrial Robots

Erik Wernholt

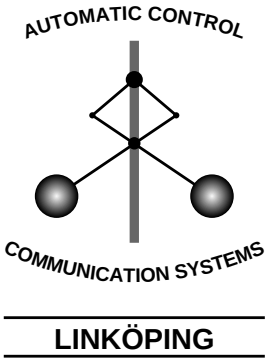

Division of Automatic Control and Communication Systems
Department of Electrical Engineering
Linköping University, SE–581 83 Linköping, Sweden
WWW: `http://www.control.isy.liu.se`
Email: `erikw@isy.liu.se`

Linköping 2004

On Multivariable and Nonlinear Identification of Industrial Robots

Department of Electrical Engineering,
Linköping University,
SE–581 83 Linköping,
Sweden.

ISBN 91-85295-89-2
ISSN 0280-7971
LiU-TEK-LIC-2004:60

Printed by UniTryck, Linköping, Sweden 2004

Abstract

The main objective of the thesis is the identification of flexibilities and nonlinearities in mathematical models of industrial robots. In particular, a nonparametric frequency-domain estimation method for the multivariable frequency response function (MFRF) has been evaluated and analyzed for the robot application. Nonlinear gray-box identification has also been treated. Since identification in robotics is a much studied problem, one important part of the thesis also is to give an overview of earlier results.

For the MFRF estimation method, an approximate expression for the estimation error has been derived which describes how the estimate is affected by disturbances, the choice of excitation signal, the feedback and the properties of the system itself. The MFRF estimation method has been evaluated using both simulation data and experimental data from an ABB IRB 6600 robot. A number of different aspects regarding excitation signals and averaging techniques have been studied. It is shown, for instance, that the repetitive nature of the disturbances further limits the choice of excitation signals. Averaging the estimates over several periods of data or using experiments with identical excitation does not give any significant reduction due to the repetitive disturbances.

A three-step identification procedure is also proposed for the combined identification of rigid body dynamics, friction, and flexibilities. The procedure includes continuous-time nonlinear gray-box identification and is exemplified using experimental data.

Acknowledgments

There are several people who helped me during the work with this thesis. First of all I would like to thank my supervisor Prof. Svante Gunnarsson for guiding me in my research in an excellent way and always taking time to answer my questions. My co-supervisor Dr. Mikael Norrlöf has also been helping me with various problems and giving me valuable comments.

I am also grateful to Prof. Lennart Ljung for giving me the opportunity to join Control & Communication in Linköping and for providing such a good working atmosphere. I would like to thank all the people in the group for a productive and enjoyable climate and for the interesting lunch discussions on various topics. I would especially like to thank Martin Enqvist for the fruitful discussions and all the questions you have to put up with. Ulla Salaneck deserves extra gratitude for helping me with many practical issues.

This work has been supported by VINNOVA's center of excellence ISIS (Information Systems for Industrial Control and Supervision) at Linköpings universitet, which is gratefully acknowledged. The work in this thesis would not have been possible without the support from ABB Automation Technologies AB – Robotics. The possibility to use their robot lab for various experiments has substantially improved the results of this thesis.

I am also very grateful to Prof. Svante Gunnarsson, Dr. Torgny Brogårdh, Dr. Mikael Norrlöf, Stig Moberg, Dr. Ola Härkegård, Martin Enqvist and Ingela Lind who have proofread this thesis or various parts thereof. Thanks also to Dr. Peter Lindskog for providing the code for the nonlinear gray-box identification.

Furthermore, I would like to thank the people at ABB Robotics for guiding me and keeping my research relevant for the application. I would especially like to mention my industrial mentor Dr. Torgny Brogårdh and also Stig Moberg for all profitable discussions on various aspects of robotics and in particular identification of robots. I am also thankful to Sven Hanssen who has provided the simulation models used in the thesis and Dr. Jonas Öhr for helping me with some of the identification experiments.

I would also like to thank my family for always supporting me. Finally, I would like to thank Jessica for support and patience with me when I am physically away during various trips to ABB and conferences, as well as mentally away during intensive times of writing and thinking. You are the best!

Erik Wernholt

Linköping, November 2004

Contents

Notation

Symbols, Operators and Functions

$\mathbb{N}$	The set of natural numbers
$\mathbb{R}$	The set of real numbers
$\mathbb{C}$	The set of complex numbers
t	Time variable
s	Laplace transform variable
z	z transform variable
p	Differentiation operator, $pu(t) = \frac{du(t)}{dt}$
q	Shift operator, $qu(t) = u(t+1)$
$\mathrm{E}(x)$	Expected value of the random variable x
$\dot{x}(t)$	Derivative of $x(t)$ with respect to time
$\in$	Belongs to
θ	Vector of (unknown) parameters
$\mathcal{M}$	Model structure, see (3.20)
N	Number of samples
T	Sample time
φ	Vector of joint coordinates, $\varphi = (\varphi_1, \ldots, \varphi_n)^T$
τ	Vector of motor torques
$M(\varphi)$	Inertia matrix in the dynamic equations (2.6)

$C(\varphi, \dot{\varphi})$	Velocity dependent term in the dynamic equations (2.6)
$g(\varphi)$	Gravitational term in the dynamic equations (2.6)
φ_m, φ_a	Joint coordinates for motor and arm
J_m, J_a	Moments of inertia of the motor and arm
r	Gear ratio
k, d	Spring stiffness and damping
F_v, F_c	Viscous and Coulomb friction parameters
$u(t)$	Input signal at time t
$y(t)$	Output signal at time t
$v_\tau(t)$, $v_u(t)$	Input disturbances at time t
$v_\varphi(t)$, $v_y(t)$	Output disturbances at time t
$r(t)$	Reference signal at time t
$\mathbf{r}(t)$	Matrix of reference signals, where column i corresponds to the reference signal applied in experiment i (cf. (6.5)).
$\mathcal{T}$	Permutation matrix $\mathbf{r}(t) = \mathcal{T} r_0(t)$ (cf. (6.5))
$R(\cdot)$	Frequency domain version of $r(t)$
$\mathbf{R}(\cdot)$	Frequency domain version of $\mathbf{r}(t)$
$\Phi_u(\omega)$	Spectrum for the signal $u(t)$
$\Phi_{yu}(\omega)$	Cross spectrum between $y(t)$ and $u(t)$
$F(\cdot)$	Controller
$G(\cdot)$	Transfer function from input to output
$\hat{G}(\cdot)$	Estimate of the transfer function $G(\cdot)$
$\Delta G(\cdot)$	Relative error for $\hat{G}(\cdot)$ (cf. (6.3))
$\hat{y}(t\|\theta)$	A model's prediction of $y(t)$ given θ and data up to time $t-1$
$\varepsilon(t, \theta)$	Prediction error, $y(t) - \hat{y}(t\|\theta)$

Abbreviations and Acronyms

CAD/CAM	Computer Aided Design/Computer Aided Manufacture
DH	Denavit-Hartenberg, a parameterization of kinematic models
DOF	Degrees Of Freedom
FRF	Frequency Response Function
IRB	Industrial RoBot, used in names for ABB robots
LTI	Linear Time Invariant
MFRF	Multivariable Frequency Response Function
MFRFE	Multivariable Frequency Response Function Estimate
MIMO	Multiple Input Multiple Output
SISO	Single Input Single Output
SVD	Singular Value Decomposition
TCP	Tool Center Point

1

Introduction

In the manufacturing industry of today, the three most important factors are quality, cost, and productivity. For an increasing number of applications, industrial robots are used to meet these demands. Robot manufacturers must therefore resolve the conflicting requirements of price reduction and increased performance.

A standard industrial robot (see Figure 1.1) consists of a mechanical arm with a number of links connected by joints, where each joint is actuated by an (electric) motor via a transmission[1]. The movements are controlled by a computer system. Usually the robot has six joints, giving six degrees-of-freedom and the ability to control both the position of the tool and its orientation in the workspace. The dynamics of a robot are coupled, which means that movements of one joint will affect the other joints. A robot is therefore a truly multivariable system. The dynamics are also nonlinear, both with respect to the operating point and other nonlinearities such as, for example, friction, backlash, and nonlinear stiffness in the transmission. In addition, the robot arm and transmission are more or less flexible[2], which introduces resonances in the system and also a measurement problem, since only a subset of the system states typically are measured.

A trend is to build robots with a bend-over-backwards capability (like the ABB IRB 6600 in Figure 1.1), which means that to reach something behind the robot, you can simply swing the arm backwards instead of having to rotate the machine.

[1] Sometimes the transmission is left out and the motor shaft is connected directly to the joint. This is often called *direct drive*.

[2] The word *flexible* have at least two different meanings. It is sometimes used to describe the positive property of easy customization and the ability to adapt to new, different, or changing requirements. Throughout this thesis, the word *flexible* will denote elastic effects, which is a negative property.

Figure 1.1 *The ABB IRB 6600 robot (ABB, 2004).*

The mechanical structure of such a robot is typically non-symmetric, which increases the dynamic coupling effects and therefore makes the robot control problem harder.

One common solution to the conflicting requirements of price reduction and increased performance is to use cheaper hardware, which gives deteriorated mechanical properties, in combination with a more advanced robot controller. Maybe additional sensors are needed, but adding sensors will increase the price. The number of sensors is therefore usually kept at the minimum level of only measuring the motor positions (before the transmission gearbox and flexibilities), even though it is the tool position on the arm side (after the gearbox and flexibilities) that is the objective to control. The relationship between motor and arm positions is described using a dynamic model. For the design of an advanced robot controller, accurate dynamic robot models are therefore crucial.

The development rate of new industrial robots is also high, with several kinds of robots and different configurations to tune each year. For top performance, there could also be a need to re-tune robots at the customer site due to wear or other changing conditions. This means that there is an increasing need for an automated way of estimating accurate dynamic models. Good models are also needed for model based diagnosis of robots in order to increase reliability and reduce maintenance time.

Two main routes to obtain these models are *physical modeling* and *system identification*. For the modeling route, basic physical laws and other well-established relationships are used to come up with a model. System identification, on the other hand, uses experimental data to adjust parameters in a selected model structure. Often, a combination of these two routes is used. A physical model is built where some parameters and/or parts are unknown. These unknown parameters/parts are then estimated using system identification methods. This procedure is often called *gray-box identification*, to be compared with the system identification extreme when the parameters have no immediate physical interpretation, called *black-box identification*.

1.1 Problem Statement

The ultimate goal for robot identification could be to find an accurate global nonlinear flexible model, suitable for, *e.g.*, control design (both the controller structure and tuning), simulation, analysis, and diagnosis. The identification of such a complex model is a huge task, both in finding suitable model structures and efficient identification procedures, and is still a topic for further research. However, under certain simplifying assumptions, a subset of the parameters can be identified. By for example using a low-frequency excitation, the flexibilities have a minor influence and a rigid model is approximately valid. The parameters of a global nonlinear rigid model can then be estimated. This is a much studied subproblem (see the overview in Section 4.3).

Another common approximation is to use local linear flexible models. The term *local* stems from the fact that the robot is excited locally around a certain operating point in the workspace, and *linear* means that the influences from other nonlinearities, such as backlash, friction, and nonlinear stiffness, are ignored or reduced by a certain excitation. An estimate of the global nonlinear flexible model can hopefully be found by combining the knowledge gained from the global nonlinear rigid model and a number of local linear flexible models from different operating points. However, some nonlinearities might not show up in this way and there are also possible problems of biased estimates and a too complex and time consuming identification procedure. Therefore, more structured methods for the identification of the global nonlinear flexible model are needed.

Identification can also be done in many ways. Using black-box or gray-box models, linear or nonlinear models, linear or nonlinear optimization techniques, time-domain or frequency-domain data/models, the excitation trajectories can be optimized, and the number of sensors can vary. For the identification of rigid body dynamics, all states are measured (or estimated by simple filtering and/or differentiating) and one can therefore use linear regression models. For the flexible body dynamics, all states are typically not measured and more advanced identification methods are needed.

Figure 1.2 gives an overview of some common model structures and identification procedures mentioned above. The global nonlinear flexible model is de-

noted $\mathcal{M}(\theta^{RB}, \theta^{FB}, \theta^{NL})$ where the parameter vector θ is divided into rigid body parameters, θ^{RB}, flexible body parameters, θ^{FB}, and parameters describing the nonlinearities, θ^{NL}. The global nonlinear rigid model, $\mathcal{M}^{GNR}(\theta^{RB}, \theta^{NL})$, is obtained by ignoring flexibilities (denoted by $\theta^{FB} = 0$). For the local linear flexible model, $\mathcal{M}^{LLF}_{X_0}(\theta^{RB}, \theta^{FB})$, the global model $\mathcal{M}(\theta^{RB}, \theta^{FB}, \theta^{NL})$ is linearized around the operating point $X = X_0$ and nonlinearities are ignored (denoted by $\theta^{NL} = 0$).

A number of different identification methods exist, based on these model approximations. Nonparametric frequency-domain methods give estimates of the input-output transfer function $G(\Omega)$ at certain frequencies Ω_k, where $\Omega = i\omega$ for a continuous-time model and $\Omega = e^{i\omega}$ for a discrete-time model. This can be used together with a given model structure $G(\Omega, \theta^{RB}, \theta^{FB})$ and the unknown parameters can then be estimated by curve fitting in the frequency domain. Estimated rigid body parameters, $\hat{\theta}^{RB}$, from the rigid body identification can be used to some extent, giving mainly θ^{FB} left to estimate. Time-domain black-box methods give a discrete-time model $G(q)$ which, among many things, also can be used for curve fitting in the frequency domain.

Summing up the mentioned ideas: *The final goal for the robot identification could be to find efficient procedures for automated tuning of flexible model structures with a minimum number of additional sensors.*

The focus in this thesis will be on identifying flexibilities and nonlinearities (shaded boxes in Figure 1.2). In particular, a nonparametric frequency domain estimation method, described in Guillaume et al. (1996), for the multivariable frequency response function (MFRF) will be evaluated and analyzed. Nonlinear gray-box identification will also be treated. Since identification in robotics is a much studied problem, one important part of the thesis also is to give an overview of earlier results.

1.2 Outline of the Thesis

The application studied in this thesis is the industrial robot. Chapter 2 gives an introduction to the robotics area, including modeling and control.

In Chapter 3 different system identification methods and model structures are presented. A survey on system identification in robotics can be found in Chapter 4.

System identification is based on measurements of input and output signals and therefore the quality of these measurements is an important factor. Different aspects of how to design a good experiment are treated in Chapter 5.

The nonparametric frequency domain estimation method for the MFRF is described in Section 3.4.3. Chapter 6 presents an error analysis for the method. Experimental results and simulation results using the MFRF estimation method are shown in Chapter 7 and Chapter 8, respectively.

In Chapter 9 a three-step identification procedure is proposed for the combined identification of rigid body dynamics, friction, and flexibilities. The procedure includes continuous-time nonlinear gray-box identification and is exemplified using experimental data. Finally some conclusions are drawn in Chapter 10.

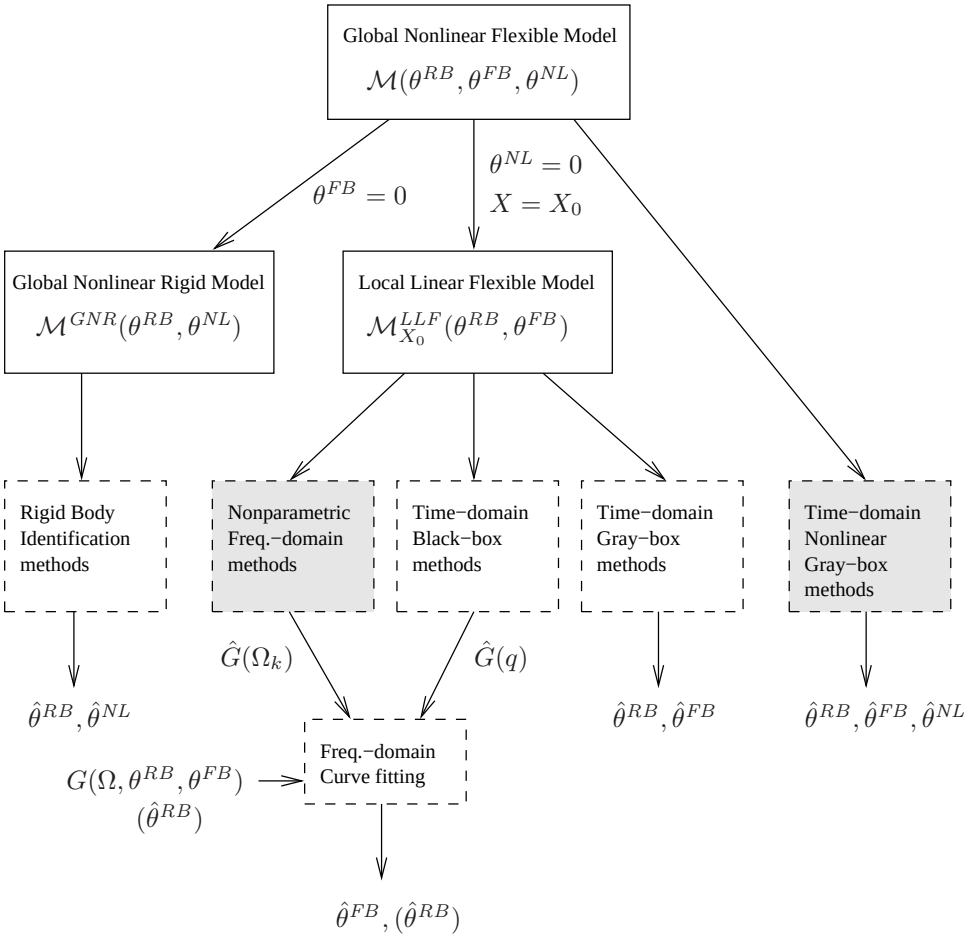

Figure 1.2 *Overview of the robot identification problem and some common subproblems and identification methods. The shaded boxes denote what will be treated in this thesis.*

1.3 Contributions

The main contributions of the thesis are

- The survey on system identification in robotics in Chapter 4.
- The error analysis for the MFRF estimation method (Guillaume et al., 1996) in Chapter 6 from which some properties of the estimation error can be explained.
- Insight into the choices of excitation signals and averaging techniques when using the MFRF estimation method for closed loop identification of an industrial robot. This is illustrated in Chapter 7 for experimental data and Chapter 8 using simulation data.
- The proposed three-step identification procedure in Chapter 9 for combined estimation of rigid body dynamics, friction, and flexibilities using continuous-time nonlinear gray-box identification. The procedure is illustrated using experimental data.

Some of the material of this thesis has been, or will be, published elsewhere. The modeling part in Chapter 2 is mainly based on Wernholt and Östring (2003). The results in Chapter 6 will appear in Wernholt and Gunnarsson (2004b) and Chapter 9 can also be found in Wernholt and Gunnarsson (2004a).

2

Robotics

In this chapter, some important properties of industrial robots will be examined. First an introduction to robotics is given in Section 2.1, followed by a historical background in Section 2.2. Modeling of industrial robots is described in Section 2.3 and finally some aspects of the robot control problem is presented in Section 2.4.

2.1 Introduction

Robotics is a quite general term and *is concerned with the study of those machines that can replace human beings in the execution of a task, as regards both physical activity and decision making* (Sciavicco and Siciliano, 2000). Here the term is restricted to the discipline of *industrial robotics* concerning robot design, control and applications in industry.

The word *robot* was first introduced by the Czech playwright Karel Capek in his 1920 play *Rossum's Universal Robots*, the word *robota* being the Czech word for work. The term has been applied to a great variety of devices, such as humanoids (trying to mimic humans), domestic robots like robot vacuum cleaners and robot lawn movers, underwater vessels, military missiles, autonomous land rowers, *etc.* Almost anything that operates with some degree of autonomy, usually under computer control, has at some point been called a robot. This thesis deals with industrial robots (see Figure 1.1 for an example), which consist of a mechanical arm with a number of joints, where each joint is actuated by an (electric) motor via a transmission. The movements are controlled by a computer system. This type of robot is often called *robot manipulator* or just *manipulator*. According to a widely accepted definition of the Robot Institute of America (Spong and Vidyasagar, 1989),

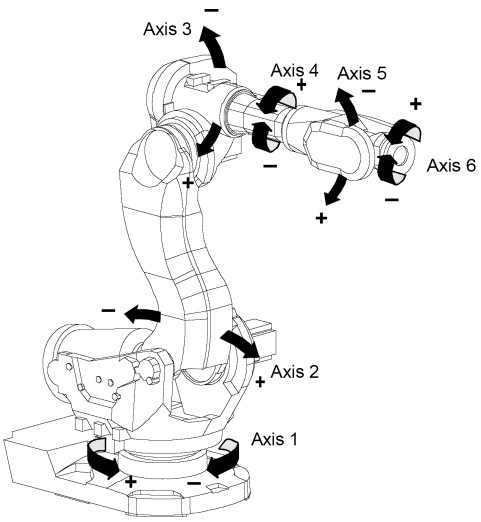

Figure 2.1 *The ABB IRB 6600 robot with its six revolute joints. Axes 1-3 position the end effector (not shown in this figure) and axes 4-6 constitute the wrist.*

a robot is a reprogrammable multifunctional manipulator designed to move materials, parts, tools or specialized devices through variable programmed motions for the performance of a variety of tasks.

The mechanical structure of a robot manipulator consists of a sequence of rigid bodies (*links*) connected by revolute or prismatic *joints*, also called *axes*. Prismatic joints give relative translational motion between links, whereas the revolute joints give relative rotational motion between the links. The manipulator is characterized by an *arm* that ensures mobility, a *wrist* that confers dexterity, and an *end effector* that performs the required task. Usually the robot has six joints, giving six *degrees-of-freedom (DOF)* and the ability to control both the position of the end effector and its orientation in the workspace. See Figure 2.1 for an example. The portion of the environment that can be reached by the robot's end effector is called the robot *workspace*. Its shape and volume depend both on the manipulator structure and mechanical joint limits. The motors are typically electric or hydraulic, and occasionally pneumatic. Both geared and and direct-drive robots exist, with different pros and cons (see Section 2.3.3).

Many different manipulator structures exist, where the main differences are due to the two different types of joints and how these are combined. Some classifying manipulator structures are: Cartesian, cylindrical, spherical, SCARA, and anthropomorphic (Sciavicco and Siciliano, 2000). One can also distinguish between manipulators with an open or closed kinematic chain, which refers to how the links are connected. Here we will only consider manipulators with an open kinematic

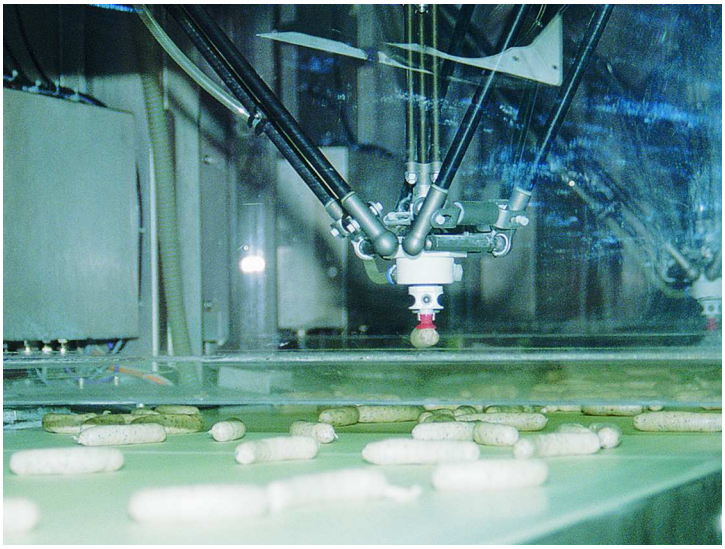

Figure 2.2 *Picking sausages with the ABB Flexpicker (ABB, 2004).*

chain (also called serial type). In particular, we will restrict our treatment to the anthropomorphic manipulator, depicted in Figure 2.1, where only revolute joints are used. This type of robot is also called *elbow-type robot* due to its similarities with a human arm. See Figure 2.2 for an example of a robot with a closed kinematic chain (also called parallel kinematics).

The area in which a robot works is called a *robot cell* or *work cell*. For many applications it is common to use multiple robots in a work cell. A dedicated device, called *positioner*, is often used to handle the work object. The positioner controls the work object and all the other devices are coordinated to move relative to the work object when it moves. The axes of the positioner are often referred to as *external axes* and are usually controlled by the robot controller. An example of a robot cell with multiple robots could be two robots welding the same workpiece in different areas and on two different sides. A positioner first moves the work to present its upper side while the robots wait. Then the robots perform their welds while the positioner waits. Next, the positioner indexes the work to present its lower side to the waiting robots. Finally, the robots perform their welds on the lower side. See also Figure 2.3 for an example of a spot welding line with multiple robots.

Three main factors for the use of industrial robots in the manufacturing industry are: reduction of manufacturing costs, increase of productivity, and improvement of product quality standards. In addition, a robot can eliminate harmful or alienating tasks for the human operator. Industrial robots are therefore essential components for the realization of automated manufacturing systems. Industrial robots are nowadays used in a wide range of applications, like spot welding (see

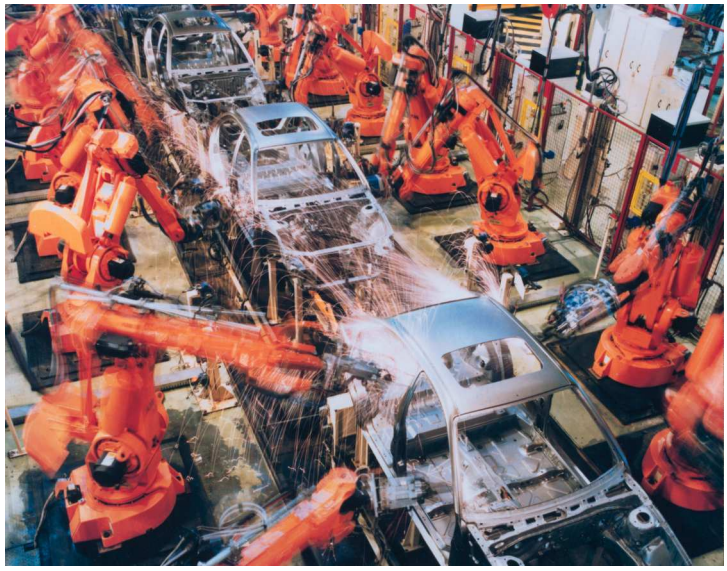

Figure 2.3 *A spot-welding line using ABB IRB 6400 robots (ABB, 2004).*

Figure 2.3), arc welding, material handling, gluing, painting, polishing, grinding, and many more. Demands on productivity and cost cut in different types of industry further increases the use of robots and they are rapidly applied to new areas. One example is the food industry (see Figure 2.2) which, according to Westerlund (2000), probably will become the second largest robot user after the automotive industry.

As was mentioned in Chapter 1, a trend is to build weaker and less symmetric mechanical structures in order to reduce cost and increase the robot workspace. Simultaneously, much work is done to decrease the weight of the moving parts of the robot due to cost and safety issues. This makes elastic effects in the robot more evident, and the control problem typically gets much harder. Usually, the only measured variables are the motor positions, which means that a dynamic model is needed to compensate for the flexibilities in the transmission and in the robot arm and to estimate the position of the tool. In this chapter, some important properties of this type of robot will be examined starting from the modeling aspect and then briefly mention some aspects of the robot control problem. Many books and articles have been written on modeling and control of robots. See for example Spong and Vidyasagar (1989), Craig (1989), Sciavicco and Siciliano (2000), and Spong et al. (1993). First, however, a historical background of industrial robots will be given.

2.2 Historical Background

Industrial robots have become an essential component in the manufacturing industry of today, reducing cost while increasing productivity and quality. Still, in a historical perspective the industrial robot is a fairly new invention and a historical background could therefore be interesting. The historical background is by no means complete. To reduce the scope, the manufacturer ABB and the European market will be in focus, with some comments on other manufacturers and markets. The facts are mainly based on Westerlund (2000).

Technically, one could say that the industrial robot originates from hydraulic assembly machines that arrived in the 1950s and from the NC machines (numerically controlled turning and milling machines). The first industrial robot, an Unimate robot from the company Unimation, was installed in 1961 to serve a die casting machine in General Motor's factory in Trenton, New Jersey. Unimation was started by the great entrepreneur Joseph Engelberger, often called "The Father of Robotics", and the engineer and innovator George Devol. The big breakthrough came in 1964 when General Motors ordered 66 Unimate robots. In Europe, the first industrial robot was installed in 1967 when Svenska Metallverken in Upplands Väsby, Sweden, bought a Unimate robot. In 1969, Unimation installed its first large spot-welding line with 26 robots, used for spot-welding car bodies at General Motors.

In the 1970s, more and more companies started using robots. In 1973, there was a total of about 3000 robots in operation around the world, of which a third were produced by Unimation. At that time, 71 companies worldwide manufactured industrial robots. Technically, the robots mainly used hydraulic actuators and usually combined revolute and prismatic joints.

A milestone in the history of industrial robots is when the Swedish company Asea[1] presented its first prototype of a robot in October 1973. The robot was called IRB 6, which meant a lifting capacity of six kilos, and contained several new technical innovations. It was fully electrical, both the drive and the control systems, and it was an elbow type robot as well as being the first robot to be controlled by a microcomputer. Another key feature was to use harmonic drive planetary gears, which are compact and provide high gear ratio, in combination with DC motors. The IRB 6 was a success and the start of the Asea department for workshop automation. The IRB managed to carry out many more tasks than the competing robots at that time, with advantages such as higher speed, higher repetitive accuracy (thanks to a patented linkage system) and simpler programming. The design of the IRB 6 became a model for robot development during the 1970s, and it is the most copied industrial robot in the world.

In Japan, they were very quick to apply the new technology of industrial robots, which meant that they could increase productivity and take new market shares. Pretty soon they developed their own robots and in 1980, 19000 industrial robots were manufactured in Japan by approximately 150 different manufacturers, such as

[1] The Swedish company Asea merged with the Swiss company Brown Boveri in 1987, which resulted in a change of name to ABB.

Kawasaki, Yaskawa, Mitsubishi Heavy Industries, Kobe Steel and Fanuc. Between 1980 and 1988, the number of robots in operation worldwide increased tenfold and 1988, the figure was 256000. Of these, 175000, or 68%, had been installed in Japan.

Europe, apart from Scandinavia, awoke quite late to industrial robots. One reason is that there was no shortage of labor there. The industrial robot made its big breakthrough in Europe during the latter part of the 1970s. During the 1980s, the automotive industry in Europe and America discovered that the Japanese investment in robotized spot-welding produced a more consistent quality and, therefore, welding became a prioritized area. At the end of the 1980s, there was also a rapid growth in the field of assembly.

By the end of the 1980s, most manufacturers with an annual production volume below 1000 robots had to start looking for a partner. Usually large companies bought up small, specialized companies. During the last decade of the twentieth century, the largest companies on the European market were ABB, Fanuc, Yaskawa (Motoman), Kuka, Comao, and Renault Automation/ACMA. ABB was more than twice as big as its closest rival on the European market.

In the mid 1980s, a big shift in technology took place among the robot manufacturers when AC motors replaced the DC motors. AC motors offered better cooling, which meant that the performance could be increased. Continuous improvements in the robot control system also took place. In 1994, ABB launched a new control system, S4, which greatly improved the robot performance with respect to accuracy and cycle time. With the S4 control system, the controller used a full dynamic model and could control the six robot axes as well as all the welding parameters and up to six external axes. The control system was also able to communicate with other systems, making integration with other automation equipment possible. ABB's latest controller, IRC5, was released 2004 and offers many new features. One powerful innovation is the MultiMove, allowing synchronized control of up to 4 robots from the same controller. The IRC5 controller and its ABB robot family can be seen in Figure 2.4.

One might wonder what the future holds for the industrial robot? According to ABB (see Westerlund, 2000), industrial robots are today employed in roughly 20 different fields, with around 900 potential fields of use in the future. It could be that a "robot revolution" lies ahead of us. However, entering these new fields will be a great challenge for robot manufacturers. Among several things, the robot must, to a greater extent, be able to perceive what is going on in the environment and then additional sensors will be needed. The robot must also be user friendly and the software much easier to program. Probably a lighter mechanical structure will be needed and, above all, the price must be reduced.

2.3 Modeling

We will here derive some models for the mechanical arm of the industrial robot. The modeling will be carried out at different levels of complexity, starting with rigid body kinematics and dynamics, then adding flexibilities to better mimic the

Figure 2.4 *ABB robot family with the IRC5 controller (ABB, 2004).*

behavior of a real robot. These different modeling levels have corresponding system identification levels, see Chapter 4. Finally, a short section on modeling of actuators and sensors is given.

The material in this section is mainly based on Wernholt and Östring (2003), Sciavicco and Siciliano (2000), and Spong and Vidyasagar (1989).

2.3.1 Kinematics

Kinematics of a robot refers to the geometric relationship between the joint variables and the end effector position and orientation in task space. The motion of the end effector in task space is usually defined in Cartesian coordinates with respect to a reference frame.

To be able to describe the robot kinematics in a convenient way, various coordinate systems are needed. Therefore a coordinate frame is attached to each link, to the base (base frame or reference frame), and to the end effector (end effector frame or tool frame).

Joint coordinates are given by the vector $\varphi = (\varphi_1, \varphi_2, \ldots, \varphi_n)^T$, where n is the number of joints. A realization of the vector φ is called a *configuration* of the robot.

The position of the tool frame, the *tool center point (TCP)*, can be expressed by a vector $x \in \mathbb{R}^3$. The orientation of the tool frame with respect to the base frame is represented by a *rotation matrix*, $R \in \mathbb{R}^{3\times3}$. The rotation matrix belongs to a group of matrices called *SO(3)*, where *SO* stands for *Special Orthogonal group* with the properties $R^T R = I$, $\det R = +1$. Even though the matrix R has 9 elements, the SO(3) conditions makes it possible to parameterize it by a parameter vector r of lower dimension. Many representations occur in the literature, like the Euler angles and roll-pitch-yaw angles (using 3 parameters), and axis/angle and unit quaternions (using 4 parameters). Using only three parameters will give singularities for certain orientations, which would be cumbersome. In the ABB

controller, the unit quaternions are used for the representation of orientation. For details on different representations, see, for example, Spong and Vidyasagar (1989) and Funda et al. (1990).

Position Kinematics

The *forward kinematic problem* is to determine the mapping

$$X = \begin{pmatrix} x(\varphi) \\ r(\varphi) \end{pmatrix} = f(\varphi) \tag{2.1}$$

from joint space to task space, where X also is called the robot *location*. The computation of this function is quite straightforward and can be done iteratively from the base frame to the first link, then on to the second and so on until the tool frame is reached. In each step, the relation is determined by geometric properties of the links and a single joint variable.

The *inverse kinematic problem* is to determine the inverse of the mapping, *i.e.*, given a position and rotation of the tool frame calculate the corresponding robot joint configuration. This is a much harder problem and the problem has in general many solutions while, for a serial link robot as in Figure 2.1, the forward kinematic problem has a unique solution.

A systematic way of building kinematic models is the *Denavit-Hartenberg representation* (see, for example, Spong and Vidyasagar, 1989). In Wernholt and Östring (2003), the DH representation is illustrated for an ABB IRB 7600 robot.

Velocity Kinematics

The *velocity kinematics* gives the relationship between the joint velocities and the corresponding end effector linear and angular velocities. Similar to (2.1) the velocity kinematics can be written as

$$V = \begin{pmatrix} v \\ \omega \end{pmatrix} = J(\varphi)\dot{\varphi} \tag{2.2}$$

where $J(\varphi) \in \mathbb{R}^{6\times n}$ is the *manipulator Jacobian*, and V represents the linear and angular velocities of the tool frame relative to the base frame. The Jacobian is an important quantity in the analysis and control of robot motion. Since it is a function of the configuration φ, those configurations for which it looses rank are of special interest. They are called *singularities* and can be interpreted as points in the workspace where a serial type robot looses one or more degrees of freedom. When planning a trajectory, singular points should be avoided. The Jacobian also describes the transformation from tool contact forces to corresponding joint torques. One way of calculating the Jacobian is to differentiate (2.1) with respect to time, see Spong and Vidyasagar (1989) for details.

2.3.2 Dynamics

A dynamic robot model describes the time evolution of the robot joints as a function of applied torques and forces. The main focus of this thesis is identification of unknown parameters in this type of model, and therefore the structure of dynamic robot models is of interest.

There are two common methods to obtain the dynamic model. The first is based on the *Euler-Lagrange* formulation and is systematic and conceptually simple. This method will be briefly described below. The second method is based on the *Newton-Euler* formulation and allows obtaining the model in a recursive form. See, for example, Spong and Vidyasagar (1989) for details.

First, the dynamic model for a rigid robot is derived (Equations (2.6), (2.9), and (2.10)). This model will then be extended to include some flexibilities.

Rigid Body Dynamics

Mechanical systems can be described using the Euler-Lagrange formulation, given that the system is subject to holonomic constraints and the constraint forces satisfy the principle of virtual work. A constraint on the k coordinates $r_1, \ldots, r_k$ is called holonomic if it is of the form $g(r_1, \ldots, r_k) = 0$, and non-holonomic otherwise. If a system is subject to l holonomic constraints, the constraint system has l fewer degrees of freedom than the unconstrained system. Then a new set of, so called, generalized coordinates $\varphi_1, \ldots, \varphi_n$ is introduced where $r_i = r_i(\varphi_1, \ldots, \varphi_n)$, $n = k - l$, and all φ_i are independent. The principle of virtual work requires that the constraint forces do no work during displacements that are consistent with the constraints. If this is the case, only external forces need to be considered, which is the case for the rigid bodies considered here.

For the industrial robot the joint variables, φ, are considered as generalized variables since these define the degrees of freedom for the robot. Now define the *Lagrangian* function according to

$$L(\varphi, \dot{\varphi}) = K(\varphi, \dot{\varphi}) - P(\varphi) \tag{2.3}$$

where $K(\varphi, \dot{\varphi})$ is the *kinetic energy*, and $P(\varphi)$ is the *potential energy* of the system.

The total kinetic energy of the robot can be calculated as the sum of each link's kinetic energy like

$$K(\varphi, \dot{\varphi}) = \sum_{j=1}^{n} [\frac{1}{2} m_j v_j^T v_j + \frac{1}{2} \omega_j^T I_j \omega_j] = \frac{1}{2} \dot{\varphi}^T D(\varphi) \dot{\varphi} \tag{2.4}$$

where m_j is the mass of link j, I_j is the inertia matrix of link j, and v_j and ω_j are the linear and angular velocities of link j, which can be derived using Jacobian matrices similar to (2.2). I_j and ω_j must be expressed in the same coordinate system, and usually a body fixed coordinate system is used which makes I_j constant in time. The matrix $D(\varphi)$ is symmetric and positive definite.

For a rigid robot, the potential energy $P(\varphi)$ is due to gravity only. For a flexible robot elastic effects need to be included as well. The dynamics of the robot are described by Lagrange's equations

$$\frac{d}{dt}\frac{\partial L}{\partial \dot{\varphi}_j} - \frac{\partial L}{\partial \varphi_j} = \tau_j \ , j = 1, \ldots, n \tag{2.5}$$

where $\tau_1, \ldots, \tau_n$ are generalized input forces. Inserting kinetic and potential energy for the Lagrangian above gives the *dynamic equations*

$$M(\varphi)\ddot{\varphi} + C(\varphi, \dot{\varphi})\dot{\varphi} + g(\varphi) = \tau \tag{2.6}$$

where $M(\varphi)$ is the *inertia matrix*, $C(\varphi, \dot{\varphi})\dot{\varphi}$ is referred to as the velocity dependent term, containing the centrifugal and Coriolis effects, and $g(\varphi)$ is the gravitational term. The elements of the matrix $C(\varphi, \dot{\varphi})$ are defined as (m_{ij} is the i, j element of $M(\varphi)$)

$$c_{kj} = \sum_{i=1}^{n} \frac{1}{2}\{\frac{\partial m_{kj}}{\partial \varphi_i} + \frac{\partial m_{ki}}{\partial \varphi_j} - \frac{\partial m_{ij}}{\partial \varphi_k}\}\dot{\varphi}_i \tag{2.7}$$

and

$$g(\varphi) = -\frac{\partial V}{\partial \varphi} \tag{2.8}$$

The Lagrangian dynamics of (2.6) have a number of important properties that are helpful in the analysis and design of the control system (Spong and Vidyasagar, 1989; Sciavicco and Siciliano, 2000). Of particular interest here is the *linearity* with respect to the *dynamic parameters*, which are sometimes called the *standard inertial parameters*. Each link gives ten inertial parameters: body mass, mass location, and the inertia matrix (only six elements due to symmetry). The robot dynamic model (2.6) can then be rewritten as

$$H(\varphi, \dot{\varphi}, \ddot{\varphi})\theta = \tau \tag{2.9}$$

or as the energy difference model

$$\Delta h(\varphi, \dot{\varphi})\theta = \Delta\mathcal{H} = \mathcal{H}(t_b) - \mathcal{H}(t_a) = \int_{t_a}^{t_b} \tau^T \dot{\varphi} dt \tag{2.10}$$

where $\theta \in \mathbb{R}^{10n}$ is the parameter vector and n is the number of links (Kozlowski, 1998). $\mathcal{H}$ is the total energy of the system. Equations (2.9) and (2.10) will be extensively used for identification of rigid body dynamics, see Section 4.3 for further details.

Flexible Body Dynamics

In an industrial robot, there are various sources of flexibility, such as elastic deformation of bearings and gears and deflection of the links under load. For many

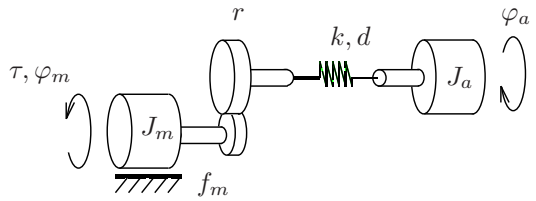

Figure 2.5 *The two-mass flexible model of the robot arm.*

robots, particularly those using harmonic drives for the torque transmission (see Section 2.3.3), the joint flexibility is significant.

A trend in robotics is to build lighter robots. The weight of the robot must of course be but into relation to the allowed payload. The load-to-mass ratio also depends on the size of the robot. The large ABB IRB 6600 robot can handle 225 kg and weights about 1700 kg, whereas their smallest robot IRB 140 can handle 5 kg and weights 98 kg. An example of a lightweight robot is the 7 DOF DLR lightweight robot in Albu-Schäffer and Hirzinger (2001), which handles 7 kg and weights 18 kg. This includes actuators as well as many additional sensors. This lightweight robot will of course not have the same performance as the traditional industrial robot regarding, for example, workspace, position accuracy, acceleration, and stiffness. All these properties are crucial for most industrial applications. There are however many reasons for using lightweight robots, like reduced mass and power consumption as well as safety issues (reduced mass of moving parts). Due to these reasons, it is also interesting to reduce the weight of industrial robots. Lightweight manipulators are used today in a variety of applications, ranging from space robotics to less known tasks like exploration of hazardous environments or nuclear waste retrieval. Service robotics and health care are two other areas of application. However, a lighter robot, will result in a weaker mechanical structure and enhance the effects of the flexibility of the materials. In addition to joint flexibilities, also flexibilities in the link structure then become important.

Flexible manipulators are actually described by partial differential equations, characterized by an infinite number of degrees of freedom. Obviously, dealing directly with infinite dimensional models is impractical both for estimation, simulation, and control design purposes. Hence it is necessary to introduce methods to describe flexibility with a discrete number of parameters. Three different approaches are generally used: *assumed modes*, *finite elements* and *lumped parameters*. See Theodore and Ghosal (1995) for a comparison of the first two approaches and Khalil and Gautier (2000) for an example of the last approach. Assumed modes are also treated in Bascetta and Rocco (2002), which, in addition, gives a good overview of the three different approaches. Here, the lumped parameters approach will be used, where each elastic link is divided into a number of masses, connected by spring-damper pairs.

The simplest flexible modeling approach is to only consider joint flexibility, *i.e.* elastic effects in the transmission between the motor and the joint. Considering

only one joint, that results in a *two-mass flexible model* according to Figure 2.5, where J_m and J_a are the moments of inertia of the motor and arm respectively, r is the gear ratio, k and d are the spring stiffness and damping (modeling the flexibility), f_m is the viscous friction of the motor, and τ is the motor torque. The equations describing the dynamics are

$$J_m\ddot{\varphi}_m + f_m\dot{\varphi}_m + rk(r\varphi_m - \varphi_a) + rd(r\dot{\varphi}_m - \dot{\varphi}_a) = \tau \tag{2.11a}$$

$$J_a\ddot{\varphi}_a - k(r\varphi_m - \varphi_a) - d(r\dot{\varphi}_m - \dot{\varphi}_a) = 0 \tag{2.11b}$$

The two-mass flexible model can be generalized to multivariable systems. A commonly adopted approximation then is to model the motors as simple rotating inertias, ignoring that the motors actually are moving due to the movements of the arm. This simplified model is obtained under the assumption that the kinetic energy of each rotor is mainly due to its own rotation, as discussed in Spong (1987). Gyroscopic forces between each rotor and the other links are then neglected. Such an approximation introduce minor errors for a traditional industrial robot which is fairly rigid. However, for lightweight robots where the masses of a flexible link and of its actuator could be comparable, neglecting or oversimplifying the dynamic effects of the motors could yield severe errors (Bascetta and Rocco, 2002).

For the generalized two-mass flexible model, the multivariable rigid body dynamics (2.6) is combined with a motor and a spring-damper pair for each joint, giving the dynamic equations

$$M_m\ddot{\varphi}_m + F_m\dot{\varphi}_m + RK(R\varphi_m - \varphi_a) + RD(R\dot{\varphi}_m - \dot{\varphi}_a) = \tau \tag{2.12a}$$

$$M(\varphi_a)\ddot{\varphi}_a + C(\varphi_a, \dot{\varphi}_a)\dot{\varphi}_a + g(\varphi_a) - K(R\varphi_m - \varphi_a) - D(R\dot{\varphi}_m - \dot{\varphi}_a) = 0 \tag{2.12b}$$

where τ now is the vector of applied motor torques, φ_a is the vector of arm joint variables (previously φ), and φ_m is the vector of motor joint variables. Diagonal matrices describing the joint dynamics are defined as $M_m = \text{diag}[J_{m1}, \ldots, J_{mn}]$, $F_m = \text{diag}[f_{m1}, \ldots, f_{mn}]$, $D = \text{diag}[d_1, \ldots, d_n]$, $K = \text{diag}[k_1, \ldots, k_n]$, and $R = \text{diag}[r_1, \ldots, r_n]$. See also Spong (1987) for a derivation of the dynamic equations.

2.3.3 Actuators and Sensors

Two basic components in the robot system are *actuators* and *sensors*. It is, of course, outside the scope of this thesis to give an overview of all different actuators and sensors used in various types of robot systems, including a description of their pros and cons. Here, the focus will be on the actuators and sensors used for the particular industrial robot used in the experiments, *i.e.*, the ABB IRB 6600 (see Chapters 7 and 9). See, for example, Sciavicco and Siciliano (2000, pp. 295-320) for are more detailed overview.

Actuators

A robot actuating system is in general constituted by a power supply, a power amplifier, a motor, and a transmission.

The *power amplifier* (or power controller) has the task of modulating the power flow (provided by the power supply) according to a control signal and transmit this power to the motor in terms of suitable force and flow quantities. For electric motors, it is common to use transistor amplifiers which are suitably switched by using pulse-width modulation techniques.

The joint motion typically demands low speeds with high torques. A motor usually provides the opposite, *i.e.*, high speeds with low torques. To overcome this, a *transmission* (gearbox) can be used. Various types are used depending on the robot structure, desired performance, etc. One example is the *harmonic drives*, which are very popular today due to their low backlash, compact size, and high torque transmission. Using a transmission will reduce the nonlinear coupling terms in the dynamic model but at the same time introduce gearbox flexibilities, backlash and friction. In some (rare) cases the motor is directly connected to the joint, without the use of any transmission, which is called *direct drive*. Using direct drive will make the coupling effects significant and in addition the control of the motors will be more difficult. The use of direct-drive actuators is not yet popular for industrial robots in view of their cost, the size of the motors (as well as the brakes), and a more difficult control problem. In addition, more accurate (and expensive) sensors will be needed to measure the joint position, compared to measuring the motor position before the gearbox (resolution increased by the gear ratio).

Two types of *motors* are often used; namely electric motors (for small and medium size robots) and hydraulic motors (for large size robots). In addition pneumatic motors are sometimes used, for example, to open and close the jaws of a gripper tool. Here, only electric motors will be considered and, in particular, AC permanent magnet motors since these are used as actuators for the industrial robot used in the experiments. *AC permanent magnet motors* are extremely fast, compact, and robust. A drawback, however, is that the generated torque changes periodically with the rotor position. The resulting torque ripple is caused by distortion of the stator flux linkage distribution, variable magnetic reluctance at the stator slots, and secondary phenomena such as, for example, the power amplifier (Holtz and Springob, 1996). The ripple caused by the variable magnetic reluctance is proportional to the current, which here will be approximated by the commanded torque, τ_c, from the robot controller (neglecting the fast power controller). Since the torque ripple is periodic in the rotor position φ, it can be modeled as a sum of sinusoids like

$$v_\tau(t) = \sum_{n\in\mathbb{N}_a} a_n \sin(n\varphi(t) + \phi_{a,n}) + \tau_c(t) \sum_{n\in\mathbb{N}_b} b_n \sin(n\varphi(t) + \phi_{b,n}) \tag{2.13}$$

where the number of components in $\mathbb{N}_a$ and $\mathbb{N}_b$ depends on the specific motor type and the level of approximation (Gutt et al., 1996). The applied torque τ can therefore be seen as a sum of the commanded torque τ_c and a disturbance term v_τ. For an example, see Table 8.1 in Section 8.1.

Sensors

Using sensors is of crucial importance to achieve high-performance robotic systems. There are various types of sensors available, often divided into sensors that measure the internal state of the robot (proprioceptive sensors) and sensors that provide knowledge about the surrounding environment (heteroceptive sensors). Examples of proprioceptive sensors are encoders and resolvers for joint position measurements and tachometers for joint velocity measurements. Heteroceptive sensors include, for example, force sensors for end effector force measurements and vision sensors for object image measurements when the manipulator interacts with the environment.

It is common to restrict the number of sensors by only measuring the rotor position (of the motor) for each joint. Due to the transmission and other sources of flexibilities, advanced dynamic models can then be used to accurately estimate the movements of the robot arm. Measurements of the rotor position is normally obtained by using Tracking Resolver-to-Digital Converters (Hanselman, 1990). The position error, due to non-ideal resolver characteristics, can be be described as a sum of sinusoids like (Hanselman, 1990)

$$v_\varphi(t) = \sum_{n \in \mathbb{N}_c} c_n \sin(n\varphi(t) + \phi_{c,n}) + e_\varphi(t) \tag{2.14}$$

where $e_\varphi(t)$ is Gaussian noise, added to take into account measurement noise. v_φ is hereafter denoted output disturbance. For an example, see Table 8.1 in Section 8.1.

2.4 Control

The robot motion control problem is the problem of determining the time history of inputs to the actuators required to cause the end effector to execute a commanded motion. In general, the motion control problem is divided into three stages,

- motion planning,
- trajectory generation, and
- trajectory tracking.

See also Figure 2.6. Each stage will now be described briefly.

2.4.1 Motion Planning

Motion planning on the highest level involves finding a *path* in the operational space, which denotes the locus of Cartesian points or some other representation, that the end effector has to follow in the execution of the assigned motion. In industrial applications this part is either done by using a teach pendant (see Figure 2.7) or by using a system separate from the robot control system, for example a CAD/CAM tool.

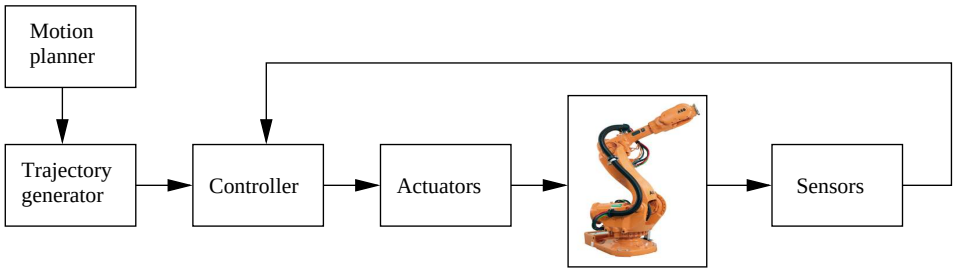

Figure 2.6 *Block diagram showing the components in the robot control problem.*

Figure 2.7 *An example of a teach pendant: The ABB IRC5 FlexPendant (ABB, 2004).*

2.4.2 Trajectory Generation

The goal of the trajectory generation stage is to generate reference inputs to the control system which ensures that the manipulator executes the planned trajectories.

Given the path representation in Cartesian space from the motion planning stage, this path first has to be transformed into a path representation in joint space. This is in general not possible to do analytically. Instead the path must be transformed using the *inverse kinematic model* of the robot manipulator at discrete points. These points are then interpolated, for example by using splines as in Nyström and Norrlöf (2003).

The generated path is a pure geometric description of the motion. A *trajectory*, on the other hand, is a path on which a time law is specified. Trajectory generation therefore deals with the problem of generating a trajectory with position, speed, acceleration, and jerk (derivative of acceleration) given as functions of time. Since

the trajectories must be *feasible*, *i.e.*, the manipulator must be able to follow the generated trajectories, the actual robot dynamics and kinematics must be taken into account. The goal often is to find optimal paths where the maximum speed and acceleration are used. Therefore, the trajectory generation problem is important for the performance of the robot.

2.4.3 Trajectory Tracking

The trajectory tracking problem can be defined as the problem of controlling the robot joints according to the trajectory calculated by the trajectory generator.

There are many control techniques and methodologies that can be applied to the control of manipulators. The control method and its implementation can have significant impact on the performance of the manipulator and consequently on the range of possible applications. The mechanical design of the manipulator will also influence the type of controller needed. For example, the nonlinear coupling effects between different joints varies greatly between a Cartesian robot and an elbow type robot. If a gearbox is used or not will also greatly affect the control problem, as was mentioned in Section 2.3.3. Using a gearbox will reduce the nonlinear coupling effects but at the same time introduce flexibilities, backlash and friction. Using a direct-drive robot, on the other hand, will make the coupling effects significant and in addition the control of the motors will be more difficult. Here, we will consider geared elbow-type robots. It is outside the scope of this thesis to give an overview of all available control methods. For more details on different aspects of robot control, there are numerous references, such as Spong and Vidyasagar (1989); Craig (1989); Sciavicco and Siciliano (2000); Spong et al. (1993). However, to get a feeling for the problem, some words will be said about a commonly used control technique.

A standard procedure in robotics today is to measure only the motor position (to increase performance, additional sensors are sometimes added). Due to the gearbox flexibilities, there will be some dynamics between the motor position, φ_m, and the arm position, φ_a. Therefore, the generated arm trajectory, φ_a^{ref}, must be transformed to a corresponding motor trajectory, φ_m^{ref}, using a flexible dynamic model. A common architecture for the robot controller is shown in Figure 2.8, using both feedback and feedforward controllers. X is the end effector Cartesian location which should follow the path created by the motion planner.

Since the trajectory is known beforehand, it can be used in a feedforward controller. The generated trajectories are feasible so the feedforward controller should ideally give zero tracking error on the motor side, $e(t) = \varphi_m^{ref}(t) - \varphi_m(t)$. Due to model errors and disturbances, there will still be a non-zero tracking error and this is handled by the feedback controller. A common choice for the feedforward controller is to use *computed torque* (Spong and Vidyasagar, 1989) which in principle means the inverse of the robot dynamics. For a rigid robot described by (2.6), the feedforward controller would output

$$\tau_f = M(\varphi^{ref})\ddot{\varphi}^{ref} + C(\varphi^{ref}, \dot{\varphi}^{ref})\dot{\varphi}^{ref} + g(\varphi^{ref}) \tag{2.15}$$

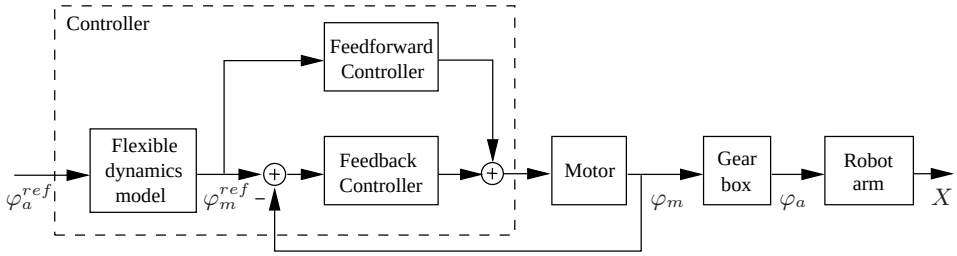

Figure 2.8 *Block diagram showing the controller and a robot with gearbox flexibilities. The dashed block corresponds to the Controller block in Figure 2.6.*

where φ^{ref} is the reference trajectory. This is a complicated expression that must be evaluated at a high sampling rate and is therefore often approximated by removing slowly varying parts. These are instead handled by the feedback controller. Adding flexibilities further complicates the feedforward controller.

For the feedback controller, the simplest control strategy is called *independent joint control* and means that each joint axis is controlled as a SISO system. Coupling effects are then treated as disturbances and what is left to control is a two-mass flexible system like (2.11). For example a simple PID controller will usually give satisfactory behavior. Since the feedforward controller is expected to give the main performance, the feedback controller is mainly tuned for disturbance rejection. The controller must be robust to modeling errors as well as uncertainties in the robot load and variations in the workspace. The arm inertia, J_a, in (2.11) will, for example, vary as a function of the configuration, φ. To improve the performance of the feedback controller, sometimes a gain scheduling technique is used with the varying arm inertia, J_a, as one of the scheduling variables. A second step would be to include some coupling effects of major influence. For example, axes two and three are for some configurations highly coupled. Of course, more advanced control strategies could be applied as well, see the previously suggested references.

3

System Identification

Linear time-invariant dynamic systems and models are the foundation of control theory and system identification and are described in many textbooks (see, for example, Rugh, 1996; Ljung, 1999). In Section 3.1, some useful properties will be briefly reviewed. This section can be skipped by readers already familiar with the subject. The system identification procedure is described in Section 3.2, with details on model structures and how to compute the estimates in Sections 3.3 and 3.4, respectively. The chapter is ended by some notes on model validation, closed-loop identification and bias and variance in the estimates.

3.1 Preliminaries

Consider a *continuous-time* system with a scalar input $u(t)$ and a scalar output $y(t)$. The system is said to be *time-invariant* if its response to a certain input signal does not depend on absolute time. It is said to be *linear* if its output response to a linear combination of inputs is the same linear combination of the output responses of the individual inputs. In addition, it is said to be *causal* if the output at a certain time only depends on the input up to that time. In the following, only causal systems will be treated.

A linear time-invariant (LTI) system can be completely described by its *impulse response* $g(\tau)$ as

$$y(t) = \int_0^\infty g(\tau)u(t-\tau)d\tau \tag{3.1}$$

An LTI system can also be represented by a *transfer function* $G(s)$, which is ob-

tained by taking the Laplace transform of the impulse response, *i.e.*,

$$G(s) = \int_0^\infty g(t)e^{-st}dt \tag{3.2}$$

We then have the relation

$$Y(s) = G(s)U(s) \tag{3.3}$$

between $Y(s)$ and $U(s)$, the Laplace transforms of the output and input, respectively. The function $G(p)$, where p is the differential operator $pu(t) = \frac{d}{dt}u(t)$, will be called the *transfer operator* (sometimes, with abuse of notation, $G(p)$ will be called transfer function as well). This makes it possible to write (3.1) as

$$y(t) = G(p)u(t) \tag{3.4}$$

We will exclusively work with observations of inputs and outputs in *discrete-time*. We thus assume that $y(t)$ and $u(t)$ are observed at the *sampling instants* $t_k = kT,\ k = 1, 2, \ldots$ where the interval T will be called the *sample time*. Often in computer controlled applications, the input signal $u(t)$ is kept constant between the sampling instants like

$$u(t) = u_k, \quad kT \le t < (k+1)T \tag{3.5}$$

which is called *zero-order hold*. Inserting (3.5) in (3.1) gives a relation between y and u at the sampling instants

$$y(kT) = \sum_{l=1}^{\infty} g_T(l)u_{k-l} \tag{3.6}$$

where $g_T(l)$ is the discrete-time *impulse response* defined as

$$g_T(l) = \int_{(l-1)T}^{lT} g(\tau)d\tau \tag{3.7}$$

Taking the z-transform of $g_T(l)$ gives the discrete-time *transfer function*

$$G_T(z) = \sum_{k=0}^{\infty} g_T(k)z^{-k} \tag{3.8}$$

and replacing z with the shift operator q, $qu(t) = u(t+T)$, gives the corresponding discrete-time *transfer operator*.

Evaluation of the transfer function at the point $z = e^{i\omega T}$ ($s = i\omega$ for continuous-time) will describe the system response to a sinusoidal input $u(t) = \cos\omega t$ like

$$y(t) = |G_T(e^{i\omega T})| \cos(\omega t + \arg G_T(e^{i\omega T})) \tag{3.9}$$

The complex-valued function

$$G_T(e^{i\omega T}), \quad -\pi/T \le \omega \le \pi/T \tag{3.10}$$

is therefore called the *frequency response function* or just the *frequency function*. It is common to graphically display this function as $\log|G_T(e^{i\omega T})|$ and $\arg G_T(e^{i\omega T})$ plotted against $\log\omega$ (for $0 < \omega \leq \pi/T$) in a *Bode plot*. For continuous-time descriptions, the frequency function $G(i\omega)$ is defined for $-\infty < \omega < \infty$.

One might wonder how the continuous-time and discrete-time frequency functions are related. It is possible to show that

$$|G(i\omega) - G_T(e^{i\omega T})| \leq \omega \cdot T \cdot \int_0^\infty |g(\tau)|d\tau \tag{3.11}$$

where $g(\tau)$ is the continuous-time impulse response (see, for example, Ljung and Glad, 1994, p. 75). The frequency response functions agree quite well for low frequencies and a rule of thumb is that the agreement usually is good enough for frequencies below one tenth of the sampling frequency ($\omega < 2\pi/(10T)$). A reason for the difference is that the influence from the zero-order hold sampling (3.5) has been neglected. One can show that a zero-order hold will give a contribution like

$$G_{zoh}(s) = \frac{1 - e^{-sT}}{s} G(s) \tag{3.12}$$

where $G_{zoh}(s)$ is the new continuous-time transfer function where the sampling effects are added (Phillips and Nagle, 1990).

Consider now the Fourier transform, defined as

$$U(i\omega) = \int_0^\infty u(t)e^{-i\omega t}dt \tag{3.13}$$

for a continuous-time signal $u(t)$ and

$$U_T(e^{i\omega T}) = \sum_{l=0}^{\infty} u_l e^{-i\omega Tl} \tag{3.14}$$

for a discrete-time signal. These transforms are related as

$$U_T(e^{i\omega T}) = \frac{1}{T} \sum_{k=-\infty}^{\infty} U(i(\omega - k\frac{2\pi}{T})) \tag{3.15}$$

If the bandwidth of the continuous-time signal is larger than half the sampling frequency, higher frequencies will be shifted in and appear as lower frequencies. This error is called *alias error* and can be avoided by using an anti-alias filter before sampling the signal. If the bandwidth is less than half the sampling frequency, no information will be lost and the continuous-time and discrete-time Fourier transforms will coincide for $-\pi/T \leq \omega \leq \pi/T$.

Of course, in a real situation, only a limited number of data points u_l, $l = 1, 2, \ldots, N$ are collected. It is then common to consider the Discrete Fourier Transform (DFT), defined as

$$U_N(\omega_k) = \frac{1}{\sqrt{N}} \sum_{l=1}^{N} u_l e^{-i\omega_k Tl} \tag{3.16}$$

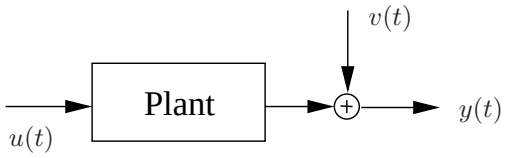

Figure 3.1 *Plant subject to system identification. The signals $u(t)$ and $y(t)$ are the system input and output, respectively, while $v(t)$ is a disturbance signal acting on the system.*

with

$$\omega_k = k\frac{2\pi}{NT}, \quad k = 1, 2, \ldots, N \tag{3.17}$$

Depending on the properties of the original infinite length signal, the DFT (3.16) may differ from the discrete-time Fourier Transform (3.14). Assuming a periodic signal and measuring an integer number of periods, (3.16) and (3.14) will coincide for the DTF frequencies (3.17). In other cases, there will be *leakage errors* due to the limited time window. This error can be reduced by using a windowed signal (typically giving less attention to samples in the beginning and the end of the data record). See, for example, Ljung (1999) and Pintelon and Schoukens (2001b) for suggestions on suitable windows.

3.2 The System Identification Procedure

Consider the setting in Figure 3.1, where $u(t)$ is the plant input and $y(t)$ is the measured plant output, corrupted by the disturbance $v(t)$. Assume now that we, for some reason, want to model this system. The model could be used both as a means for achieving deeper knowledge about the system and as a design tool, for example as a basis for simulations or for controller design. One common use of models is prediction, where we want to predict future output values. This is, for example, used in weather forecasts.

Two main routes for obtaining these models are *physical modeling* and *system identification*. Modeling involves using basic physical laws and other well-established relationships (which, in a sense, means using previous experience based on previous empirical work). On the other hand, system identification uses experimental data to find a suitable model. In this chapter the focus, obviously, will be on the latter route.

The system identification procedure involves finding a model that describes the input-output data sufficiently well, according to some criterion. The search for this model will be carried out among a set of candidate models. System identification therefore includes several steps, like:

1. Design the experiments.
2. Collect experimental data from the system.

3. Select a set of models or the model structure to represent the system.
4. Determine the "best" model in the set, guided by the data.
5. Validate the model.

In each step, there are numerous options which inevitably cannot be described in detail here. Still, some particular options with relevance to our studied problem will be pointed out. For a detailed treatment, the reader is referred to, for example, Ljung (1999), Söderström and Stoica (1989), and Pintelon and Schoukens (2001b).

The design of good experiments for use in identification is covered separately in Chapter 5. The second step, the actual collection of experimental data, depends on the considered system, measurement equipment, *etc.*, and will not be treated here. The last three steps are covered in the following sections.

3.3 Model Structures

As was mentioned previously, the identification procedure involves a search for the best model among a set of candidate models, called the *model set*. The selection of this model set is the most important and, at the same time, the most difficult choice in the identification procedure. Physical insight and a priori knowledge about the system are often of great assistance. The model set is just a collection of models. In order to facilitate the numerical search, the model set can be parameterized by a parameter vector θ belonging to the parameter set $D_{\mathcal{M}}$. This parameterization of the model set is called a *model structure* and is denoted by $\mathcal{M}$.

Some options to consider in the selection of a suitable model structure are:

- Linear versus nonlinear models.
- Parametric versus nonparametric models.
- Black-box versus gray-box models.
- Discrete-time versus continuous-time models.
- Linear-in-the-parameters versus nonlinear-in-the-parameters.

Most of these options can be combined, giving a wide range of possible model structures to choose from. For each choice, there are a number of identification methods for the computation of the parameter estimate. These methods will be discussed in the next section. The model structure selection will also greatly affect how hard the problem of computing the parameter estimate will be. Each of these options will now be briefly explained.

Consider once more the setting in Figure 3.1 and the aim to find a model describing the collected input-output data. The first choice to make is if to use a *linear* or *nonlinear* model. Almost every real life system is nonlinear, including the industrial robot that is studied in this thesis. The theory of nonlinear systems is very involved and therefore nonlinear systems are often approximated by linear

models. This is done under the assumption that the behavior can be linearized in the operating region. Whether this is a valid assumption or not depends on the application. For a detailed discussion on linear models of nonlinear systems, see Enqvist (2003) and Pintelon and Schoukens (2001b, Ch. 3).

The second choice is between a *parametric* or *nonparametric* model. A nonparametric model could, for example, be the impulse response (time domain) or the frequency response function (frequency domain) at a large number of points. The only assumption made then is that a linear input-output relation exists. For a parametric model, on the other hand, some additional knowledge and/or assumptions are used to reduce the model's degrees-of-freedom by parameterizing it by a limited number of parameters. An example could be a transfer function model, parametrized by its poles and zeros. For a parametric model, the physical insight will typically be larger and it can be seen as a concentration of information. Usually a nonparametric model is simpler to create since less knowledge about the system is needed.

Assume now that the system in Figure 3.1 can be modeled by a parametric linear time-invariant model like

$$y(t) = G(p, \theta)u(t) + H(p, \theta)e(t) \tag{3.18}$$

in the *continuous-time* case and

$$y(t) = G(q, \theta)u(t) + H(q, \theta)e(t) \tag{3.19}$$

in the *discrete-time* case. The plant transfer function, $G(\cdot, \theta)$, describes the input-output relation and the term $H(\cdot, \theta)e(t)$, where $e(t)$ is a white disturbance signal with zero mean, is used to describe the impact of the disturbance $v(t)$ on the output $y(t)$. $G(\cdot, \theta)$ and $H(\cdot, \theta)$ are parametrized by the parameter vector θ. The model structure $\mathcal{M}$ can then be written more formally as

$$\mathcal{M}: \quad D_{\mathcal{M}} \ni \theta \rightarrow \mathcal{M}(\theta) = \{G(\cdot, \theta), H(\cdot, \theta)\} \tag{3.20}$$

which means the mapping from the parameter vector θ, belonging to the parameter set $D_{\mathcal{M}}$, to a particular model $\mathcal{M}(\theta)$. For details on model sets and model structures, see Ljung (1999, pp. 107-108).

Sometimes the model structure $\mathcal{M}$ is obtained after careful modeling, with some unknown parts or parameters left to estimate. This type of model structure is called *gray box*. Similarly, a model structure whose parameters do not reflect physical considerations in the system is called *black box*. Nonlinear gray-box models will be treated in Chapter 9.

The transfer functions $G(\cdot, \theta)$ and $H(\cdot, \theta)$ can be parameterized in many different ways, *e.g.*, as rational functions where the parameter vector θ contains the coefficients in the numerator and denominator polynomials. The following general *black-box model* structure is often used

$$A(\cdot, \theta)y(t) = \frac{B(\cdot, \theta)}{F(\cdot, \theta)}u(t) + \frac{C(\cdot, \theta)}{D(\cdot, \theta)}e(t) \tag{3.21}$$

where, in discrete-time,

$$A(q,\theta) = 1 + a_1 q^{-1} + \ldots + a_{n_a} q^{-n_a} \tag{3.22}$$

and similarly for $C(q,\theta)$, $D(q,\theta)$, and $F(q,\theta)$, while

$$B(q,\theta) = b_1 q^{-n_k} + b_2 q^{-n_k-1} \ldots + b_{n_b} q^{-n_k-n_b+1} \tag{3.23}$$

where n_k is the number of time delays in the system. By setting some of the polynomials to unity, different special cases are achieved. One common case is the ARX model

$$A(q,\theta)y(t) = B(q,\theta)u(t) + e(t) \tag{3.24}$$

A reason for its wide use is that the parameter estimate can be easily calculated, see (3.38).

Another common model parametrization is the *state space model*

$$\dot{x}(t) = A(\theta)x(t) + B(\theta)u(t) + K(\theta)e(t) \tag{3.25a}$$
$$y(t) = C(\theta)x(t) + D(\theta)u(t) + e(t) \tag{3.25b}$$

or

$$x(t+T) = A(\theta)x(t) + B(\theta)u(t) + K(\theta)e(t) \tag{3.26a}$$
$$y(t) = C(\theta)x(t) + D(\theta)u(t) + e(t) \tag{3.26b}$$

where here for simplicity the *innovations form* is considered (Ljung, 1999, p. 99). In this description, $x(t) \in \mathbb{R}^n$ is the state vector and $A(\theta)$, $B(\theta)$, $K(\theta)$, $C(\theta)$, and $D(\theta)$ are matrices (vectors) of suitable dimensions. A nice property for state space models is that they work equally well for multivariable systems as for scalar systems. The state space models (3.25) and (3.26) are just choices of parameterization of the linear systems (3.18) and (3.19), respectively. Consider now the discrete-time case. Using the shift operator, (3.26) can be rewritten as

$$y(t) = G(q,\theta)u(t) + H(q,\theta)e(t) \tag{3.27}$$
$$G(q,\theta) = C(\theta)(qI - A(\theta))^{-1}B(\theta) + D(\theta) \tag{3.28}$$
$$H(q,\theta) = C(\theta)(qI - A(\theta))^{-1}K(\theta) + I \tag{3.29}$$

showing the relationship to the model (3.19). For a nonlinear system, like the robot, the dynamics can be modeled using a nonlinear state space model like

$$\dot{x}(t) = f\big(t, x(t), \theta, u(t), e(t)\big) \tag{3.30a}$$
$$y(t) = h\big(t, x(t), \theta, u(t)\big) + e(t) \tag{3.30b}$$

in the continuous-time case, with obvious modifications for the discrete-time case. Here, f and h are nonlinear functions. This type of model will be used for nonlinear gray-box identification in Chapter 9.

3.4 Calculating the Estimate

Suppose now that a model structure has been selected, according to the previous section. Depending on the choice of model structure, a number of different methods exist. It is common to distinguish between parametric and nonparametric methods and also between time-domain and frequency-domain methods. Here, we will briefly discuss parametric time-domain methods, parametric frequency-domain methods, and nonparametric frequency-domain methods. For nonparametric time-domain methods like transient-response analysis and correlation analysis, see for example Ljung (1999) and the references therein.

3.4.1 Parametric Time-domain Methods

With time-domain methods for system identification, we here mean methods that compute estimates of the unknown parameters θ using measurements of the input and output for a number of time instants, $Z^N = \{u(1), y(1), \ldots, u(N), y(N)\}$. (For simplicity, we will assume sample time $T = 1$ in the sequel.) Several methods are available in the literature but to limit the discussion, mainly the the *prediction error method* will be considered. The idea behind the prediction error method is to find the parameters that will minimize the prediction errors,

$$\varepsilon(t, \theta) = y(t) - \hat{y}(t|\theta) \tag{3.31}$$

where $\hat{y}(t|\theta)$ is the model's prediction of $y(t)$ given Z^{t-1}. For the discrete-time case (3.19), the standard predictor is

$$\hat{y}(t|\theta) = H^{-1}(q, \theta)G(q, \theta)u(t) + (1 - H^{-1}(q, \theta))y(t) \tag{3.32}$$

For the continuous-time case (3.18), a predictor can be calculated by, for example, first sampling the model. For the discrete-time state space model (3.26), the predictor $\hat{y}(t|\theta)$ is given by

$$\begin{aligned} \hat{x}(t+1, \theta) =& A(\theta)\hat{x}(t, \theta) + B(\theta)u(t) + \\ &+ K(\theta)\left[y(t) - C(\theta)\hat{x}(t, \theta) - D(\theta)u(t)\right] && \text{(3.33a)} \\ \hat{y}(t|\theta) =& C(\theta)\hat{x}(t, \theta) + D(\theta)u(t) && \text{(3.33b)} \end{aligned}$$

For the minimization of the prediction errors (3.31), one could choose different norms. A common choice is the quadratic criterion, given by

$$V_N(\theta) = \frac{1}{N}\sum_{t=1}^{N}\frac{1}{2}\varepsilon^2(t, \theta) \tag{3.34}$$

Other norms than ε^2 might be useful for, for example, robustness against outliers (Ljung, 1999). The criterion is usually minimized by a numerical search method, for example the Gauss-Newton method (Ljung, 1999, Ch. 10). This is the case also for the nonlinear gray-box identification method used in Chapter 9.

In some special cases, like the ARX model (3.24) with a quadratic criterion (3.34), there exists an analytical solution. For an ARX model, the predictor can be written as a linear regression

$$\hat{y}(t,\theta) = \phi^T(t)\theta \tag{3.35}$$

$$\phi(t) = [-y(t-1)\cdots -y(t-n_a)\ u(t-n_k)\cdots u(t-n_k-n_b+1)]^T \tag{3.36}$$

$$\theta = [a_1 \cdots a_{n_a}\ b_1 \cdots b_{n_b}]^T \tag{3.37}$$

Since the prediction error here is *linear in the parameters*, the minimizing parameter vector to (3.34) is the solution to a standard least-squares problem

$$\hat{\theta}_N = \arg\min_\theta V_N(\theta) = \left[\frac{1}{N}\sum_{t=1}^{N}\phi(t)\phi^T(t)\right]^{-1}\frac{1}{N}\sum_{t=1}^{N}\phi(t)y(t) \tag{3.38}$$

which is usually computed using a QR factorization (see Ljung, 1999)).

For state space models, there is also the possibility to use *subspace methods*, which basically estimate the matrices of the state space model by solving a sequence of least-squares problems. See, for example, the book Van Overschee and DeMoor (1996) for an overview.

3.4.2 Parametric Frequency-domain Methods

A parametric frequency-domain identification method estimates the unknown parameters θ from *frequency-domain data* Z^N which, in most cases, is obtained by a DFT from the raw time-domain data like

$$Z^N = \{U_N(\omega_1), Y_N(\omega_1), \ldots, U_N(\omega_N), Y_N(\omega_N)\} \tag{3.39}$$

The data set could also be obtained directly from the system using a measurement device providing frequency domain data.

If we assume that the system can be described by (3.18) or (3.19), we have the following (approximate) relations

$$Y_N(\omega_k) = G(i\omega_k,\theta)U_N(\omega_k) + H(i\omega_k,\theta)E_N(\omega_k) \tag{3.40}$$

in continuous time and

$$Y_N(\omega_k) = G(e^{i\omega_k T},\theta)U_N(\omega_k) + H(e^{i\omega_k T},\theta)E_N(\omega_k) \tag{3.41}$$

in discrete time. For non-periodic signals, the relations are only approximate since a transient term then should be added as well. For (3.40) to hold, we have also assumed that the bandwidth of the original continuous-time signals is less than half the sampling frequency such that the continuous-time and discrete-time Fourier transforms, (3.13) and (3.14), coincide.

A common criterion for the parameter estimate is the *(weighted) least squares* criterion

$$V_N(\theta, Z^N) = \sum_{k=1}^{N} |Y_N(\omega_k) - G(i\omega_k, \theta)U_N(\omega_k)|^2 W_k \tag{3.42}$$

for continuous time and

$$V_N(\theta, Z^N) = \sum_{k=1}^{N} \left|Y_N(\omega_k) - G(e^{i\omega_k T}, \theta)U_N(\omega_k)\right|^2 W_k \tag{3.43}$$

for discrete time, where the *weight functions* W_k can be selected using the noise model $H(\cdot, \theta)$. If the noise model depends on θ, an additional term should be added as well (Ljung, 1999; Pintelon and Schoukens, 2001b). The criterion can be made quadratic in θ by parameterizing the model $G(\cdot, \theta)$ as a rational function and multiply $Y_N(\omega_k) - G(\cdot, \theta)U_N(\omega_k)$ by the denominator, see Pintelon and Schoukens (2001b) for details. For systems with a large dynamic range, which is the case for the highly resonant industrial robot we are studying, the *(weighted) logarithmic least squares* criterion is suggested

$$V_N(\theta, Z^N) = \sum_{k=1}^{N} \left|\log \frac{Y_N(\omega_k)}{U_N(\omega_k)} - \log G(e^{i\omega_k T}, \theta)\right|^2 W_k \tag{3.44}$$

which has improved numerical stability as well as robustness with respect to outliers. From a theoretical point of view, logarithmic least squares will give inconsistent (biased) estimates, but for systems with a fairly good signal-to-noise ratio, this is of minor practical importance. See, again, Pintelon and Schoukens (2001b, pp. 206-207) for details.

Relationship Between Time-domain and Frequency-domain methods

First, one can note that there is a one-to-one relationship between time-domain and frequency-domain data, so no information is lost by taking the DFT of the time-domain data. The only difference is that some information is more easily accessible in one domain than in the other. It is also possible to reformulate an identification problem from time domain to frequency domain, and vice versa, so in that sense, they are equivalent (see, for example, Ljung, 1999). However, the complexity of the identification methods will vary depending on the selected domain and there can also be some numerical differences.

For time-domain methods, discrete-time models are the natural choice. For frequency domain methods, on the other hand, the choice of models is more general. This is due to the fact that the differential or difference equations are replaced by algebraic equations in the related frequency variable, and then there are no major differences in the calculation of the model estimates. For a discussion on similarities and differences using time-domain or frequency-domain identification methods, see for example Pintelon and Schoukens (2001b, pp. 368-373) and Ljung (1999, pp. 227-233).

3.4.3 Nonparametric Frequency-domain Methods

Nonparametric frequency-domain identification methods means that the plant frequency response function (FRF) is estimated without using a certain model set described by a number of parameters. Most nonparametric estimation methods consider only scalar systems, like the ETFE described below. Here we will also consider an estimation method, described in Guillaume et al. (1996), for the multivariable frequency response function (MFRF).

Estimates of the FRF are an interesting intermediate step in the identification process. Using these estimates, the quality of the measurements is assessed and one gets a feeling for the complexity of the modeling problem. In a second step, a parametric model can be estimated, *e.g.* by minimizing the distance between the model and the estimated FRF, see (3.44), or directly from time-domain or frequency-domain data, as was previously described.

The Empirical Transfer Function Estimate (ETFE)

Using the DFT of the input and output, $U_N(\omega_k)$ and $Y_N(\omega_k)$, the *empirical transfer function estimate (ETFE)* is defined as

$$\hat{\hat{G}}_N(e^{i\omega_k T}) = \frac{Y_N(\omega_k)}{U_N(\omega_k)} \tag{3.45}$$

It is possible to show that the variance of this estimate does not approach zero as the number of data tends to infinity, unless the data is periodic (Ljung, 1999). Therefore, the estimate is often smoothed using a weighting function

$$\hat{G}_N(e^{i\omega T}) = \frac{\sum_k \alpha_k(\omega)\hat{\hat{G}}_N(e^{i\omega_k T})}{\sum_k \alpha_k(\omega)} \tag{3.46}$$

The smoothing will reduce the variance but introduce a bias (see Section 3.7 for bias and variance expressions). The width of the smoothing, *i.e.*, the variance/bias trade-off, is determined by the user. The ETFE is closely related to spectral estimation, described next.

Spectral Estimation (SPA)

Using the DFT, the *periodogram* of a signal $u(t)$ can be calculated as

$$\hat{\hat{\Phi}}_u(\omega) = |U_N(\omega)|^2 \tag{3.47}$$

and is a (crude) estimate of the signal (power) *spectrum* (Ljung, 1999). Similarly

$$\hat{\hat{\Phi}}_{yu}(\omega) = Y_N(\omega)\overline{U}_N(\omega) \tag{3.48}$$

is an estimate of the *cross spectrum*, where $\overline{(\cdot)}$ denotes complex-conjugate. The periodograms are smoothed (see, for example, Ljung, 1999, pp. 180-183) to get

estimates of the spectrum and cross spectrum, $\hat{\Phi}_u(\omega)$ and $\hat{\Phi}_{yu}(\omega)$, which are used in the *spectral analysis (SPA)* to form an estimate like

$$\hat{G}_N(e^{i\omega T}) = \frac{\hat{\Phi}_{yu}(\omega)}{\hat{\Phi}_u(\omega)} \tag{3.49}$$

The Multivariable Frequency Response Function Estimate (MFRFE)

For multivariable systems, nonparametric estimation methods are not that common. The identification method that will be described here can be seen as a generalization of the ETFE to multivariable systems and is described in for example Guillaume et al. (1996). In the sequel, the estimate will be called the multivariable frequency response function estimate (MFRFE).

Let $U_N(\omega_k)$ and $Y_N(\omega_k)$ be the DFTs of the sampled signals, where $\omega_k = k\frac{2\pi}{NT}$, $k = 1, 2, \ldots, N$. If the sampled signals are periodic, the following linear relation will hold exactly

$$Y_N(\omega_k) = G(e^{i\omega_k T})U_N(\omega_k) \tag{3.50}$$

where $G(e^{i\omega_k T}) \in \mathbb{C}^{p\times m}$ is the MFRF. Note that if the sampled signals are not periodic, the DFT will introduce leakage errors due to the limited time window and (3.50) will no longer hold exactly (see Pintelon and Schoukens, 2001b, Sec. 2.2.2). This is the main reason why only periodic excitation is considered.

To be able to extract $G(\omega_k)$ from data, at least m different experiments are needed. The data vectors from the different experiments can then be collected into matrices (bold face in the sequel) where each column corresponds to one experiment. The relation between the input and output can then be written as

$$\mathbf{Y}_N(\omega_k) = G(e^{i\omega_k T})\mathbf{U}_N(\omega_k) \tag{3.51}$$

where $\mathbf{U}_N(\omega_k) \in \mathbb{C}^{m\times m}$ and $\mathbf{Y}_N(\omega_k) \in \mathbb{C}^{p\times m}$. If $\mathbf{U}_N(\omega_k)$ has full rank, an estimate of $G(\omega_k)$ can be formed as

$$\hat{G}_N(e^{i\omega_k T}) = \mathbf{Y}_N(\omega_k)\mathbf{U}_N^{-1}(\omega_k) \tag{3.52}$$

Note that the full rank condition of $\mathbf{U}_N(\omega_k)$ puts restrictions on the excitation signals. See Guillaume et al. (1996) for some examples. Chapter 6 will also deal with problem when selecting the reference signal for closed-loop identification. If more than m experiments are carried out, $\mathbf{U}_N(\omega_k)^{-1}$ can be replaced by the pseudo-inverse.

When the measurements are corrupted by disturbances, the relation (3.51) will no longer hold exactly. The estimator (3.52) can still be used, but the estimate will contain errors due to the disturbances. For an analysis of the errors, see Chapter 6. To reduce the variance of the estimate, averaged versions of $\mathbf{Y}_N(\omega_k)$ and $\mathbf{U}_N(\omega_k)$

can be used like

$$\hat{G}_{N,M}(e^{i\omega_k T}) = \hat{\mathbf{Y}}_{N,M}(\omega_k)\hat{\mathbf{U}}^{-1}_{N,M}(\omega_k) = \\ = \left(\frac{1}{M}\sum_{i=1}^{M}\mathbf{Y}_N^{[i]}(\omega_k)\right)\left(\frac{1}{M}\sum_{i=1}^{M}\mathbf{U}_N^{[i]}(\omega_k)\right)^{-1} \tag{3.53}$$

where $\mathbf{U}_N^{[i]}(\omega_k)$ and $\mathbf{Y}_N^{[i]}(\omega_k)$, $i = 1, 2, \ldots, M$ are the DFTs of M synchronized input/output records (for example different periods in a periodic data set). It is, of course, also possible to smooth the estimate similar to (3.46).

3.5 Model Validation

The estimation procedure will give the "best" model within the chosen model structure. The problem of model validation is to decide whether the "best" model is "good enough". In Ljung (1999), three aspects of the problem is listed:

1. Does the model agree sufficiently well with the observed data?
2. Is the model good enough for my purpose?
3. Does the model describe the "true system"?

To answer these questions, one should confront the model with as much information about the true system as is practical. This includes a priori information, measurement data, and using the model. The last question is intriguing, but actually Question 2 is the one that matters in practice. Ljung (1999, Ch. 16) lists a number of tools for model validation. One useful tool is *residual analysis*, which involves an analysis of the prediction errors (also called model residuals). For physically parameterized models, the estimated parameters can also be compared with what is reasonable values from a priori knowledge. An important validation tool is to evaluate the model's input-output behavior. For example, this can be done by comparing model estimates in a Bode plot (both spectral analysis and parametric models). The model's ability to reproduce the input-output data in terms of simulations and predictions is also an important tool. This is often measured using the *model fit*, defined in Ljung (1999) as

$$\text{fit} = 100\left(1 - \frac{\sqrt{\sum_{t=1}^{N}(y(t) - \hat{y}(t))^2}}{\sqrt{\sum_{t=1}^{N}(y(t) - \bar{y})^2}}\right) \tag{3.54}$$

where $y(t)$ is the measured output, $\hat{y}(t)$ is the predicted (simulated) output and $\bar{y}$ is the mean value of the measured output.

Cross validation is another important point during model validation, which means that the model should be evaluated on fresh data sets. It is not so impressing that a model can reproduce the data used for the model estimation. Using fresh data is a much harder test and passing such a test gives confidence in the estimated model.

3.6 Closed-loop Identification

It is sometimes necessary to perform identification experiments under the presence of output feedback, *i.e.* in closed loop. The reason may be an unstable plant, or that it is has to be controlled for production, economic, or safety reasons. Consider a closed-loop system

$$y(t) = G_0(q)u(t) + v(t) \tag{3.55}$$
$$u(t) = r(t) - F_y(q)y(t) \tag{3.56}$$

where $F_y(q)$ denotes the controller and $G_0(q)$ is the true system. In this setting, typically $r(t)$ is considered the excitation signal. Depending on whether $r(t)$ is known or not, different identification methods can be used.

A problem with closed-loop data is that many of the identification methods that work well in open loop, fail when applied directly to closed-loop data. The reason is that there will be a nonzero correlation between the input signal and the disturbance in the measured output signal. This is, for example, the case for the nonparametric methods mentioned in Section 3.4.3. Prediction error methods works fine as long as the true system can be described by the model and the data is informative enough (see, for example, Chapter 5 for some notes regarding informative data). Another problem with closed-loop data is that the data set typically contains less information about the open-loop system.

A common classification of closed-loop identification methods are *direct*, *indirect*, and *joint input-output* methods. In the direct approach, the identification method is directly applied to the measured input-output data without any assumptions on how the data was generated. Indirect methods assume that the controller is known and the idea is to first estimate the closed-loop system from the reference signal to the output signal. Using the known controller, the open-loop system can then be calculated. Joint input-output methods estimate the controller and the open-loop system by considering the input and output jointly as outputs from an augmented system driven by the reference signal. The controller must then be parameterized as well. A drawback for the last two approaches is that the controller must be linear in order to use linear models for the estimate of the closed loop system and the augmented system, respectively.

As was previously mentioned, the direct approach gives problems for many identification methods, with prediction error methods as one exception. The estimates will typically get biased and the bias depends on the properties of the feedback as well as the signal-to-noise ratio. Bias and variance expressions will be given in Section 3.7 both for open-loop and closed-loop data. The indirect and joint input-output approaches convert the closed-loop problem to an open-loop one, where the reference signal plays the role of an input. Since the reference signal is uncorrelated with the output disturbance, these approaches can be used together with all the open-loop methods.

For a detailed treatment of the subject, the interested reader is referred to, for example, Ljung (1999), Forssell (1999), and Forssell and Ljung (1999).

3.7 Bias and Variance

The model quality is often measured by the statistical concepts *bias* and *variance*. Bias can be defined as the (average) difference between the true system and the estimated model, whereas variance is a measure of how much the estimate will vary between different measurements (noise realizations).

The bias term is mostly affected by the model set. Small bias is obtained for large, flexible model sets, and/or for model sets that are well-adapted to the given system.

Consider a true system given by

$$y(t) = G_0(q)u(t) + v(t) = G_0(q)u(t) + H_0(q)e(t) \tag{3.57}$$

where $u(t)$, for an open-loop system, is considered the excitation signal. For a closed-loop system, the input is selected like

$$u(t) = r(t) - F_y(q)y(t) \tag{3.58}$$

where $F_y(q)$ is the controller and $r(t)$ is the reference signal. Note that by setting $F_y = 0$ gives us the open-loop case where $u(t) = r(t)$. The input spectrum $\Phi_u(\omega)$ can be written as

$$\Phi_u(\omega) = \underbrace{|S_0(e^{i\omega T})|^2\Phi_r(\omega)}_{\Phi_u^r(\omega)} + \underbrace{|F_y(e^{i\omega T})|^2|S_0(e^{i\omega T})|^2\Phi_v(\omega)}_{\Phi_u^e(\omega)} \tag{3.59}$$

where $\Phi_v(\omega)$ is the noise spectrum, $\Phi_r(\omega)$ is the spectrum of the reference signal and $S_0(q) = (1 + F_y(q)G_0(q))^{-1}$ is the sensitivity function. $\Phi_u^r(\omega)$ is the part of the input spectrum originating from the reference signal and $\Phi_u^e(\omega)$ is the part originating from the output noise (due to output feedback). For open-loop data, $\Phi_u^e(\omega) = 0$.

It is outside the scope of this thesis to present bias and variance expressions for all methods presented in Section 3.4. However, to get a feeling for the problem, one prediction error method and the nonparametric ETFE will be considered.

3.7.1 Parametric Methods

Assume now that we want to identify a model of (3.57) using a prediction error method with the model

$$y(t) = G(q,\theta)u(t) + H(q,\theta)e(t) \tag{3.60}$$

For a fixed noise model $H(q,\theta) = H_*(q)$ the limiting model G_* ($N \to \infty$) is, according to (13.53) in Ljung (1999),

$$G_* = \arg\min_G \int_{-\pi/T}^{\pi/T} \left|G_0(e^{i\omega T}) + B(e^{i\omega T}) - G(e^{i\omega T},\theta)\right|^2 \frac{\Phi_u(\omega)}{|H_*(e^{i\omega T})|^2} d\omega \tag{3.61}$$

$$|B(e^{i\omega T})|^2 = \frac{\lambda_0}{\Phi_u(\omega)} \cdot \frac{\Phi_u^e(\omega)}{\Phi_u(\omega)} \cdot |H_0(e^{i\omega T}) - H_*(e^{i\omega T})|^2 \tag{3.62}$$

where $\lambda_0 = \mathrm{E}e^2(t)$ is the noise variance. The bias term B will be small in frequency ranges where either (or all) of the following holds

- The noise model is good ($H_0 - H_*$ is small)
- The feedback contribution to the input spectrum (Φ_u^e/Φ_u) is small
- The signal to noise ratio is good (λ_0/Φ_u is small)

The variance of the estimated transfer function $\hat{G}_N$ can be obtained from asymptotic black-box theory (order of both G and H tend to infinity, as well as N) like

$$\operatorname{Cov} \hat{G}_N = \frac{n}{N} \frac{\Phi_v(\omega)}{\Phi_u^r(\omega)} \tag{3.63}$$

(see Ljung, 1999, Eq. (13.55)). The noise-to-signal ratio determines how well the transfer function is estimated. The variance is also increased if more parameters n are used, which highlights the trade-off between bias and variance (the bias is typically reduced if more parameters are used). Note that it is only the part of the input spectrum originating from the reference signal that will reduce the variance.

Prediction error methods will give consistent estimates, even for closed-loop data, given that the true system can be described in the model set and that the data is informative enough. In particular, it is important to have a flexible noise model to reduce bias effects.

3.7.2 Nonparametric Methods

As an example of a nonparametric method, we will consider the ETFE. For open-loop data, we have (Ljung, 1999)

$$\mathrm{E}\hat{\hat{G}}_N(e^{i\omega T}) = G_0(e^{i\omega T}) + \frac{\rho_1(N)}{U_N(\omega)} \tag{3.64}$$

$$\operatorname{Cov} \hat{\hat{G}}_N(e^{i\omega T}) = \frac{1}{|U_N(\omega)|^2}(\Phi_v(\omega) + \rho_2(N)) \tag{3.65}$$

where $\rho_1 \leq C_1/\sqrt{N}$ and $\rho_2 \leq C_2/N$ for some constants C_1 and C_2. The properties of the ETFE highly depends on whether the data is periodic or not. If the data is periodic, $C_1 = 0$ and $|U_N(\omega)|^2$ increases like const $\cdot\, N$ for the excited frequencies. This gives an unbiased ETFE and the variance variance decays like $1/N$. If the data is nonperiodic, the ETFE will be asymptotically unbiased and the variance will be equal to the noise-to-signal ratio. In that case, the ETFE is a very crude estimate.

Nonparametric estimation methods usually works under the assumption that the input $u(t)$ is uncorrelated with the output disturbance $v(t)$. This is no longer true for closed-loop data and therefore the estimates usually are biased. The estimates using ETFE or SPA tend to (Ljung, 1999, p. 191)

$$\hat{G}(e^{i\omega T}) = \frac{G_0(e^{i\omega T})\Phi_r(\omega) - F_y(e^{-i\omega T})\Phi_v(\omega)}{\Phi_r(\omega) + |F_y(e^{i\omega T})|^2\Phi_v(\omega)} \tag{3.66}$$

as the number of data goes to infinity and where Φ_r and Φ_v denote the spectrum of $r(t)$ and $v(t)$. If there is no noise in the system, the estimate will tend to the true system. For systems with a large signal-to-noise ratio, the bias can also be negligible. If, on the other hand, the noise dominates over the reference signal, the estimate will tend to the inverse of the controller.

4

System Identification in Robotics

There are many available system identification methods, and the techniques of system identification have a wide application area. Therefore, one might ask the question: *Why dedicate a chapter for the topic of system identification in robotics*? The robot application is associated with many challenging problems for system identification methods, such as a multivariable nonlinear system, closed loop identification (to stay centered around the operating point), oscillatory behavior, (deterministic) disturbances, and nonlinearities such as, *e.g.*, friction and backlash. In addition, the robot dynamics can be modeled quite accurately using known mechanical relations, as was pointed out in Chapter 2. These dynamic equations have particular features that can be exploited by the identification method.

Since identification in robotics is a much studied problem, the purpose of this chapter is to give an overview of earlier results related to the identification of kinematics, rigid body dynamics, flexibilities and nonlinearities.

4.1 Introduction

System identification in robotics can be divided into, at least, three different levels or application areas (see, for example, Albu-Schäffer and Hirzinger, 2001). These levels involve the estimation of the

- kinematic description of the robot (including elastostatic effects)
- dynamic model of the robot, often divided into
  - rigid body dynamics, and

  - flexible body dynamics

- joint model

The robot kinematics can, for example, be described by the DH-parameters, giving four parameters for each link to estimate. The rigid body dynamics are described by the center of mass, mass, and inertia matrix for each link. By flexible body dynamics, we here mean elastic effects in the robot structure, for example in the links. The joint model involves motor inertia, gearbox elasticity and damping, backlash, motor characteristics, and friction parameters. In addition to these three levels, one can also consider the estimation of load dynamics (Kozlowski, 1998, Ch. 6) and adaptive control (Ortega and Spong, 1989) as parts of the system identification problem. Another important area left out in this chapter is the identification of sensor and actuator disturbances (Jahns and Soong, 1996). These disturbances were briefly described in Section 2.3.3.

Nominal parameter values for the kinematics and rigid body dynamics can often be obtained from CAD models on the basis of their geometry and type of material. These values are often not accurate enough, due to simplifications in the modeling and complex dynamic effects, such as joint friction, that cannot be sufficiently modeled. To obtain high accuracy, these parameters must be tuned by the use of experimental data. Some parts of the joint model, like the motor characteristics, can be measured before assembly whereas things like friction depends on the assembly, and therefore must be estimated after assembly.

In a majority of the literature on robot identification (see, for example, Kozlowski (1998) and the references in this chapter), a rigid body model is assumed and flexibilities, if any, are assumed to be located at the joint level. This can partly be explained by a previous use of fairly rigid robots. The assumption has also been verified, for example by using modal analysis (Behi and Tesar, 1991). With the increasing use of new mechanical structures (bend-over-backwards capability, non-symmetric structure, lightweight robots) and new applications in industry where higher performance is demanded with respect to position accuracy and speed, elastic effects become even more evident and must be dealt with. Therefore, finding procedures for the identification of flexibilities is important.

In Section 4.2, the identification of kinematics will be briefly described. Section 4.3 gives an overview of rigid body identification. Finally, identification of (joint) flexibilities and nonlinearities is covered in Section 4.4.

4.2 Kinematics

The kinematic parameters describe the geometric relation between joint variables and the end effector location (position and orientation). These parameters also define the inverse kinematics (see Section 2.3.1), which is used during the path planning (see Section 2.4.1) to transform a Cartesian path to a corresponding path in joint space. The quality of this mapping will determine the robot's accuracy and it is therefore crucial to have a correct kinematic description. The identification of

kinematic parameters is also called *kinematic calibration* or *robot calibration* and many different techniques exist, see Hollerbach (1989) for a survey.

However, the general idea is to consider the forward kinematics (2.1) of the robot and perform a first order Taylor expansion of the location X with respect to the kinematic parameters θ like

$$\Delta X = \frac{\partial f(\varphi, \theta)}{\partial \theta} \Delta\theta \tag{4.1}$$

where $\Delta X = X - f(\varphi, \theta_0)$ is the deviation in end effector location from the predicted location and $\Delta\theta = \theta - \theta_0$ is the corresponding parameter deviation from the nominal value θ_0. The matrix $\frac{\partial f(\varphi,\theta)}{\partial \theta}$ should be evaluated for $\theta = \theta_0$. This system of equations can be solved in a least-squares sense for $\Delta\theta$ by considering a number of locations (see corresponding solution below in (4.4) and (4.5)). In addition to the robot link parameters (for example DH parameters), θ should include additional parameters describing, for example, elastostatic effects (deflection due to gravity) and the mounting of the robot base and the end effector.

To be able to calculate the deviation ΔX, measurements of the end effector location X are needed. These measurements can be either relative or absolute. Examples of relative measurements could be to approach the same point from different directions or measuring an object with known geometry (but unknown absolute position). Zhong et al. (1996) suggest the use of a trigger probe as end effector to touch constraint planes in the workspace (the location of the planes are not necessarily known exactly). Using relative measurements, many of the kinematic error parameters $\Delta\theta$ can be estimated. For absolute measurements, two main routes can be seen. The first one uses some mechanical apparatus that allows constraining the end effector at given locations with a priori known precision. The second route uses direct measurement systems of the end effector location in the Cartesian space, for example using a laser tracking system. This is the kind of system used in Abderrahim and Whittaker (2000), where the Denavit-Hartenberg parameters are estimated by combining measurements of the end-effector caused by movements of each joint, one at a time. See also Khalil and Besnard (2002) for a treatment of elastostatic effects due to joint and link flexibilities.

4.3 Rigid Body Dynamics

The identification of rigid body dynamics is based either on the robot dynamic model (2.9), also called the *differential model*[1]

$$H(\varphi, \dot{\varphi}, \ddot{\varphi})\theta = \tau \tag{4.2}$$

or the energy (difference) model (2.10), also called the *integral model*

$$\Delta h(\varphi, \dot{\varphi})\theta = \Delta\mathcal{H} = \mathcal{H}(t_b) - \mathcal{H}(t_a) = \int_{t_a}^{t_b} \tau^T \dot{\varphi} dt \tag{4.3}$$

[1]The names *differential model* and *integral model* are according to Kozlowski (1998).

where $\theta \in \mathbb{R}^{10n}$ is the parameter vector and n is the number of links. The two models are both linear in the parameters, which are the same in the two models. The integral model (4.3) consists of only one equation, compared to the n equations in the differential model (4.2). The differential model is, in that respect, richer in information than the integral model. An advantage with the integral model is that the joint acceleration $\ddot{\varphi}$ is not needed. For easier treatment, only the differential model will be considered from now on. See, for example, Gautier and Khalil (1988) and Kozlowski (1998) for treatments of both the differential and integral models.

Traditionally, flexibilities are ignored during the identification of rigid body dynamics, which is motivated by the use of low-frequency trajectories that do not excite flexibilities. The identification of rigid body dynamics is usually combined with the identification of a (simple) friction model in order to reduce bias in the estimated parameters.

The model representation (4.2) is redundant, *i.e.*, there are infinitely many parameter values that give the same dynamic model. For a particular robot, a number of the parameters are zero or linearly dependent, and all parameters are therefore not identifiable. To find the minimum number of parameters, called *base parameters*, that characterize the dynamic model, different approaches can be found in the literature. The most basic distinction is if the problem is solved using a numerical or analytical method.

Consider now N samples of data, $\{\varphi(t_i), \dot{\varphi}(t_i), \ddot{\varphi}(t_i), \tau(t_i)\}, i = 1, 2, \ldots, N$, which are related according to (4.2) like

$$\underbrace{\begin{pmatrix} H(\varphi(t_1), \dot{\varphi}(t_1), \ddot{\varphi}(t_1)) \\ H(\varphi(t_2), \dot{\varphi}(t_2), \ddot{\varphi}(t_2)) \\ \cdots \\ H(\varphi(t_N), \dot{\varphi}(t_N), \ddot{\varphi}(t_N)) \end{pmatrix}}_{\Phi} \theta = \underbrace{\begin{pmatrix} \tau(t_1) \\ \tau(t_2) \\ \cdots \\ \tau(t_N) \end{pmatrix}}_{Y} \tag{4.4}$$

Numerical methods are mainly based on QR or SVD factorizations of the regressor matrix Φ. The sequence $\{\varphi(t_i), \dot{\varphi}(t_i), \ddot{\varphi}(t_i)\}, i = 1, 2, \ldots, N$, should then be sufficiently rich so that all parameters are excited. One option is to use random numbers for $\varphi(t_i)$, $\dot{\varphi}(t_i)$, and $\ddot{\varphi}(t_i)$. See, for example, Gautier (1990) and Sheu and Walker (1989) for details and Pfeiffer and Hölzl (1995) for an example. Many analytical methods have also been proposed, based on symbolical manipulations of the model equations. For closed form solutions, see for example, Mayeda et al. (1990) and Gautier and Khalil (1990).

Having a minimal parameter-linear description $H_b\theta_b = \tau$, measurements from a large number of time instants are needed to avoid an ill-conditioned regressor matrix Φ_b (similar to (4.4)). Both joint position and velocity can be measured, but it is common to only measure joint position. If the robot dynamic model (4.2) is used, joint acceleration (and velocity) must be reconstructed. Since the identification is done off-line, the reconstruction is typically done using anti-causal filters (no phase shift) and central difference algorithms. The joint torques can, in rare cases of torque sensors at the joints, be measured directly. Otherwise they

can, for example, be estimated from current measurements in the case of electric actuators.

To obtain the measurements, the robot is moved along a trajectory and joint motion and torque are measured. Finally the base parameters can be estimated, for example, by a *weighted least squares (WLS)* method like

$$\hat{\theta}_b = \arg\min_{\theta_b} \frac{1}{2}(Y - \Phi_b\theta_b)^T W(Y - \Phi_b\theta_b) = (\Phi_b^T W \Phi_b)^{-1}\Phi_b^T WY \tag{4.5}$$

where many different weighting matrices W occur in the literature, see Gautier and Poignet (2001); Swevers et al. (1997) for examples. Other estimation methods are for example treated in Gautier and Poignet (2001), which contains a comparison between WLS and the extended Kalman filter. In Gautier et al. (1994), total least squares estimation is used and Presse and Gautier (1993) use Bayesian estimation techniques.

To make the parameter estimation problem (4.5) well conditioned, the excitation trajectory is often generated using an optimization scheme to obtain maximum excitation of all base parameters. This involves nonlinear optimization with motion constraints on joint positions, velocities, and accelerations. Different optimization criteria exists, for example to minimize the condition number of Φ_b (Pfeiffer and Hölzl, 1995; Gautier and Khalil, 1991) or $-\log\det(\Phi_b^T W \Phi_b)$ (Swevers et al., 1997). Often, a scaled version of the matrix Φ_b is used in the criterion to obtain parameter estimates with approximately the same relative accuracy. The matrix is scaled like $\bar{\Phi}_b = \Phi_b \operatorname{diag}(\bar{\theta}_b)$ where $\bar{\theta}_b$ contains a priori known parameter values.

For the optimization, the excitation trajectory must be parameterized, which can be done in many different ways. The most general one is perhaps Armstrong (1989), where the optimization variables are a sequence of joint accelerations. Gautier and Khalil (1991) use a sequence of joint positions and velocities as variables. Afterwards, a continuous trajectory is obtained by interpolating a 5th order polynomial between these points, assuming zero initial and final acceleration. A problem is to be sure that the resulting trajectory fulfills all constraints and also there is no guarantee of optimality. In Swevers et al. (1997), the trajectory is parameterized as a finite Fourier series, and the optimization variables are then the coefficients in this series. Pfeiffer and Hölzl (1995) instead optimize the trajectory such that the trajectory always follows the steepest descent of the optimization criterion (time is discretized).

Grotjahn et al. (2001) suggest that the base parameters are divided into three groups; gravitational parameters θ_g, diagonal parameters θ_{Md}, and off-diagonal parameters θ_{Mod}. Equation (4.2) is then rewritten like

$$\underbrace{H_{Md}(\varphi,\ddot{\varphi})\theta_{Md} + H_{Mod}(\varphi,\ddot{\varphi})\theta_{Mod} + H_{Mg}(\varphi,\ddot{\varphi})\theta_g}_{M(\varphi)\ddot{\varphi}} + \underbrace{H_c(\varphi,\dot{\varphi})\theta}_{C(\varphi,\dot{\varphi})\dot{\varphi}} + \underbrace{H_g(\varphi)\theta_g}_{g(\varphi)} = \tau \tag{4.6}$$

where references to (2.6) are shown as well. The parameter groups are identified one at a time by simple trajectories with trapezoidal velocity profile and a weighted least-squares method. The method has been successfully applied to the 6 DOF

industrial robot manutec-r15. Grotjahn et al. claim that they do not require a priori identification of the friction model, but assumes symmetric friction during the estimation of gravitational parameters and a friction model is identified later during the identification of θ_{Md}. A drawback might be that in their example, they needed measurements from 165 configurations with a total duration of about 45 min.

A different approach is taken in Chenut et al. (2000) where additional sensors are used to improve the parameter estimates. They present a parameter estimation scheme where internal and external measurements are combined. Internal refers to the previously used joint motion and joint torque measurements and external refers to torque/force measurements of the base platform. The method is illustrated in simulations and yields improved parameter estimates.

4.4 Flexibilities and Nonlinearities

As was mentioned in Section 2.3.2, there are various sources of flexibility in an industrial robot, such as elastic deformation of bearings and gears and deflection of the links under load. For many robots, particularly those using harmonic drives for the torque transmission, the joint flexibility is dominant. A two-mass model like (2.11) is then often sufficient to describe the dynamics (or coupled two-mass models for multivariable cases). As was pointed out in Section 2.3.2, a trend is to build weaker robot arms which also introduces significant flexibilities in the links and their connections. Therefore higher order models are sometimes needed in order to get a sufficiently accurate description of the system.

Identification of flexibilities is more involved than the identification of rigid body dynamics. The main reason is that now typically only a subset of the state variables are measured and one can therefore not use linear regression. This could of course be solved by adding sensors (Pfeiffer and Hölzl, 1995; Albu-Schäffer and Hirzinger, 2001). A problem is that this solution is expensive and the experiments quite involved. For a standard industrial robot where the price is constantly reduced, this solution is probably not applicable. Also, as was mentioned in the problem statement in Section 1.1, the final goal for our robot identification is to find procedures for automated tuning of flexible model structures with a minimum number of additional sensors.

In addition to flexibilities nonlinear effects like friction and backlash have to be taken into account during the identification of the joint model. These effects will significantly influence the identification of the dynamics if not properly handled. Backlash and Coulomb friction will in general reduce the notch and peak frequencies in transfer function estimates and the Coulomb friction will in addition reduce the amplitude for low frequencies (Aberger, 2000). In addition, nonlinearities can have major effects on the system operation, for example when the rotation changes direction, and accurate models describing these phenomena are therefore of importance.

The research on modeling and control of friction has come quite far, see for

example the survey article Armstrong-Hélouvry et al. (1994). However, a problem is to be able to identify all unknown parameters in these complex friction models. Hence, the traditional model with the three components; viscous, Coulomb and static friction, is still often used. This model describes the stationary velocity-force relation fairly well, whereas important dynamic effects are completely missed. For control purposes and analysis of stick-slip, limit-cycles, *etc.*, a better friction model is often needed. A fairly simple dynamic model for friction that captures most of the friction behavior is presented in Canudas de Wit et al. (1995) and is often called the LuGre model. This includes the Stribeck effect, hysteresis, spring-like characteristics for stiction, and varying break-away force. Still, most of the friction models considered in the literature on identification in robotics are fairly simple. One reason might be that the model is sufficient during the identification of the rigid body dynamics, even though there are already some results on biased estimates due to a too simple friction model (Grotjahn et al., 2001). Another reason might be lack of measurements or that many friction problems are solved by better hardware (for example, lubricants). From now, when talking about friction, we mean more than just viscous friction, which give minor difficulties during identification and can be described by a linear model.

Backlash in mechanical systems is, for example, described in the survey article Nordin and Gutman (2002), where they use the definition: "the play between adjacent movable parts (as in a series of gears)". The width of the backlash is the most essential parameter. This width can experimentally be determined only by additional position sensors. Controlled systems with backlash often exhibit steady-state errors or, even worse, limit cycles whereby the system oscillates.

There is a vast amount of literature available concerning the identification of joint parameters, strongly differing in both the model's level of detail and identification methods. The identification is done in time domain or frequency domain, based on physical or unstructured models, using linear or nonlinear optimization techniques. There are also major differences in how the nonlinearities are handled. Some estimate friction separately in a first step, and then in a second step estimate the joint dynamics. In this second step, they either compensate for the estimated friction, or use special excitation that will give minor frictional contribution. Using this route, linear identification methods can be applied. The other route is to use a nonlinear model structure describing the joint dynamics as well as friction and other nonlinearities.

In Pham et al. (2001) the estimation of physical parameters in a two-mass flexible model is treated through a least-squares technique similar to the one used in the estimation of rigid body dynamics. The linear-in-parameters formulation with only motor measurements is obtained through a nonlinear transformation and certain approximations that are justified by using a special trajectory that do not excite certain parameters. The identification experiments are carried out by moving one axis at a time.

In Östring et al. (2003), a method is applied where a gray-box model describing both inertial parameters and flexibilities can be identified directly in the time domain. This is done by utilizing a user-defined model structure in the System

Identification Toolbox (SITB) and experimental data from closed-loop experiments for axis 1 of an ABB IRB 1400 robot. Both black-box models and physically parameterized models are identified. Östring et al. suggest that a 3-mass model is sufficient to describe the dynamics. See also Nissing and Polzer (2000), where the identification of a physically parameterized two-mass model in state space form is treated. The three unknown physical parameters are estimated by using an iterative Gauss-Newton method. The experimental data comes from an 1 DOF hydraulic flexible arm.

In Berglund and Hovland (2000), a general method is described for the identification of masses, springs and dampers. The identification is based on an estimated Frequency Response Function (FRF) in combination with the solution of an inverse eigenvalue problem. See also Hovland et al. (2001) for an extension to systems containing coupled inertia terms, which is the case for multivariable systems. Another frequency-domain method is used in Khorrami et al. (1995), where recursive estimation of a two-mass model (for each joint) is treated. The parameters are estimated in the frequency domain using the ETFE or a time-varying version of the ETFE. The model is used for input pre-shaping (for example a notch filter for the reference signal).

In Johansson et al. (2000) they apply and evaluate different subspace identification methods (N4SID and MOESP) for identification of axis 1 and 4 of an ABB IRB 2000 robot. They suggest the use of the MOESP algorithm for the identification of a black-box state-space model combined with a friction model.

Black-box identification is also treated in Ferretti et al. (1994b), where a 6 DOF industrial robot is considered. A third order black-box transfer function is estimated for each joint. The excitation signal, applied as velocity reference for the controller, is a constant (to avoid effects of static friction) plus white noise. To eliminate, or at least minimize, the dynamic coupling among the links, different configurations are used for the identification of each joint dynamics. This is done by using a CAD model and symbolic manipulations of the robot dynamic equations. They also compute a physically parameterized expression of the transfer functions obtained from symbolic manipulations of the dynamic equations. They outline that a comparison of the estimated and physically parameterized transfer functions yields a system of nonlinear equations which could be solved for the physical parameters. No physical parameters are presented, but a similar procedure is used in Isaksson et al. (2003) for the estimation of initial values.

As was previously mentioned, there are some solutions where additional sensors are used for the identification. In Pfeiffer and Hölzl (1995), the joint parameters (stiffness, damping, and motor inertia) are estimated by fixation of the links. Between each link and link fixation a force sensor is applied. A slightly different procedure is used in Ferretti et al. (1994a), where joint stiffness is estimated by constraining the robot end effector and using a force sensor to measure the constraint forces. Another method, requiring additional sensors, is *experimental modal analysis*. It is a widespread method in the mechanical engineering society used to determine a structure's dynamic characteristics; namely, resonant frequencies, damping values, and the associated pattern of structural deformation called mode

shapes. Parametric identification using experimental modal analysis is, for example, treated in Behi and Tesar (1991). Using accelerometers in 11 points and an impact hammer, transfer functions are estimated and modal parameters and mode shapes are obtained by curve fitting the system transfer functions. The oscillation of the system is produced by the deformations of the shoulder and elbow joints (joints 2 and 3) about their axes of rotation and the deflection of the base plate relative to the foundation (giving two DOF). Therefore, four spring-damper pairs are used and springs, dampers and masses are then derived from the estimated modal matrix. See also Avitabile (2001) for a good introduction to modal analysis.

For the identification of nonlinearities such as friction and backlash, a number of references could be given. One interesting method is presented in Chen et al. (2002) which is based on open loop experiments with binary input signals. By using the difference of the input-output signals from two experiments with different magnitudes, the friction can be ignored while doing the identification of the linear system. In a second step, the friction is estimated using the dc level of the linear system and a constant input. Isaksson et al. (2003) consider gray-box identification of a two-mass model with backlash, where black-box modeling is used to find initial parameter values. See also Hovland et al. (2002) for estimation of backlash and spring stiffness using an extended Kalman filter (EKF). Identification of backlash and friction is also treated in Angerer et al. (2004) and Kara and Eker (2004). In Chapter 9 of this thesis, nonlinear gray-box identification will also be treated, using a model that includes Coulomb friction and nonlinear spring stiffness.

5

Experiment Design

The design of an identification experiment includes several choices, like where and what to measure, when to measure the signals, what signals to manipulate and how to manipulate them in an optimal way. Obviously, this cannot be treated in depth here, but still some comments will be made. The material is mainly based on Ljung (1999); Pintelon and Schoukens (2001b). The interested reader is therefore referred to these books and the references therein.

5.1 Introduction

For a complex process, questions like *where* and *what* to measure must be answered. It might not even be obvious what are the input and output signals. When these things have been cleared out, another question is *when* to measure. This typically involves what sampling time T to use in the sampling process. For a successful sampling, also presampling filters should be considered to avoid alias effects (Ljung, 1999, Sec. 13.7). The optimal sampling time depends both on the system and what kind of models/methods to use. It is usually no problem to sample (too) fast during the data acquisition. However, when estimating a parametric discrete-time model, very small sampling times (compared to the natural time constants of the system) might lead to numerical problems and model fits in high-frequency bands. This can often be solved by decimating the data before the estimation. A too large sampling time, on the other hand, will lead to very bad results. An advice is to use a sampling frequency about ten times the bandwidth of the system. Related to this choice is also the number of data points, N, which often will determine the variance in the estimates as will be described below.

The choice of input signals has a very substantial influence on the observed data, and therefore also on the estimated models. This choice will determine the operating point of the system and which parts and modes of the system that will be excited. A general advice here is to let the experiment condition resemble the situation for which the model is going to be used.

There are two different aspects often associated with the choice of input $u(t)$; the second-order properties, like its spectrum $\Phi_u(\omega)$ (and cross spectrum $\Phi_{ue}(\omega)$ in the case of output feedback), and the "shape" of the signal. For a linear system, asymptotically only the spectrum will have effect. For a limited number of data, and especially for a nonlinear system, the signal shape will have influence as well. Both these properties will be treated. First, however, we will introduce the concept of informative experiments.

5.2 Informative Experiments

Informative experiments relates to the concept of informative data sets (see Definitions 8.1 and 8.2 in Ljung (1999) for details). If a data set is *informative enough* with respect to a model set, we can discriminate between different models in the set. An informative data set can discriminate between all LTI models. A related concept regarding the input signal is *persistently exciting (of order n)* (see Ljung, 1999, Definition 13.1), which relates to the number of parameters that can be estimated. A sum of n sinusoids will be persistently exciting of order $2n$, which makes it possible to identify all parameters in an nth order SISO system (numerator and denominator polynomials of order n). The input $u(t)$ is called *persistently exciting* if its spectrum $\Phi_u(\omega) > 0$ for almost all ω. Such a signal will give an *informative* data set in the open loop case.

A problem when talking about optimal excitation signals (with respect to bias and variance in the estimates) is that this often is in conflict with another important property, namely *validation power*. For an nth order system, the optimal signal might be a sum of n sinusoids, but this signal will not be able to reveal if the true system is of a higher order. The signal should therefore be *rich* enough to be able to validate (and invalidate) the estimated models.

For closed loop identification, there are a number of fallacies that must be avoided. First, some identification methods, like for example ordinary spectral analysis, will give erroneous results since the input now is correlated with the output noise. The experiment can also be non-informative even if the input in itself is persistently exciting. The guiding principle is to avoid a too simple controller and use a reference signal which is rich enough for the system (similar to the discussion about the input signal for the open loop case).

5.3 Selection of Power Spectrum

When selecting an excitation signal we should first make sure that the estimated model will be acceptable in terms of bias. When the bias may be significant it is

wise to let the experiment resemble the situation under which the model is going to be used. Once this is achieved, the signal spectrum can be further optimized with respect to variance. What is an optimal spectrum will also depend on the chosen modeling approach. In a nonparametric frequency response estimate, there is no relation between the estimates at different frequencies and the excitation should then be designed to achieve a predefined accuracy in the frequency band of interest (for example maximizing the absolute or relative accuracy). From (3.65) we get that the spectrum

$$\Phi_u(\omega) = \text{const} \cdot \Phi_v(\omega) \tag{5.1}$$

will give about the same absolute accuracy in the estimate. To instead get the same relative accuracy,

$$\Phi_u(\omega) = \text{const} \cdot \frac{\Phi_v(\omega)}{|G_0(e^{i\omega T})|^2} \tag{5.2}$$

could be used. This corresponds to an output spectrum approximately proportional to the noise spectrum.

For the parametric case, loosely speaking, an optimal power spectrum is such that the available power is used at the frequencies where it contributes most to the knowledge of the system. According to Ljung (1999), the parameter covariance matrix P_θ will be

$$P_\theta \sim \lambda_0 \left[\mathrm{E} \left(\frac{d}{d\theta} \hat{y}(t|\theta) \right) \left(\frac{d}{d\theta} \hat{y}(t|\theta) \right)^T \right]^{-1}$$

which shows that interesting parameters must have a clear effect on the output predictions. For the open loop case, we also have the expression

$$\bar{M}(\Phi_u) = \int_{-\pi}^{\pi} \tilde{M}(\omega) \Phi_u(\omega) d\omega + M_e \tag{5.3}$$

$$\tilde{M}(\omega) = \frac{\lambda_0 G_\theta'(e^{i\omega T}, \theta_0)[G_\theta'(e^{i\omega T}, \theta_0)]^T}{2\pi\kappa_0 \Phi_v(\omega)}$$

for the *average information matrix per sample* $\bar{M}(\Phi_u)$ (Ljung, 1999, pp. 416-417). Here G_θ' is the gradient of G with respect to the parameters, κ_0 depends on the selected norm in the criterion, and M_e is a term independent of Φ_u. The information matrix should be large in order to get a small covariance matrix. To achieve this, the input power should be spent at frequencies where $\tilde{M}(\omega)$ is large, that is where the Bode plot is sensitive to parameter variations (G_θ' large). Often a sufficient guidance on where to spend the input power is found by varying the parameters in the model and checking how the Bode plot changes.

A problem is that in many cases the true system (which we want to identify) is needed in order to calculate the optimal input spectrum. In a practical situation, this can be approximately solved by using a two-step procedure where first a preliminary system model is estimated using a flat amplitude spectrum for the

input signal. In a second step, the preliminary system model is used to calculate an optimal input spectrum.

Calculating the optimal input spectrum is quite involved, especially for closed loop experiments, and outside the scope of this thesis. The optimal spectrum will depend on the criterion, limits on the input and output signals, and the true system, including the noise characteristics. See, among many references, Ljung (1999) and Pintelon and Schoukens (2001b).

5.4 Selection of Excitation Signal

Given an (optimal) input spectrum and limitations on the input amplitude and other constraints, we must now select a particular excitation signal that fulfills all the requirements.

For signals that have a specified maximum peak value, it is convenient to use the, so called, *crest factor* (Pintelon and Schoukens, 2001b) as a measure of the signal quality. The crest factor of a signal is given by the ratio of the peak value of the signal to its effective root mean square (rms) value, where *effective* means that only the signal power in the frequency band of interest is used for the rms calculation. The crest factor gives an idea of the compactness of the signal. Signals with an impulsive behavior have a large crest factor and will, for a given peak value, inject much less power into the system than a signal with a small crest factor. Typically, the crest factor will get larger for signals with only a few spectral lines, compared to a flat signal spectrum. The goal could now be rephrased as: *Achieve a desired input spectrum for a signal with as small crest factor as possible.*

One way of achieving a certain spectrum could be to use a stepped sine excitation, consisting of a series of single sine measurements at the specified frequencies. Advanced digital signal processing algorithms (especially the Fast Fourier Transform) have lead to the use of more complex input signals. Instead of exciting the system frequency by frequency, broadband spectrum signals are generated. This gives considerable reduction of measurement time. Many different kinds of signals exist, which can be divided into general purpose signals and optimized signals.

The general purpose signals have a flat amplitude spectrum and a quite low crest factor and can be applied without any optimization. The only parameters to be selected are the bandwidth of the excitation signal and the frequency resolution of the measurement (typically $1/T_0$ for periodic signals with period T_0 and $1/(N \cdot T)$ for nonperiodic signals). Some common choices are swept sine (chirp), Schroeder multisine (sum of sinusoids), pseudo-random binary sequence (PRBS), random noise, random burst, and pulse-impact testing (see Pintelon and Schoukens, 2001b, for details).

Periodic signals have certain advantages which can be used to avoid leakage and reduce variance in nonparametric estimates like, for example, the ETFE. Leakage is also avoided by using burst, or time-limited signals where the whole system response is captured. In this thesis, we will exclusively use periodic signals since most of the results are on nonparametric frequency response estimates. In particular, chirp

and multisine signals will be considered.

A *chirp signal* is a sinusoid with a frequency that changes continuously over a certain frequency band $f_1 \leq f \leq f_2$ like

$$u_0(t) = A\sin(2\pi f_1 t + \pi/T_0(f_2 - f_1)t^2 + \phi) \ , \quad 0 \leq t \leq T_0, \tag{5.4}$$

with amplitude A, and phase ϕ. In order to get a periodic signal, f_1 and f_2 must be a multiple of $f_0 = 1/T_0$. The chirp signal will usually have a crest factor of 1.45, which is about the same as for a single sinusoid which have $\sqrt{2}$.

The *multisine signal* can be written as

$$u_0(t) = \sum_{k=1}^{F} A_k \sin(2\pi f_k t + \phi_k), \tag{5.5}$$

with amplitudes A_k, phases ϕ_k, and frequencies $f_k = l_k f_0 = l_k/T_0$ with $l_k \in \mathbb{N}$. The phases ϕ_k are chosen to get a low crest factor. For the *Schroeder multisine*, the phases are selected according to (Schroeder, 1970)

$$\begin{aligned} &\phi_1 \text{ arbitrary} \\ &\phi_k = \phi_1 - \frac{k(k-1)\pi}{F}, \quad 2 \leq k \leq F \end{aligned}$$

For a flat amplitude spectrum, $A_k = A$, the crest factor typically gets 1.7. The signal is preferably calculated using FFT. The multisine signal is very flexible since the user can specify exactly which frequencies to use. The Schroeder phases are however calculated under the assumption of a flat amplitude spectrum. In other cases, the crest factor can get fairly large. To solve this, we have to look for optimized signals.

In Pintelon and Schoukens (2001b), two different algorithms are proposed for optimizing the crest factor of a multisine signal. Here we will use the iterative optimization procedure described in Van der Ouderaa et al. (1988), which is referred as the clipping algorithm in the literature. The algorithm works as follows:

Algorithm 5.1 (Clipping algorithm)

1. *Start with a given amplitude spectrum and initial phases.*
2. *Combine amplitude and phases.*
3. *Inverse DFT.*
4. *Clip time signal.*
5. *DFT.*
6. *Reset amplitude spectrum to its original value, but keep the new phases.*
7. *Exit if crest factor does not decrease any longer, otherwise continue from step 2.*

The clipping level is changed from a low value in the beginning (*e.g.*, $0.7 \cdot u_{max}$) to almost no clipping in the end (*e.g.*, $0.999 \cdot u_{max}$). Depending on the required crest factor, the algorithm could need a few hundred iterations to several thousands. To further reduce the crest factor, the concept of *snowing* could be used, which means that additional frequencies are added. This will often allow a higher input power at the user specified frequencies to the price of "wasting" some of the total power. See Pintelon and Schoukens (2001b) for details. They also give examples of other optimized signals like, for example, the discrete interval binary sequence, where the switching sequence is optimized to achieve the user specified spectrum.

5.5 Experiment Design in Robotics

The design of experiments in robotics has already been briefly mentioned in Chapter 4 when talking about system identification in robotics. As was pointed out there, the identification is usually divided into kinematics, rigid body dynamics, and flexibilities. The experiment design for each of these stages will now be briefly mentioned.

The experiment design will of course differ depending on the robot structure. Here, the anthropomorphic manipulator will be considered (see Figure 2.1 for an example). For this kind of robot it is necessary to use feedback control while data are collected, both for safety reasons and in order to compensate for gravitational effects[1]. The proposed excitation signals in the literature usually differs depending on where in the robot control system excitation signals can be applied. Using an experimental control system, like in Chapter 7, makes it possible to use any kind of off-line computed reference signals. In other cases, one is restricted to the movements that are possible to program in the commercial robot system, typically point-to-point movements along lines and arcs with a specified velocity and acceleration.

For the kinematic calibration, the experiment design involves the selection of a number of robot configurations. For each of these configurations, the end effector location, X, is measured together with the motor joint angles, φ. Each configuration gives a collection of equations like (4.1). Combining these gives a system of equations similar to (4.4) which can be solved in a least squares sense. The robot configurations could be optimized in order to give a well-conditioned problem.

For rigid body dynamics identification, the excitation signal is a trajectory that should excite the rigid body dynamics and friction parameters without introducing any oscillations due to flexibilities. Therefore a low frequency excitation is preferred. The trajectory is often optimized to give a well-conditioned problem. For the optimization, the excitation trajectory is parameterized, for example as a sequence of joint positions and velocities (Gautier and Khalil, 1991) or as a finite Fourier series (Swevers et al., 1997). See Section 4.3 for details.

[1] The feedback control is actually necessary only for those axes that are affected by gravitation. Axis one could therefore be estimated in open loop.

Identification of flexibilities is quite involved and it is therefore common to estimate local linear flexible models (see Figure 1.2) for a number of different configurations. Combining these estimates with an estimated global nonlinear rigid model might give enough knowledge about the global nonlinear flexible model. For the local model approximation to be valid, the resulting movements of the robot arm should be of fairly low amplitude. Nonlinear effects must also be handled. The influence of static friction can, for example, be reduced by using an excitation signal which avoids zero velocity as much as possible (for example, by using a square wave as velocity reference). Suitable excitation signals for the identification of a local linear flexible model can be obtained using the ideas presented in the previous sections. For example by using a broadband signal in the whole frequency band where notch and peak frequencies in the frequency function are expected. The broadband signal is then superimposed onto the square wave. Excitation signals for flexibilities can be optimized both regarding which configurations to consider and what type of broadband signal to use, including the signal spectrum.

5.6 Dealing with Transients

When applying an input signal to a system, the system response will contain transient effects as well as the system steady state response as will be illustrated by the following example.

Example 5.1 (Transients)
Consider a simple scalar system

$$\dot{y}(t) = y(t) + u(t), \quad y(0) = 0$$

where the input is selected as

$$u(t) = \begin{cases} 0 & \text{if } t < 0 \\ \sin(2\pi t) & \text{if } t \geq 0 \end{cases}$$

The output signal $y(t)$ from this system is plotted in Figure 5.1 for the first five periods of data. As can be seen, the output signal differs quite much from the steady state response (dotted line) for the first periods. In the same figure, the output spectrum is plotted for five periods. In steady state there should only be output power at 1 Hz.

For parametric methods, usually transient effects are handled by estimating the initial conditions of the system using additional parameters (Ljung, 1999; Pintelon and Schoukens, 2001b).

The nonparametric methods mentioned in Section 3.4.3, assume that (3.50) holds in order to avoid errors. This will hold as long as the difference between the initial and final conditions of the system is zero (Pintelon and Schoukens, 2001b, Sec. 5.3.2.2). This is, for example, the case with periodic excitation in steady state

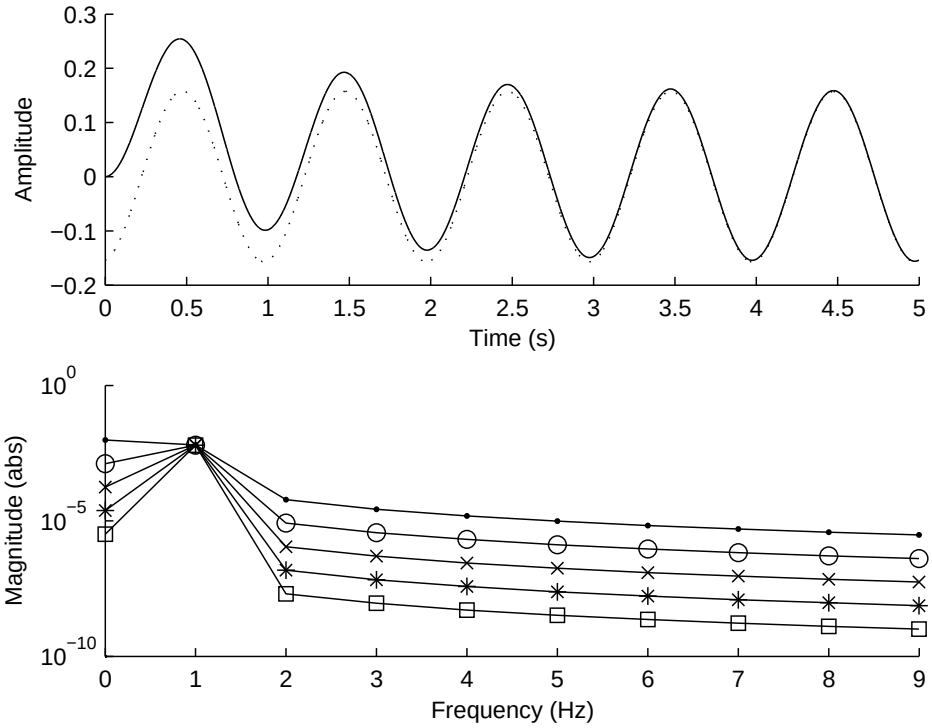

Figure 5.1 *Illustration of the transient effects in Example 5.1. Top: The output signal for five periods of data (solid line) together with the steady state response (dotted line). Bottom: The output spectrum for the five different periods (top line, period one, bottom line, period 5).*

(no difference between the output signal from one period to the next). The same is true for burst excitation if the whole system response is collected.

The waiting time to reach steady state mainly depends on the damping of the system. In a real situation, it is enough to wait until the transient effects are less than other sources of errors, such as disturbances. According to Schoukens et al. (2000), the required waiting time, T_w, can be approximately estimated by

$$T_w = \frac{\tau}{2} \ln \left(\epsilon^2 \frac{\tau}{2T_{tot}} \right) \tag{5.6}$$

where τ is the dominating time constant of the system in the considered frequency band, T_{tot} is the length of the data record (typically one period of data), and ϵ^2 is

the system signal-to-noise ratio

$$\epsilon^2 = \frac{|G(i\omega)U(\omega)|^2}{\sigma^2(\omega)} \tag{5.7}$$

where $\sigma(\omega)$ is the noise power. In case of very low noise levels, $1/\epsilon$ can be chosen as the desired relative error. Transient effects will also be illustrated in Section 7.2.1 for the MFRF estimation method (3.52) using experimental data.

6

MFRF Estimation – Error Analysis

Accurate dynamic models are needed in many applications and it is therefore crucial to use identification methods that produce good model estimates. In this chapter, we will study the method for estimating the multivariable frequency response function (MFRF), described in Section 3.4.3. In particular, an approximate expression for the estimation error for closed loop identification is derived. Using this expression some properties of the estimation error can be explained. Of particular interest is how the model quality is affected by the properties of the disturbances, the choice of excitation signal in the different input channels, the feedback and the properties of the system itself. The expression will be illustrated in Chapter 7 using experimental data from a real industrial robot and in Chapter 8 using simulation data.

The chapter is organized as follows. Section 6.1 presents the frequency domain identification method that will be used in the chapter and Section 6.2 deals with the problem of selecting the excitation signals. Finally, the approximate error expression is derived in Section 6.3.

6.1 The Identification Method

Consider the setting in Figure 6.1, where F is the controller and G is the plant to identify. The plant has m input channels and p output channels. The controller takes as input the difference between the reference signal r and the measured plant output y, and u is the commanded plant input. Due to disturbances v_u and v_y, the plant input will be $u_p = u + v_u$ and the measured plant output $y = y_p + v_y$, *i.e.*, the sum of the true output y_p and the output disturbance v_y.

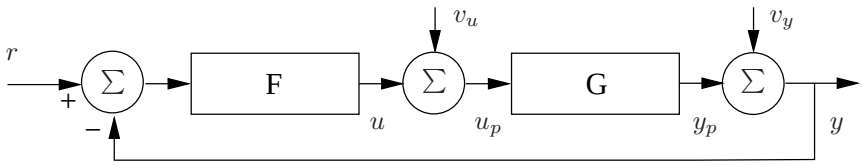

Figure 6.1 *Block diagram showing the setup for closed loop identification.*

The identification method, described more in detail in Section 3.4.3, requires input-output data (u and y in Figure 6.1) from (at least) as many experiments as the number of input channels. The sampled data are transformed using DFT and collected into matrices $\mathbf{U}_N(\omega_k) \in \mathbb{C}^{m\times m}$ and $\mathbf{Y}_N(\omega_k) \in \mathbb{C}^{p\times m}$, where each column corresponds to one experiment. The relation between the input and output can then be written as

$$\mathbf{Y}_N(\omega_k) = G(e^{i\omega_k T})\mathbf{U}_N(\omega_k) \tag{6.1}$$

where $G(e^{i\omega_k T}) \in \mathbb{C}^{p\times m}$ is the multivariable frequency response function (MFRF). We will in the sequel use $G(\omega_k)$ as a short notation for $G(e^{i\omega_k T})$. If $\mathbf{U}_N(\omega_k)$ has full rank, an estimate of $G(\omega_k)$ can be formed as

$$\hat{G}_N(\omega_k) = \mathbf{Y}_N(\omega_k)\mathbf{U}_N^{-1}(\omega_k) \tag{6.2}$$

The MFRF estimation method assumes that (6.1) holds, which is the case for periodic data from the system steady state response (also called stationary response). The error analysis conducted in this chapter will only consider stationary errors, *i.e.*, transient errors are neglected.

In order to evaluate the quality of the estimated models, some quality measures are needed. In this thesis we will mainly look at the *relative error* of the estimate, defined as

$$\Delta G_N(\omega_k) = \frac{\hat{G}_N(\omega_k) - G(\omega_k)}{G(\omega_k)} \tag{6.3}$$

For MIMO systems, which is the case here, the relative error is calculated element-wise. For an easier comparison, the magnitude of the relative error, $|\Delta G_N(\omega_k)|$, is averaged over the excited frequency interval, Ω, as in

$$\overline{|\Delta G_N|} = \frac{1}{N_\Omega}\sum_{\omega_k\in\Omega} |\Delta G_N(\omega_k)| \tag{6.4}$$

where N_Ω is the number of excited frequencies. The subscript N will from now on be omitted for easier notation.

For bias and variance expressions, see, for example, Pintelon and Schoukens (2001a), which handles the SISO case in the presence of correlated input/output errors (closed loop data).

6.2 Excitation Signals

The selection of excitation signals is an important step in the design of good experiments, which has already been discussed in Chapter 5.

As was mentioned in Section 6.1, we need (at least) the same number of experiments as the number of inputs. Consider therefore the matrix $\mathbf{r}(t) \in \mathbb{R}^{p\times m}$ of reference signals, where column i corresponds to the reference signal applied in experiment i. *How should* $\mathbf{r}(t)$ *be selected?* To be noted is that we need $p \geq m$ in order to make $\mathbf{U}_N(\omega_k)$ full rank (see (6.8) where $G_u(\omega_k) \in \mathbb{C}^{m\times p}$). In addition to the reference signal, the controller could be considered as a tuning parameter for the identification experiment. That is not considered here.

We will here restrict our selection of $\mathbf{r}(t)$ to

$$\mathbf{r}(t) = \mathcal{T} r_0(t) \tag{6.5}$$

where $r_0(t)$ is a scalar signal (for example a multisine signal), and $\mathcal{T}$ is a permutation matrix. Two cases of $\mathcal{T}$ will be used for comparison[1]

$$\mathcal{T}_1 = \begin{pmatrix} 1 & 0 & 0 \\ 0 & 1 & 0 \\ 0 & 0 & 1 \end{pmatrix} \quad \mathcal{T}_2 = \begin{pmatrix} 1 & 1 & 1 \\ 1 & -1 & 1 \\ 1 & 1 & -1 \end{pmatrix} \tag{6.6}$$

where the second matrix maximizes $\det \mathcal{T}$ (only the set (-1,0,1) is allowed for the elements) and is suggested in Guillaume et al. (1996) for the open loop case.

6.3 Error Analysis

Consider once more the block diagram in Figure 6.1 for the case $v_y \neq 0$ and/or $v_u \neq 0$. How is the relative error (6.3) affected by the disturbances? We will here mainly consider the DFT matrices (bold face) of the signals, where column i corresponds to experiment i. Now let $\mathbf{V}(\omega_k)$ denote the sum of the contributions from both input and output disturbances, *i.e.*

$$\mathbf{V}(\omega_k) = \mathbf{V}_y(\omega_k) + G(\omega_k)\mathbf{V}_u(\omega_k) \tag{6.7}$$

As measurements, we will consider the control signal, u, and the measured output signal, y, given by

$$\mathbf{U}(\omega_k) = G_u(\omega_k)(\mathbf{R}(\omega_k) - \mathbf{V}(\omega_k)) \tag{6.8}$$

$$\mathbf{Y}(\omega_k) = G(\omega_k)\mathbf{U}(\omega_k) + \mathbf{V}(\omega_k) = G_c(\omega_k)\mathbf{R}(\omega_k) + S(\omega_k)\mathbf{V}(\omega_k) \tag{6.9}$$

respectively, where

$$S(\omega_k) = (I + G(\omega_k)F(\omega_k))^{-1} \tag{6.10}$$

$$G_u(\omega_k) = (I + F(\omega_k)G(\omega_k))^{-1}F(\omega_k) \tag{6.11}$$

$$G_c(\omega_k) = G(\omega_k)F(\omega_k)S(\omega_k) \tag{6.12}$$

[1] Assuming $p = m = 3$, which is the case in this thesis.

Lemma 6.1
Consider the setting in Figure 6.1 with the estimator $\hat{G}(\omega_k)$ *given by* (6.2) *and* $p = m$. *The estimation error (neglecting leakage effects in the DFT:s) is*

$$\tilde{G}(\omega_k) = \hat{G}(\omega_k) - G(\omega_k) = \mathbf{V}(\omega_k)\mathbf{U}^{-1}(\omega_k)$$

with $\mathbf{V}(\omega_k)$ *and* $\mathbf{U}(\omega_k)$ *given by* (6.7) *and* (6.8), *respectively.*

Proof: *From* (6.2) *one gets*

$$\tilde{G}(\omega_k) = \hat{G}(\omega_k) - G(\omega_k) \tag{6.13}$$

$$= (\mathbf{Y}(\omega_k) - G(\omega_k)\mathbf{U}(\omega_k))\mathbf{U}^{-1}(\omega_k) \tag{6.14}$$

Inserting $\mathbf{Y}(\omega_k) = G(\omega_k)\mathbf{U}(\omega_k) + \mathbf{V}(\omega_k)$ *from* (6.9) *then immediately gives the desired result.* □

Using (6.8) the error expression can be rewritten as

$$\tilde{G}(\omega_k) = \mathbf{V}(\omega_k)((\mathbf{R}(\omega_k) - \mathbf{V}(\omega_k))^{-1}G_u^{-1}(\omega_k) \tag{6.15}$$

where

$$G_u^{-1}(\omega_k) = G(\omega_k) + F^{-1}(\omega_k) \tag{6.16}$$

For large signal-to-noise ratios one can use the approximation $(\mathbf{R}(\omega_k) - \mathbf{V}(\omega_k))^{-1} \approx \mathbf{R}^{-1}(\omega_k)$, which gives

$$\tilde{G}(\omega_k) \approx \mathbf{V}(\omega_k)\mathbf{R}^{-1}(\omega_k)(G(\omega_k) + F^{-1}(\omega_k)) \tag{6.17}$$

From Lemma 6.1, one immediately notes that $\mathbf{U}$ should be large in order to get a small estimation error. To fulfill this, one could either increase the amplitude of the reference signal, or make the transfer function G_u large. From (6.15) and (6.16) one can see that a high gain controller will give a smaller estimation error. This could at first seem to be in conflict with standard results for spectral analysis, see Section 3.7.2, claiming that F should be as small as possible. The difference is explained by the fact that here the controller $u(t) = F(q)(r(t - y(t))$ is used.

By choosing $F = -G^{-1}$ (which corresponds to a marginally stable system), the estimation error would be zero. Of course, that is unrealistic since the true system is unknown and the signal amplitudes would be infinitely large. A more practical point is that close to instability, where an accurate model is needed the most, the estimation error will be smaller.

Consider now the case described in (6.5), Section 6.2, that the same scalar reference signal $r_0(t)$ is used in all experiments and for all channels using the permutation matrix $\mathcal{T}$. Equation (6.17) then gives

$$\tilde{G}(\omega_k) \approx \frac{1}{R_0(\omega_k)}\mathbf{V}(\omega_k)\mathcal{T}^{-1}(G(\omega_k) + F^{-1}(\omega_k)) \tag{6.18}$$

Using this expression, three properties of the relative error will be described:

- Non-symmetric relative error.
- Larger relative error for small elements (given that the disturbances $\mathbf{V}_{ij}$ have similar character).
- Relative error dependent on $\mathcal{T}$.

6.3.1 Non-symmetric Relative Error

For easier notation, consider the $\mathcal{T}_1$-case and a diagonal controller. Equation (6.18) then implies the expressions

$$\tilde{G}_{1,3} = \frac{1}{R_0}(\mathbf{V}_{1,:}G_{:,3} + \mathbf{V}_{1,3}F_{3,3}^{-1}) \tag{6.19}$$

$$\tilde{G}_{3,1} = \frac{1}{R_0}(\mathbf{V}_{3,:}G_{:,1} + \mathbf{V}_{3,1}F_{1,1}^{-1}) \tag{6.20}$$

where $\mathbf{V}_{1,:}$ is row 1 in $\mathbf{V}$, $G_{:,3}$ is column 3 in G, *etc.* (argument (ω_k) omitted for easier notation). In these equations $\mathbf{V}_{i,j}$ denotes the DFT of the disturbance acting on channel i in experiment j.

Equations (6.19)–(6.20) explain why the relative error will be non-symmetric. The error $\tilde{G}_{3,1}$ is influenced by the elements in the first column of G. The error $\tilde{G}_{1,3}$ is on the other hand influenced by the elements in the third column of G, and this will obviously not give the same result.

6.3.2 Larger Relative Error for Small Elements

The relative error will in general be larger for small elements in G, which can be seen as follows. By comparing the expression

$$\tilde{G}_{1,1} = \frac{1}{R_0}(\mathbf{V}_{1,:}G_{:,1} + \mathbf{V}_{1,1}F_{1,1}^{-1}) \tag{6.21}$$

with $\tilde{G}_{3,1}$ from (6.20) and using the assumption that all $\mathbf{V}_{ij}$ have same character, the magnitude of $\tilde{G}_{1,1}$ and $\tilde{G}_{3,1}$ will be approximately the same. Dividing by $G_{1,1}$ and $G_{3,1}$, respectively, then gives that the relative error will be larger in magnitude for the smaller element, typically for the off-diagonal element.

6.3.3 Dependence on $\mathcal{T}$

If the $\mathbf{V}_{ij}$ are independent of the excitation, the $\mathcal{T}_2$ case will give lower relative error than the $\mathcal{T}_1$ case. This is due to the fact that $\mathbf{V}\mathbf{R}^{-1} = 1/R_0\mathbf{V}\mathcal{T}^{-1}$ for the $\mathcal{T}_2$ case involves averaging two elements in $\mathbf{V}$, which obviously, in average, will reduce its value. In particular, if the $\mathbf{V}_{ij}$ are uncorrelated, the value will be reduced by a factor 2.

For the robot application, $\mathbf{V}_{ij}$ depends on the movement of the robot, and hence also on the excitation (see Section 8.1 for details). This will affect the assumption of

same magnitude for all $\mathbf{V}_{ij}$ and in addition make the components in $\mathbf{V}$ correlated. The choice of permutation matrix $\mathcal{T}$ is therefore much more involved for the robot application.

7

MFRF Estimation – Experimental Results

The aim of this chapter is to find out how different properties of the excitation signals as well as different averaging techniques affect the estimated multivariable frequency response function (MFRF) for experimental data from an ABB IRB6600 robot. Section 7.1 describes the data collection, including the experimental setup and experiment design. The results are presented in Section 7.2 and finally Section 7.3 contains some conclusions and suggestions.

7.1 Data Collection

The data used for identification are collected from an ABB IRB6600 robot (see Figure 7.1) using an experimental controller. The experiments are carried out in the research lab of ABB Automation Technologies AB – Robotics, Västerås, Sweden, which is gratefully acknowledged.

The first three axes are considered, giving a multivariable system with three inputs (commanded motor torques) and three outputs (motor joint velocities). For this kind of application it is necessary to use feedback control while data are collected, both for safety reasons and in order to keep the robot around its operation point. An experimental control system is used, which makes it possible to use off-line computed reference signals for the joint controllers (similar to φ_m^{ref} in Figure 2.8).

The excitation signals are applied as reference signals for the motor joint velocities. The experimental controller can approximately be seen as a diagonal PI-controller for the joint velocities.

The identification method, described more in detail in Section 3.4.3 and Chap-

Figure 7.1 *The ABB IRB6600 robot.*

ter 6, requires input-output data from (at least) as many experiments as the number of inputs channels. Consider therefore the matrix $\mathbf{r}(t) \in \mathbb{R}^{3\times 3}$ of reference signals, where column i corresponds to the reference signal applied in experiment i. The properties of the excitation signal $\mathbf{r}(t)$ will of course affect the quality of the estimated parameters. In particular, the corresponding DFT matrix, $\mathbf{R}_N(\omega_k)$, must have full rank for all excited frequencies. One way of creating $\mathbf{r}(t)$ is to use a scalar reference signal $r_0(t)$ and a permutation matrix $\mathcal{T}$ like $\mathbf{r}(t) = \mathcal{T} r_0(t)$, as was described in Section 6.2. Since the system is nonlinear, not only the spectrum will matter, but also the amplitude and the actual waveforms. See Chapter 5 for details on the experiment design.

The aim here is to estimate the multivariable frequency response function in the whole frequency band where notches and peaks are expected. For this purpose, a broadband excitation signal will be used which excites the frequency band $[1, 40]$ Hz with a flat amplitude spectrum. Of course the spectrum could be optimized as well, but that is not considered in this study. Many different signals exist, but here mainly the multisine signal will be considered. Another option is to use a chirp signal, which gives approximately the same behavior, which can be seen in Section 7.2.6. A problem then is that the signal "shape" is fixed, compared to the multisine signal that depend on the phases. See Section 7.2.7 for a continued

discussion on the use of different signal shapes.

The influence of static friction should also be reduced, so an excitation signal with as few zero velocity crossings as possible is preferred. This is solved by using a (smoothed) square wave in all channels and then superimpose the broadband signal in certain channels. The reference signal (matrix) can therefore be seen as a sum of the broadband signal and the square wave like

$$\mathbf{r}(t) = \mathbf{r}_{bb}(t) + \mathbf{r}_{sq}(t) \tag{7.1}$$

where

$$\mathbf{r}_{sq}(t) = \begin{pmatrix} 1 & 1 & 1 \\ 1 & 1 & 1 \\ 1 & 1 & 1 \end{pmatrix} r_{sq}(t) \tag{7.2}$$

and $r_{sq}(t)$ is a scalar signal that is smoothed by using an anti-causal moving average filter with a triangular weighting like

$$r_{sq}(t) = \sum_{k=-l}^{l} w_k x(t + kT), \quad w_k = \frac{l + 1 - |k|}{(l+1)^2} \tag{7.3}$$

where $x(t)$ is a square wave, T is the sample time and l is the filter length. In the sequel, we will use $l = 40$ and $T = 0.5 \cdot 10^{-3}$ s.

The broadband signal $\mathbf{r}_{bb}(t)$ will be selected according to Section 6.2 like

$$\mathbf{r}_{bb}(t) = \mathcal{T} r_{bb}(t) \tag{7.4}$$

where $\mathcal{T}$ is a permutation matrix and $r_{bb}(t)$ is a scalar signal. Here, a diagonal permutation matrix $\mathcal{T} = \mathcal{T}_1$ will be used most of the time. For the scalar $r_{bb}(t)$ the periodic *multisine* signal (see (5.5)) $r_{ms}(t)$ will be used according to

$$r_{ms}(t) = \sum_{k=1}^{F} A_k \sin(2\pi f_k t + \phi_k) \tag{7.5}$$

with amplitudes A_k, phases ϕ_k, signal period T_0, and frequencies $f_k = l_k f_0 = l_k / T_0$ with $l_k \in \mathbb{N}$. In the experiments, the filtered square wave, $r_{sq}(t)$, and the multisine signal, $r_{ms}(t)$, will have a period time of 5 s, giving a frequency resolution of 0.2 Hz. Their amplitudes are 14 rad/s and 12 rad/s, respectively. For the multisine, the phases ϕ_k are chosen to get a low crest factor (approximately 1.55) by using random initial phases combined with the clipping algorithm (see Section 5.4). About five periods of data are collected. To reduce (eliminate) transient effects, only the last four periods are used as estimation data. Transient effects are therefore insignificant. See Section 7.2.1 for results on transient effects.

7.2 Results

In this section, estimates of the multivariable frequency response function (MFRF) will be presented for a number of different properties of the excitation signals as

well as different averaging techniques. Of course, this is just a small collection of cases, but can still give useful insight into the problems involved.

Even though motor velocity is considered as output during the experiment design (velocity controllers), we will exclusively present estimates of the MFRF from motor torque to motor acceleration, $G_{\tau\ddot{\varphi}}$, in this chapter. The main reason is that physical properties are more easily seen in $G_{\tau\ddot{\varphi}}$, compared to the MFRF from motor torque to motor velocity, $G_{\tau\dot{\varphi}}$. In a Bode plot, $G_{\tau\ddot{\varphi}}$ should be flat (no integrators) except for resonances and friction. Note also their close correspondence

$$G_{\tau\ddot{\varphi}}(i\omega) = i\omega G_{\tau\dot{\varphi}}(i\omega) \tag{7.6}$$

corresponding to an amplitude scaling of ω and a phase shift of $\pi/2$ rad. (Actually, the presented estimates in the chapter are calculated according to (7.6), where $G_{\tau\dot{\varphi}}(i\omega)$ is estimated from the measured data.) See also Section 8.1 for a comparison between $G_{\tau\ddot{\varphi}}$ and $G_{\tau\dot{\varphi}}$.

7.2.1 Transient Effects

The considered MFRF estimation method is based on the assumption that the measurements come from the steady state system response. Transients will therefore introduce errors in the estimates. To reduce the transient effects, a periodic excitation signal can be applied and then wait until transients have declined. The required waiting time, T_w, has been discussed in Section 5.6.

In Figure 7.2 the estimates can be seen for $T_w = 0$ s and $T_w = 5$ s. The main differences can be seen for low frequencies, in particular in the off-diagonal elements. If the estimates are plotted for a number of waiting times, one can hardly see any differences in the estimate for $T_w \geq 1$ s, compared to the $T_w = 5$ s case. In the sequel, a waiting time of at least 2 s will be used.

7.2.2 Averaging Over Periods

As was mentioned in Section 3.4.3, a way of reducing the variance in the estimates is to average the DFTs from different synchronized data records like in (3.53). Here, each period is considered as a data record and these are of course synchronized. The excitation signals described in Section 7.1 will now be used, *i.e.*, we have four periods of steady state data. In Figure 7.3 the estimates from each individual period are plotted. As can be seen, the estimates are hardly separable. Averaging will in this case make almost no difference compared to just using the estimate from one period of data (see the thin lines in Figure 7.13). The underlying assumption for averaging over periods is that the disturbances acting on the input and output are independent over the periods. Here, this is probably not the case. The randomness in the estimates is therefore caused by other phenomena, which will be further discussed in Section 7.2.7.

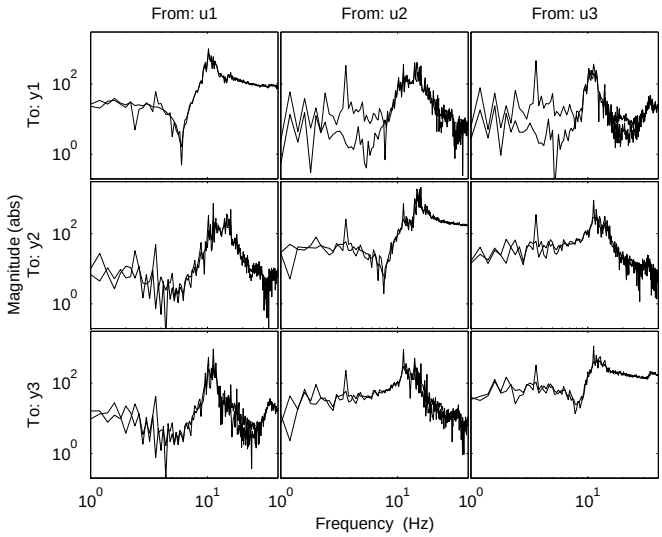

Figure 7.2 *Magnitude of the estimated MFRF with waiting times $T_w = 0$ s (thin lines) and $T_w = 5$ s (thick lines).*

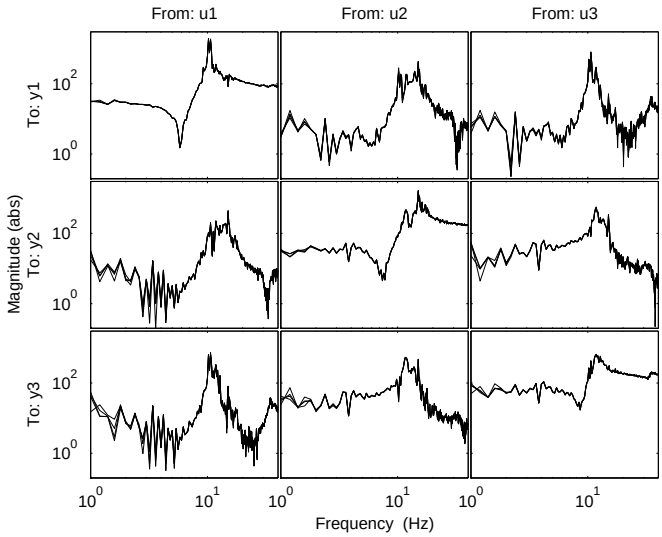

Figure 7.3 *Magnitude of the estimated MFRF for four different periods of data. The estimates are hardly separable.*

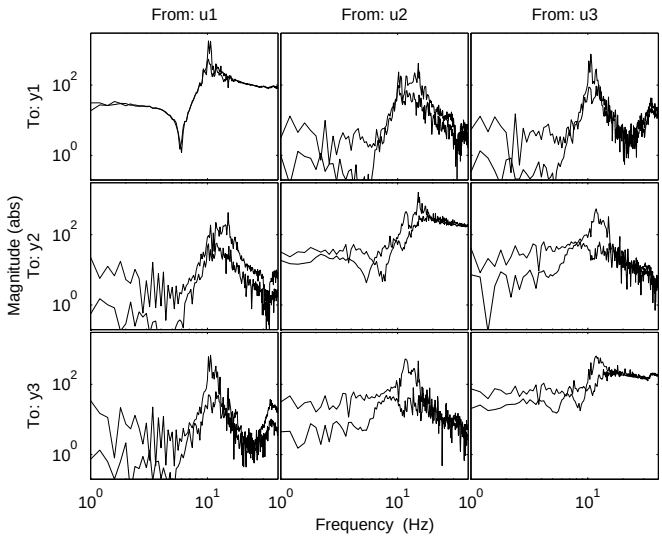

Figure 7.4 *Magnitude of the estimated MFRF using an excitation signal with square wave (thin lines) and without square wave (thick lines).*

7.2.3 Using a Square Wave

Adding a square wave to the excitation signal will both increase the energy in the excitation signal at certain frequencies as well as change its wave form. In particular, the number of zero velocity crossings is reduced. In Figure 7.4 the influence of using a square wave can be seen. Comparing the estimates with and without a square wave, one can clearly see the importance of using the square wave. Without it, the resonance peaks almost disappear and the locations of the notch frequencies are also lower. The (1,1) element is an exception, which could be explained by less friction for axis one.

7.2.4 Amplitude Dependence

The signal amplitude will, for a linear system, mainly affect the variance in the estimate. For a nonlinear system, on the other hand, the estimated linear approximation will depend on the operating point and therefore also on the signal amplitude.

The influence of different amplitudes can be seen in Figure 7.5, where the low amplitude excitation signal has the same shape as the normal amplitude excitation signal, but the amplitude is halved. It might be hard to see any differences, but zooming in on the (1,1) and (2,2) elements show that the notch frequency is reduced when the amplitude is decreased. This is in correspondence with test bench

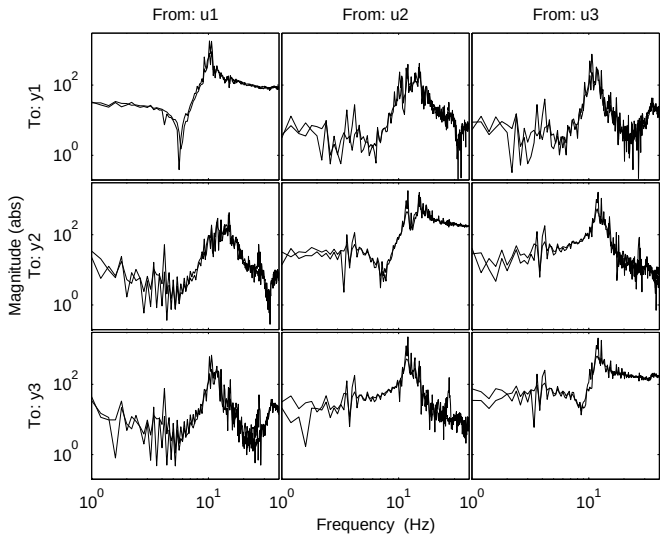

Figure 7.5 *Magnitude of the estimated MFRF for different amplitudes. Thin lines: normal amplitude, thick lines: low amplitude.*

measurements of gearbox stiffness, which gets stiffer for larger amplitudes.

7.2.5 Different Permutation Matrices $\mathcal{T}$

We will here compare the estimates using excitation signals with different permutation matrices $\mathcal{T}_1$ and $\mathcal{T}_2$ (see (6.6)). The estimates can be seen in Figure 7.6. From this figure, it is hard to draw any immediate conclusions about which one to use. A peculiar result is that for the $\mathcal{T}_2$ case, the notch frequency is larger in the (1,1) element but smaller in the (3,3) element, compared to the $\mathcal{T}_1$ case. The $\mathcal{T}_2$ case gives slightly lower estimates for the (1,2) and (1,3) elements, which actually are closer to the true values (see Section 7.2.9).

7.2.6 Multisine Versus Chirp

We will here compare the estimates using the multisine signal and the chirp signal (see (5.4)). The frequency of the chirp signal is linearly swept from 40 Hz to 1 Hz during 5 s. Repeating this signal gives a periodic signal with period time 5 s. The peak value is the same as for the multisine signal. The averaged (over four periods of data) estimates can be seen in Figure 7.7. From this figure, it is hard to draw any immediate conclusions about which signal to use.

To be noted is that for the chirp signal, a small DC-level is present (can be removed by tuning ϕ in (5.4)) which gives a slightly improved estimate due to

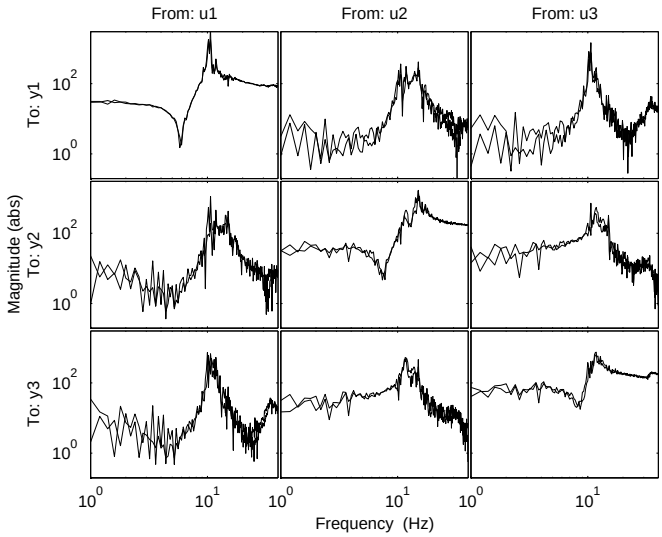

Figure 7.6 *Magnitude of the estimated MFRF for different permutation matrices, $\mathcal{T}_1$ (thin lines) and $\mathcal{T}_2$ (thick lines).*

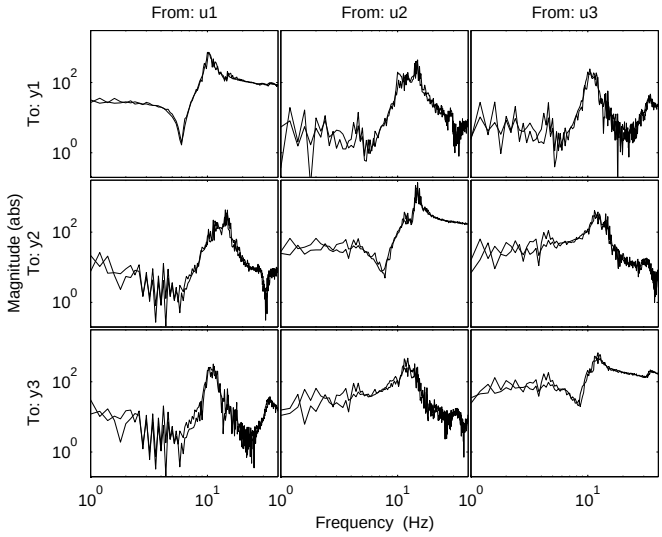

Figure 7.7 *Magnitude of the estimated MFRF using the chirp signal (thick lines) and the multisine signal (thin lines).*

the averaging. Compare Section 7.2.8 where a DC-level is added to the multisine signal.

7.2.7 Averaging Over Experiments

In Section 7.2.2 the averaging was done over multiple periods of a single periodic data set. Here, data from different experiments will be considered as well. [A data set/experiment will now denote the result from applying the reference matrix $\mathbf{r}(t)$ which, to be precise, actually corresponds to three separate experiments.]

A problem when averaging signals like in (3.53) from multiple data sets is synchronization. This must be handled, otherwise the estimate can get worse by the averaging. Consider, *e.g.*, the scenario of taking the average of two equal periodic signals (except for noise) with a phase shift of one half of the period time. This would only leave the noise components left for the estimation. Often the signals can be synchronized by using some trigger signal or by analyzing the data. If this is not the case, one can average the estimated MFRF since the phase shifts then are eliminated. Note that the inversion in the MFRF estimation method is a nonlinear operation so averaging before or after the inversion will give different results.

Here, the data sets are not synchronized so the estimated MFRFs from each data set will be averaged. The averaging can be done in different ways. Here, two ways will be considered. The first one is a simple *arithmetic mean* like

$$\hat{G}(\Omega_k) = \frac{1}{n_{exp}} \sum_{j=1}^{n_{exp}} \hat{G}^{[j]}(\Omega_k) \tag{7.7}$$

where n_{exp} is the number of experiments, Ω_k is either $i\omega_k$ or $e^{i\omega_k T}$, and $\hat{G}^{[j]}(\Omega_k)$ is the estimate from data set j, calculated according to (3.53). The second way of averaging will be denoted *logarithmic mean* and is defined as

$$|\, \hat{G}(\Omega_k) \,| = \exp\left(\frac{1}{n_{exp}} \sum_{j=1}^{n_{exp}} \log |\, \hat{G}^{[j]}(\Omega_k) \,| \right) \tag{7.8}$$

$$\arg \hat{G}(\Omega_k) = \arg\left(\frac{1}{n_{exp}} \sum_{j=1}^{n_{exp}} Y^{[j]}(\omega_k)\overline{U}(\omega_k) \right) \tag{7.9}$$

which is suggested in Pintelon and Schoukens (2001b) as a more robust averaging technique, compared to (7.7) which is prone to give larger bias errors. For a MIMO system, the phase cannot be calculated like in (7.9), but one way is to use

$$\arg \hat{G}(\Omega_k) = \frac{1}{n_{exp}} \sum_{j=1}^{n_{exp}} \arg \hat{G}^{[j]}(\Omega_k) \tag{7.10}$$

or (7.7) for estimating the phase and (7.8) for the estimation of the magnitude.

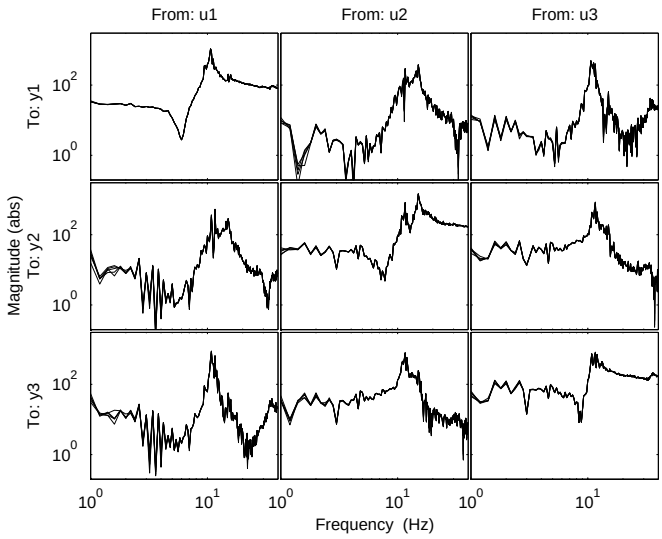

Figure 7.8 *Magnitude of the estimated MFRF for five experiments with the same excitation.*

In Section 7.2.2, the averaging over periods was unable to remove the randomness in the estimates. Using five data sets with the same reference signal $\mathbf{r}(t)$ give averaged estimates (over the periods) according to Figure 7.8. These estimates are also almost identical and no averaging will be able to reduce the randomness in the estimates.

So, *where does the randomness come from?* It cannot be caused by stochastic disturbances, since then the estimates would differ between each period and experiment. What is left is nonlinear effects and repetitive disturbances. According to Pintelon and Schoukens (2001b, Ch. 3), nonlinearities will give both systematic and stochastic contributions to the estimated frequency response function (FRF), even in the absence of other disturbances. These can be seen as bias and variance in the estimates. The stochastic contribution is actually a deterministic signal once the excitation signal is fixed, but is called stochastic since it behaves as uncorrelated (over the frequencies) noise. For a multisine excitation signal, changing the phases will give a different realization of this stochastic contribution. It is therefore suggested to use different realizations of the multisine and average the FRF over these experiments. In addition, one should only use certain frequencies (*e.g.* only odd frequencies) to reduce the nonlinear effects. See Pintelon and Schoukens (2001b) for details.

Following the suggestion, five experiments with different multisine signals $\mathbf{r}_{ms}(t)$ are carried out. The multisine signals all have the same amplitude spectrum, but the initial phases are randomly picked and therefore the optimized phases will be

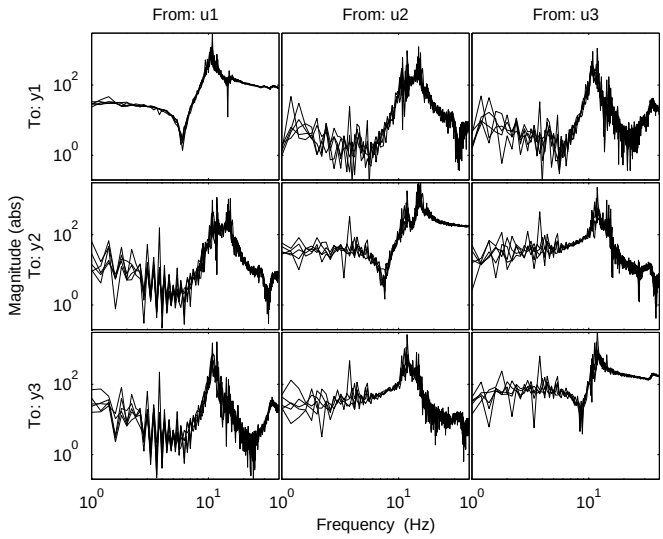

Figure 7.9 *Magnitude of the estimated MFRF for five experiments with different multisines (same amplitude but different phases).*

different in the five experiments. The corresponding five averaged estimates (over the periods) can be seen in Figure 7.9. Compared to the estimates in Figure 7.8, these estimates now vary quite much depending on the specific multisine realization.

In Figure 7.10, the averaged estimates according to (7.8) can be seen for the two cases of equal and different multisines. To be noticed is the reduced randomness in the estimate for the case of different multisines. The randomness would be further reduced if more experiments would be carried out. In addition one could of course apply some smoothing of the estimates, like in (3.46), but then there is always a trade-off between bias and variance. Figure 7.11 shows the differences between using the arithmetic mean (7.7) and the logarithmic mean (7.8). One can notice that the logarithmic mean (7.8) gives a smoother estimate and is therefore the preferred choice.

7.2.8 Averaging Over Periods with Varying Operating Point

Assuming that the disturbances can be described according to Section 2.3.3, the disturbances will depend on the actual motor position. Averaging over periods with a slightly varying operating point would then be a way of reducing the influence from such repetitive disturbances. A varying operating point can be obtained by adding a small DC-level to the velocity reference signal. Figure 7.12 shows the estimates from the four different periods of data where the motor position is changed about $\pi/2$ rad between each period. Due to a large gear ratio, this gives

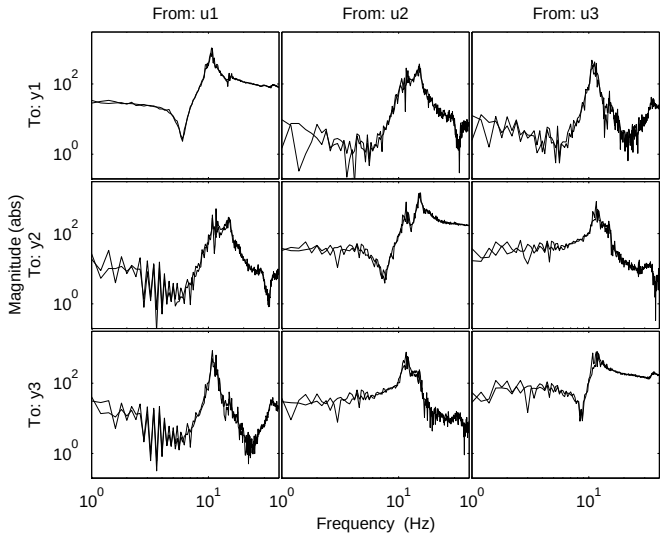

Figure 7.10 *Magnitude of the estimated MFRF, averaged over the five experiments in Figure 7.8 (thin lines) and Figure 7.9 (thick lines) using the logarithmic mean* (7.8).

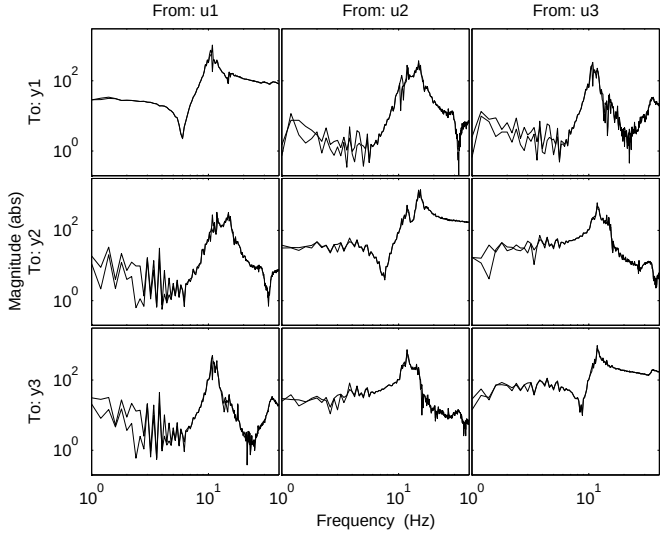

Figure 7.11 *Magnitude of the estimated MFRF using the arithmetic mean* (7.7) *(thin lines) and the logarithmic mean* (7.8) *(thick lines) for the averaging.*

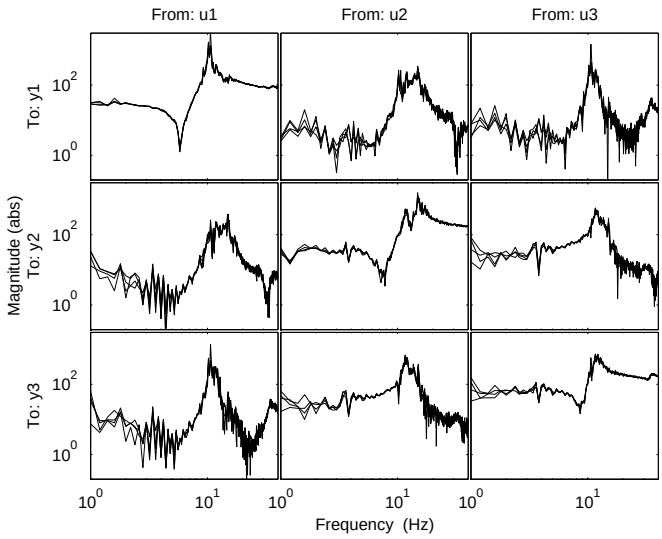

Figure 7.12 *Magnitude of the estimated MFRF for four different periods of data with a slightly varying operating point.*

an insignificant change in operating point for the robot arm.

Comparing these estimates with the ones in Figure 7.3, a considerable difference can be noted. Averaging according to (3.53) for these two cases can be seen in Figure 7.13. This shows that the randomness in the estimates are reduced by using the slightly varying operating point.

The result using a varying operating point also gives an indication that the disturbances acting on the system are indeed of the repetitive character described in Section 2.3.3. Still, the averaging over different multisine realizations is more effective than the averaging over varying operating point (compare Figures 7.10 and 7.13).

7.2.9 Single Sinusoid Versus Broadband Excitation

A possible problem with broadband excitation signals is that the injected signal power at a certain frequency is fairly low, compared to if a single sinusoid is used as excitation signal. To see the difference, a single sinusoid with the same peak value as the multisine signal is superimposed on the smoothed square wave. The single sinusoid has about the same total signal power as the multisine, which gives a much higher signal power for the excited frequency.

In Figure 7.14 the estimates from five experiments with different single sinusoids can be seen together with the averaged estimate using different multisines (thick lines in Figure 7.10). There is a close correspondence between the estimates, except

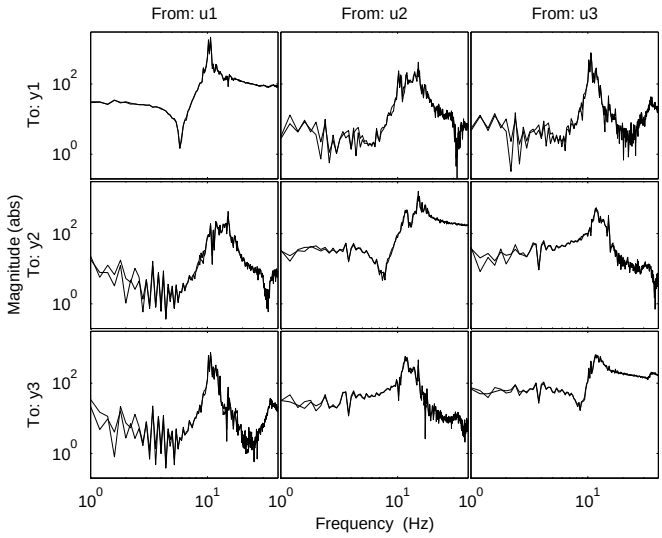

Figure 7.13 *Magnitude of the estimated MFRF using averaging over periods (cf.* (3.53)*) for a varying operating point (thick lines) and fixed operating point (thin lines).*

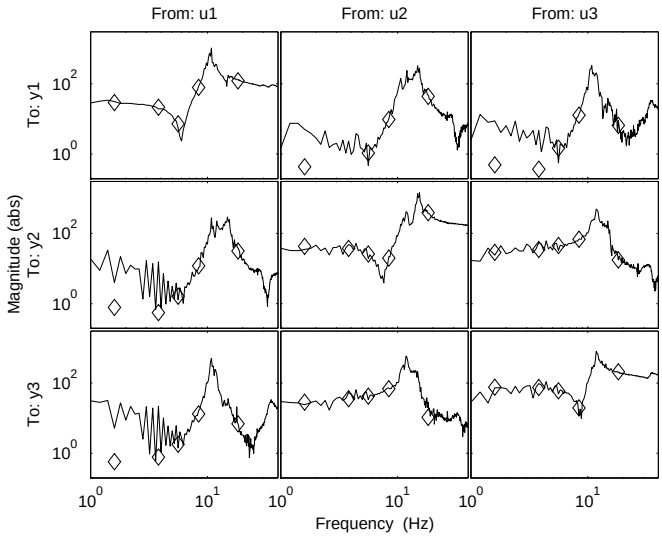

Figure 7.14 *Magnitude of the estimated MFRF using a single sinusoid (diamonds) compared to multisine signals (solid lines). Both signals are superimposed on the smoothed square wave.*

for the low frequency part of the coupling elements between axis one and axes two and three. Theoretical expressions for the low frequency coupling can be derived from the rigid body dynamics model. According to discussions with ABB, the single sinusoid estimates are closer to the theoretical values for this particular robot. Some possible reasons for this discrepancy will be further discussed in Section 8.3.2.

7.3 Conclusions

Data have been collected from an ABB IRB6600 robot using an experimental controller. Many different aspects of excitation signals and averaging techniques for the multivariable frequency response function estimate have been covered. To summarize:

- For accurate estimates, transient effects must be dealt with by a suitable waiting time until a steady state system response is reached. For this particular robot, a waiting time of 1-2 s seems to be enough.
- Static friction must also be handled and therefore a square wave, or a signal with similar properties, is needed in order to reduce the number of zero velocity crossings.
- The amplitude of the excitation signal will affect the location of notch and peak frequencies.
- The permutation matrix will also have some effect, but it is hard to draw any immediate conclusions about which one to use from these experiments.
- Another observation is that in order to reduce the randomness in the estimates, one should average estimates from several experiments with random multisines with *different realizations*. Since the averaging over several periods (and experiments with identical excitation) does not give any significant reduction, it is better to use many short data records, containing one period of data from the steady state response. In order to further reduce nonlinear effects, it would be interesting to try odd multisines, or other versions suggested in Pintelon and Schoukens (2001b).
- Finally, in order to estimate the coupling elements between axis one and axes two and three for low frequencies, a broadband excitation signal is not sufficient, at least not with the current power spectrum. This is probably caused by a too poor signal-to-noise ratio (SNR). Since we are mainly dealing with repetitive disturbances, the SNR is not significantly improved by using a longer data set. A single sinusoid applied for a very short time will thus give a better estimate. A stepped sine excitation for the low frequency part might then be a good alternative. Another option to consider is to increase the injected power for low frequencies when using the multisine signal.

8

MFRF Estimation – Simulation study

In this chapter, the multivariable frequency response function (MFRF) estimation method will be evaluated using simulation data. Of particular interest is how different properties of the excitation signals as well as different averaging techniques will affect the estimates. These are the same questions that were considered in Chapter 7 using experimental data from a real industrial robot.

The reason for using a simulation model is that it makes it possible to study the different aspects separately and is a way of trying to explain the experimental results from Chapter 7. By, for example, keeping the character of the excitation signal fixed, and changing the properties of the disturbances, and, in addition, having the true system available, it is possible to get insight into the properties of the estimated model. The results are evaluated using the approximate, but explicit, expression for the estimation error from Chapter 6.

The simulation model is described in Section 8.1 and the experiment design is treated in Section 8.2. Various results from the simulations are presented in Section 8.3. Finally, Section 8.4 contains some conclusions.

8.1 Simulation Model

The robot simulation model used in this chapter corresponds to an experimental robot with a load capacity of 250 kg (similar to the ABB IRB 6600 robot). The model is a linearized version of a nonlinear state-space model with 20 states, describing the dynamics of joints 1, 2 and 3 (see Figure 8.1) from applied motor torque τ to achieved motor position φ. The nonlinear model is similar to (2.12), but at joints 2 and 3, two additional spring-damper pairs have been added to describe

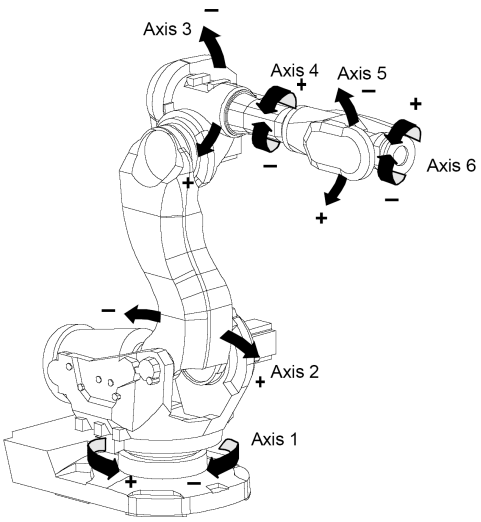

Figure 8.1 *The ABB IRB 6600 robot.*

flexibilities in other directions than the joint directions (giving 8 additional states). The nonlinear robot model is linearized at zero position and velocity, corresponding to the position in Figure 8.1. The motor torque τ is considered as input. As output, it is common to both consider the motor velocity, $\dot{\varphi}$, and acceleration, $\ddot{\varphi}$. In Figure 8.2 Bode plots can be seen for the two transfer functions $G_{\tau\dot{\varphi}}$ and $G_{\tau\ddot{\varphi}}$.

The reason for considering velocity as output is that the controllers usually are velocity controllers. However, viewing the transfer function from motor torque to motor acceleration is sometimes more informative since this should be flat (no integrators), except for resonances and friction. Note also their close correspondence

$$G_{\tau\ddot{\varphi}}(i\omega) = i\omega G_{\tau\dot{\varphi}}(i\omega) \tag{8.1}$$

corresponding to an amplitude scaling of ω and a phase shift of $\pi/2$ rad. In the sequel, mainly the transfer function from motor torque to motor acceleration will be estimated.

The data collection will be carried out in closed loop, which is schematically depicted in Figure 8.3. For this kind of application it is necessary to use feedback control while data are collected, in order to keep the robot around its operation point. Limitations according to real life experiments are imposed on the experiments, such as limitations in amplitude and bandwidth for the motor torque, velocity, and acceleration.

The input disturbance, v_τ, and the output disturbance, v_φ, are modeled ac-

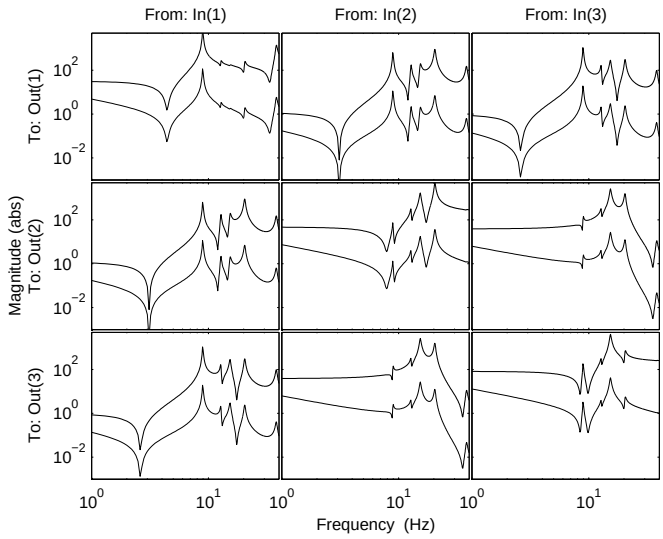

Figure 8.2 *Bode plot of the transfers functions $G_{\tau\dot{\varphi}}$ (thin lines) and $G_{\tau\ddot{\varphi}}$ (thick lines).*

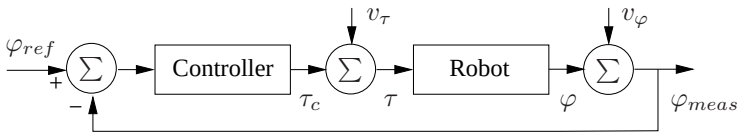

Figure 8.3 *Block diagram illustrating the simulation setup.*

cording to Section 2.3.3 like

$$v_\tau(t) = \sum_{n\in\mathbb{N}_a} a_n \sin(n\varphi(t) + \phi_{a,n}) + \tau_c(t) \sum_{n\in\mathbb{N}_b} b_n \sin(n\varphi(t) + \phi_{b,n}) \tag{8.2a}$$

$$v_\varphi(t) = \sum_{n\in\mathbb{N}_c} c_n \sin(n\varphi(t) + \phi_{c,n}) + e_\varphi(t) \tag{8.2b}$$

(see Section 2.3.3 for details.) The input disturbance is torque ripple from an AC permanent magnet motor and the output disturbance is resolver ripple from a Tracking Resolver-to-Digital Converter. Numerical values which are considered to be relevant for the robot application can be seen in Table 8.1. A small stochastic part, $e_\varphi(t)$, is added in order to model various noise sources in the measurement equipment. $e_\varphi(t)$ is chosen as Gaussian white noise with zero mean and a variance of $1.5 \cdot 10^{-10}$.

Some simplifying conditions in the system setup are that the simulation model does not include nonlinearities such as, *e.g.*, backlash in the gearbox, Coulomb

Table 8.1 *Numerical values for the disturbances in* (8.2)*. Values partly from (Uddeholt, 1998).*

n	a_n (Nm)	$\phi_{a,n}$ (rad)
3	0.06	1.45
36	0.11	0.9
72	0.08	0.2
n	b_n (-)	$\phi_{b,n}$ (rad)
18	0.04	0
n	c_n (mrad)	$\phi_{c,n}$ (rad)
2	0.40	-1.84
10	0.20	0.81
12	0.22	2.94
48	0.18	2.94

friction, or nonlinear stiffness in the springs. These nonlinearities would affect the estimation quality, which has been studied in for example Aberger (2000) for black-box identification of an industrial robot, and would be interesting to incorporate in a future study. See also Chapter 9 for nonlinear gray-box identification using a model that includes Coulomb friction and nonlinear spring stiffness.

8.2 Experiment Design

A similar experiment design will be used for the simulation study as was used in Chapter 7 for the experimental data. For details, the reader is referred to Section 7.1.

For the experiment design, the motor velocity $\dot{\varphi}(t)$ will be used as output $y(t)$, and the excitation signal $r(t)$ is therefore applied as reference velocity for the controller, which can be seen as a PI-controller for the joint velocities. Hence, $\varphi_{ref}(t)$ in Figure 8.3 is the integral of the reference signal $r(t)$. The controller used in the experiments is diagonal, and the diagonal elements are of PI-type.

The identification method, described more in detail in Section 3.4.3 and Chapter 6, requires steady state input-output data from (at least) as many experiments as the number of inputs channels. Consider therefore the matrix $\mathbf{r}(t) \in \mathbb{R}^{3\times 3}$ of reference signals, where column i corresponds to the reference signal applied in experiment i. The reference signal (matrix) will be selected similar to Section 7.1 as a sum of a broadband signal and a square wave like

$$\mathbf{r}(t) = \mathbf{r}_{bb}(t) + \mathbf{r}_{sq}(t) \tag{8.3}$$

where $\mathbf{r}_{sq}(t)$ is a smoothed square wave applied in all channels and $\mathbf{r}_{bb}(t)$ is selected

according to Section 6.2 like

$$\mathbf{r}_{bb}(t) = \mathcal{T} r_{bb}(t) \tag{8.4}$$

where $\mathcal{T}$ is a permutation matrix and $r_{bb}(t)$ is a scalar signal. For the scalar $r_{bb}(t)$ the periodic multisine signal $r_{ms}(t)$ will be used (see (5.5)).

In all the experiments, the filtered square wave has a period time of 5 s and an amplitude of 9.6 rad/s. The multisine signal has a peak value of 8 rad/s, period time $T_0 = 10$ s, and its frequency contents in the interval $[1,\ 40]$ Hz. This gives a frequency resolution of 0.1 Hz for the multisine signal. For the multisine, random initial phases are used in combination with the clipping algorithm, giving a crest factor of approximately 1.55. To reduce (eliminate) transient effects (see Section 5.6), we will here wait until no difference can be seen in the estimates from one signal period to the next.

8.3 Results

In this section, estimates of the multivariable frequency response function (MFRF) will be presented for a number of different properties of the excitation signals as well as different averaging techniques. The main purpose is to find out how the estimates are affected by these different choices and possibly explain some of the experimental results from Chapter 7.

8.3.1 Influence of $\mathcal{T}$ and Square Wave

During the experiment design there are numerous choices on how to select the excitation signal. Here the choices of permutation matrix $\mathcal{T}$ and the use of a square wave will be evaluated. Figures 8.4 to 8.7 (see the following pages) contain the magnitude of the relative errors, $|\Delta G|$, (see (6.3)) in the MFRF estimates for the following combinations of excitation signals:

	Without square wave	With Square wave
$\mathcal{T}_1$	Figure 8.4	Figure 8.6
$\mathcal{T}_2$	Figure 8.5	Figure 8.7

The averaged (over frequencies) version of $|\Delta G|$, denoted $\overline{|\Delta G|}$, can be seen in Table 8.2. These values might be easier to use for the comparison of the different excitation signals. In practice, the square wave is needed to reduce the effects of static friction (see the experimental results in Chapter 7). In these simulations no static friction is present. Instead we can study how the square wave affect the estimates via the repetitive disturbances, since these depend on the excitation signal.

Without Square Wave

First, consider the case of not using a square wave in Figures 8.4 and 8.5. From these figures and Table 8.2, a number of observations can be made:

Table 8.2 *Averaged (over frequencies) magnitude $\overline{|\Delta G|}$ of the relative error $|\Delta G|$ in the MFRF estimate (in %) for different excitation signals (cf. Figures 8.4 to 8.7).*

	Without square wave			With square wave		
$\mathcal{T} = \mathcal{T}_1$	9.23	23.41	32.20	8.17	59.67	92.50
	24.40	18.27	24.28	55.53	17.10	60.35
	33.95	31.07	18.49	80.83	61.41	15.77
$\mathcal{T} = \mathcal{T}_2$	10.13	42.20	47.00	7.76	27.15	39.11
	198.96	15.84	55.81	92.74	12.38	61.57
	186.22	69.55	14.79	165.69	61.26	11.35

- Even though the multivariable system itself, shown in Figure 8.2, is symmetric the relative error is non-symmetric (compare, for example, the (1,3) and (3,1) elements in Figure 8.5).
- The relative error is larger for small elements (compare, for example, the (1,1) and (1,2) elements in Figure 8.5).
- For the diagonal elements, the $\mathcal{T}_1$ and $\mathcal{T}_2$ cases are about the same, but for the off-diagonal elements, $\mathcal{T}_1$ is better (cf. Table 8.2).

The first two observations are in correspondence with the error analysis in Chapter 6. The last observation needs further analysis. If the disturbances would have been stochastic, independent of the excitation, then the observation in Section 6.3.3 would be valid, *i.e.*, $\mathcal{T} = \mathcal{T}_2$ would give better estimates in all elements. This can be seen in Appendix A.1, which also illustrates the other mentioned observations. Here, the properties of the disturbance will depend on the excitation, which will be analyzed next.

Analysis of Repetitive Disturbances

The repetitive disturbances (8.2) used in the simulation model will depend on the movement of the robot and hence also on the excitation. For simplicity, only the output disturbance case will be analyzed. Similar results can be obtained for the input disturbance. Since the motor velocity $\dot{\varphi}(t)$ is considered as output during the experiment design, the corresponding output disturbance, denoted $v_y(t)$, will therefore be the derivative $\dot{v}_\varphi(t)$ of the repetitive disturbance $v_\varphi(t)$ in (8.2b) like

$$v_y(t) = \dot{v}_\varphi(t) = \dot{\varphi}(t) \sum_{n \in \mathbb{N}_c} c_n n \cos(n\varphi(t) + \phi_{c,n}) + \frac{d}{dt} e_\varphi(t) \tag{8.5}$$

which hints that $v_y(t)$ is highly correlated with $\dot{\varphi}(t)$. Due to the controller we have, in the sample points, the relation $\dot{\varphi}(t) = G_c(q)r(t)$ and we therefore get the

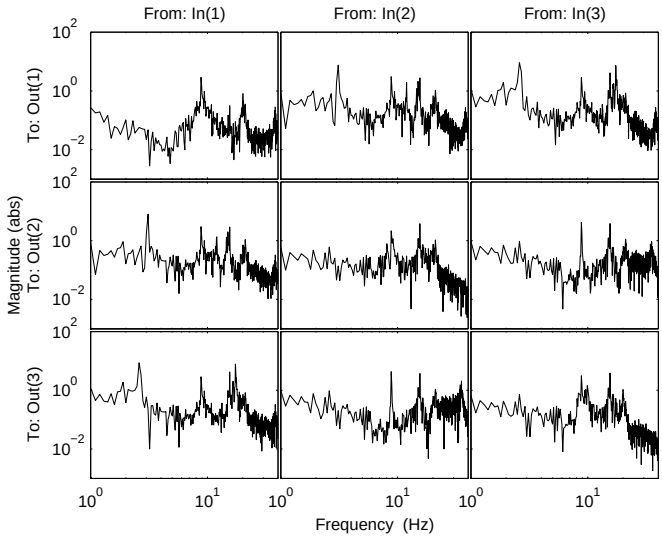

Figure 8.4 *Magnitude of the relative error, $|\Delta G|$, in the MFRF estimate for $\mathcal{T} = \mathcal{T}_1$ and repetitive disturbances.*

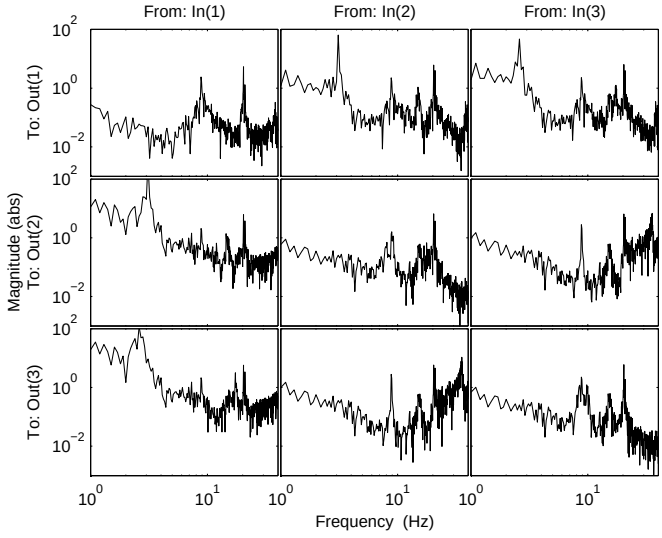

Figure 8.5 *Magnitude of the relative error, $|\Delta G|$, in the MFRF estimate for $\mathcal{T} = \mathcal{T}_2$ and repetitive disturbances.*

approximation

$$\mathbf{V}_y(\omega_k) \approx \text{const} \cdot G_c(e^{i\omega_k T})\mathbf{R}(\omega_k) \tag{8.6}$$

which gives useful understanding. To be noted is that the nonlinear relation (8.5) introduces leakage to neighboring frequencies and therefore $V_y(\omega_k) \neq 0$ even though $R(\omega_k) = 0$. Using $\mathbf{R}(\omega_k) = \mathcal{T} R_0(\omega_k)$ gives

$$\mathbf{V}_y(\omega_k) \approx \text{const} \cdot G_c(e^{i\omega_k T})\mathcal{T} R_0(\omega_k) \tag{8.7}$$

which shows that the disturbances will be drastically different in the $\mathcal{T}_1$ and $\mathcal{T}_2$ cases. With $G_c \approx I$, $\mathbf{V}_y$ will be approximately diagonal in the $\mathcal{T}_1$ case, whereas in the $\mathcal{T}_2$ case, all elements in $\mathbf{V}_y$ will have approximately the same size. This partly explains the differences.

With Square Wave

Consider now the square wave case in Figure 8.6 and Figure 8.7. Comparing the estimates using $\mathcal{T}_1$ and $\mathcal{T}_2$ shows that $\mathcal{T}_2$ gives more accurate estimates when a square wave is present (except for the (2,1), (2,3) and (3,1) elements). This can also be seen in Table 8.2. Why this remarkable difference compared to when no square wave was used?

A square wave with frequency f_0 can be represented by a Fourier series with non-zero components at frequencies $(2k+1)f_0, k = 0, 1, \ldots$. For the square wave case, these frequencies will be excited in all channels. A problem then is that the square wave will excite the repetitive disturbances in all channels as well. Since the disturbances are nonlinear, they will "leak" to neighboring frequencies so the square wave will in addition cause disturbances even at not excited frequencies. What this means in practice is that the disturbance matrices $\mathbf{V}_u$ and $\mathbf{V}_y$ will be fairly equal for $\mathcal{T}_1$ and $\mathcal{T}_2$, which was not the case when no square wave was used (the off-diagonal elements were then at least a factor five lower for the $\mathcal{T}_1$ case).

Recall now the relationship (6.1)

$$\mathbf{Y}(\omega_k) = G(e^{i\omega_k T})\mathbf{U}(\omega_k) \tag{8.8}$$

between the measured input and output matrices, $\mathbf{U}(\omega_k)$ and $\mathbf{Y}(\omega_k)$. This is the disturbance free case. Adding input and output disturbances according to Figure 6.1 gives

$$\mathbf{Y}(\omega_k) = G(e^{i\omega_k T})\big(\mathbf{U}(\omega_k) + \mathbf{V}_u(\omega_k)\big) + \mathbf{V}_y(\omega_k) \tag{8.9}$$

From this expression, it becomes evident that the signal-to-noise ratio (SNR) for the input and output matrices are important to investigate. These are defined as

$$[SNR_{\mathbf{U}}(\omega_k)]_{ij} = \frac{|[\mathbf{U}(\omega_k)]_{ij}|^2}{|[\mathbf{V}_u(\omega_k)]_{ij}|^2} \tag{8.10}$$

$$[SNR_{\mathbf{Y}}(\omega_k)]_{ij} = \frac{|[\mathbf{Y}(\omega_k)]_{ij}|^2}{|[\mathbf{V}_y(\omega_k)]_{ij}|^2} \tag{8.11}$$

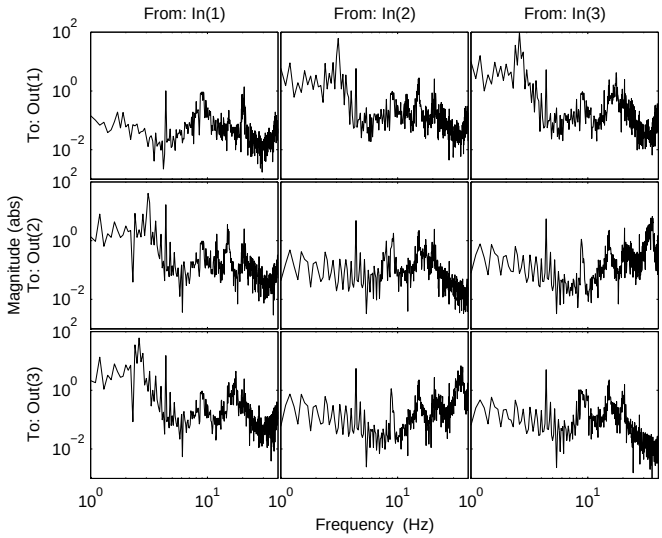

Figure 8.6 *Magnitude of the relative error, $|\Delta G|$, in the MFRF estimate for $\mathcal{T} = \mathcal{T}_1$, square wave, and repetitive disturbances.*

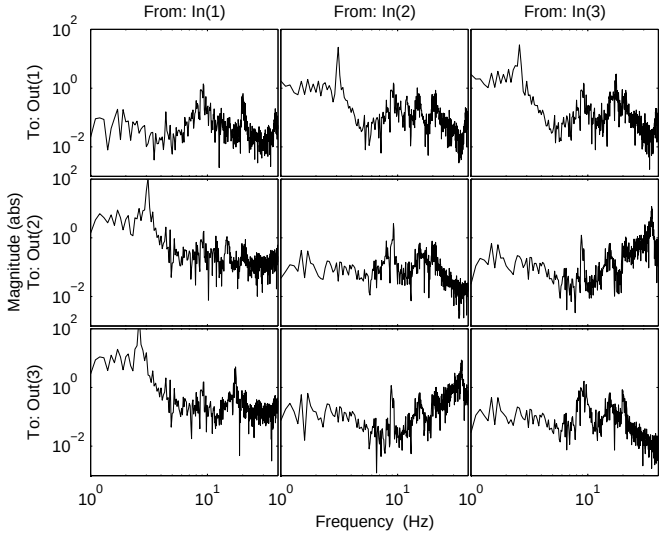

Figure 8.7 *Magnitude of the relative error, $|\Delta G|$, in the MFRF estimate for $\mathcal{T} = \mathcal{T}_2$, square wave, and repetitive disturbances.*

where $|\mathbf{U}(\omega_k)]_{ij}|^2$ is an estimate of the input spectrum for element (i, j), *etc.*

Consider now the frequencies not included in the square wave. For the $\mathcal{T}_1$ case, the off-diagonal elements of the output and input matrices will then only contain coupling effects. The coupling between axis one and axes two and three are fairly weak for low frequencies, which results in low signal values in elements (1,2), (1,3), (2,1), and (3,1). As was previously mentioned, the disturbances are present at all frequencies and therefore, the SNR for these elements will be poor. See Appendix A.2 for plots of the input and output spectrum together with disturbance spectrum and SNR.

The poor SNR values at low frequencies for the off-diagonal elements are also evident in the relative error. Compare, for example, Figure 8.4 (without square wave) and Figure 8.6 (with square wave).

As can be noted from the presented relative errors, the square wave will sometimes result in improved estimates for certain elements and frequencies. Compare, for example, the (2,2) elements in Figure 8.4 and Figure 8.6. The relative error is about the same except at the frequencies corresponding to the square wave where the relative error is lower in the square wave case.

Conclusions

If no square wave is present, $\mathcal{T} = \mathcal{T}_1$ gives the best estimates, except for the (2,2) and (3,3) elements where $\mathcal{T}_2$ gives slightly better estimates (cf. Table 8.2). When the square wave is added, $\mathcal{T}_2$ gives more accurate estimates, except for the (2,1) and (3,1) elements (cf. Table 8.2). It also seems that the differences for the $\mathcal{T}_2$ case are fairly small between using a square wave and not, with a small improvement by using the square wave.

Even though it seems that $\mathcal{T} = \mathcal{T}_2$ should be the preferred choice, we will from now on mainly consider the $\mathcal{T}_1$ case together with the smoothed square wave to get comparable results to the ones in Chapter 7.

8.3.2 Single Sinusoid Versus Broadband Excitation

As was noted in Section 7.2.9, a single sinusoid resulted in more accurate estimates for experimental data. This was particularly evident for the off-diagonal elements at low frequencies. In Figure 8.8 the estimates using a single sinusoid and a multisine signal can be seen together with the true system. For both signals, $\mathcal{T} = \mathcal{T}_1$ is used and the signals are superimposed on a smoothed square wave (The relative error using the multisine can be seen in Figure 8.6). It is evident, by comparing Figures 7.14 and 8.8, that the same phenomena is present in the simulations. The difference in the estimates using the multisine and the single sinusoid can be explained by analyzing the signal spectrum and signal-to-noise ratio (SNR). The single sinusoid has the same peak value as the multisine signal, which gives a much higher signal power for the excited frequency.

In Table 8.3, the SNR can be seen for the input and output matrices at the single sinusoid frequency. Comparing the SNR for the multisine and single sinusoid

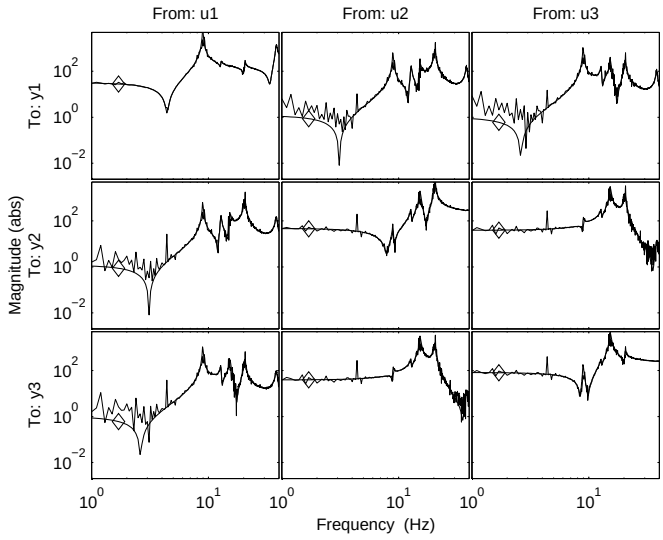

Figure 8.8 *Magnitude of the MFRF estimate for a single sinusoid (diamond) and multisine (thin lines), using $\mathcal{T} = \mathcal{T}_1$ and a square wave. Thick line: true system.*

Table 8.3 *Signal-to-noise ratio (SNR) in dB ($10 \cdot \log_{10}(SNR)$) for the input and output matrices (see (8.10) and (8.11)) in the single sinusoid and multisine cases (evaluated at the single sinusoid frequency).*

	Sinusoid			Multisine		
Input SNR	49.1	57.9	50.4	14.3	8.8	−1.9
	50.9	53.1	52.7	4.9	26.1	31.7
	54.1	53.8	51.2	−0.8	33.2	21.4
Output SNR	85.3	66.7	54.8	65.1	53.3	37.8
	67.3	86.2	78.2	39.2	62.9	66.9
	51.1	82.0	85.8	33.8	61.6	62.7

Table 8.4 *Magnitude of the relative error, $|\Delta G|$, in the MFRF estimate (in %) for the multisine and sinusoid cases (evaluated at the single sinusoid frequency).*

Sinusoid			Multisine		
0.36	0.60	0.81	19	163	309
0.29	0.32	0.42	225	19	29
0.34	0.45	0.37	431	29	23

cases shows a remarkable difference. The SNR is on average improved by a factor 100 (20 dB) using the sinusoid. Note especially the difference in the input SNR for the off-diagonal elements (except the (2,3) and (3,2) elements). For the multisine these elements are way too low. The corresponding relative errors can be seen in Table 8.4, which further emphasizes that the single sinusoid gives much more accurate estimates compared to the multisine signal. Note, however, that the multisine signal excites 400 frequencies in one experiment. Using single sinusoids will therefore drastically increase the required measurement time in order to cover all these frequencies.

8.3.3 Averaging Over Experiments

Averaging over experiments using the same excitation signal will give no improvement in the estimates for repetitive disturbances. Adopting the same idea as in Section 7.2.7, *i.e.*, averaging over experiment with different realizations of the multisine, will make a difference. For simplicity, only the $\mathcal{T}_1$ case with square wave will be considered. As could be seen in Figure 8.8, the estimate is biased due to the square wave, especially for the low frequency part of the (1,2),(1,3),(2,1) and (3,1) elements. Performing 250 experiments and averaging over these will give averaged estimates according to Figure 8.9 using the arithmetic mean and according to Figure 8.10 for the logarithmic mean. As can be noted, the logarithmic average technique still gives biased estimates for the low frequency part of the off-diagonal elements. In this respect, the arithmetic mean is the preferred choice.

Since 250 experiments is unrealistic in practice, it might be interesting to see what happens for a smaller number. Figure 8.11 shows the estimate for 20 realizations using the arithmetic mean. As can be seen, the estimate is already fairly close to the true system and actually less biased than the estimate using the logarithmic mean over 250 realizations in Figure 8.10.

8.4 Conclusions

In this chapter, a number of different aspects regarding excitation signals and averaging techniques have been studied. Especially interesting is that the same phenomena can be seen in simulations as in Chapter 7 where experimental data was used. For the analysis of the estimation errors, the expressions from Chapter 6 have been used. In addition, the signal-to-noise ratio (SNR) has been studied. The following conclusions can be made:

- The square wave will excite the repetitive disturbances in all channels.
- Permutation matrix $\mathcal{T} = \mathcal{T}_2$ gives more accurate estimates, compared to using $\mathcal{T}_1$, except for the (2,1) and (3,1) elements (cf. Table 8.2).
- The relative error is non-symmetric. This is particularly evident in the $\mathcal{T}_2$ case where the elements (2,1) and (3,1) in general are much worse than the (1,2) and (1,3) elements.

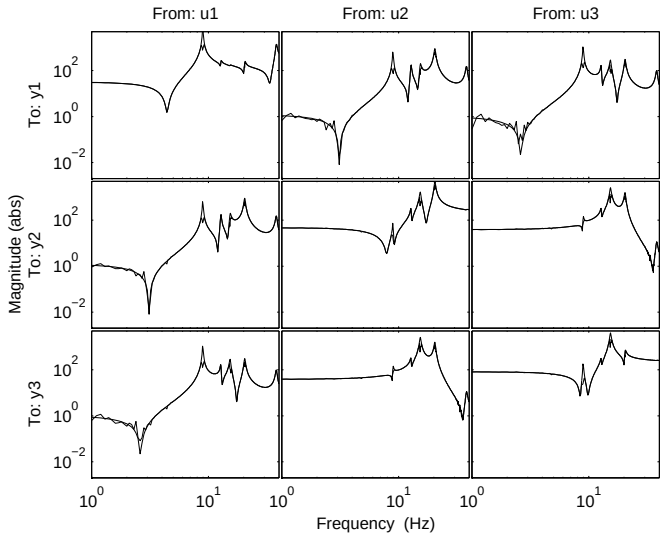

Figure 8.9 *Magnitude of the MFRF estimate averaged over 250 realizations using the arithmetic mean for $\mathcal{T} = \mathcal{T}_1$ and a smoothed square wave (thin lines). Thick lines: true system.*

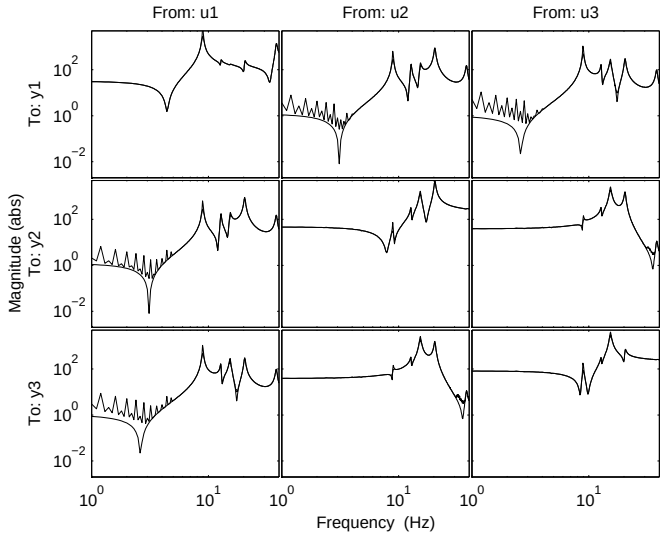

Figure 8.10 *Magnitude of the MFRF estimate averaged over 250 realizations using the logarithmic mean for $\mathcal{T} = \mathcal{T}_1$ and a smoothed square wave (thin lines). Thick lines: true system.*

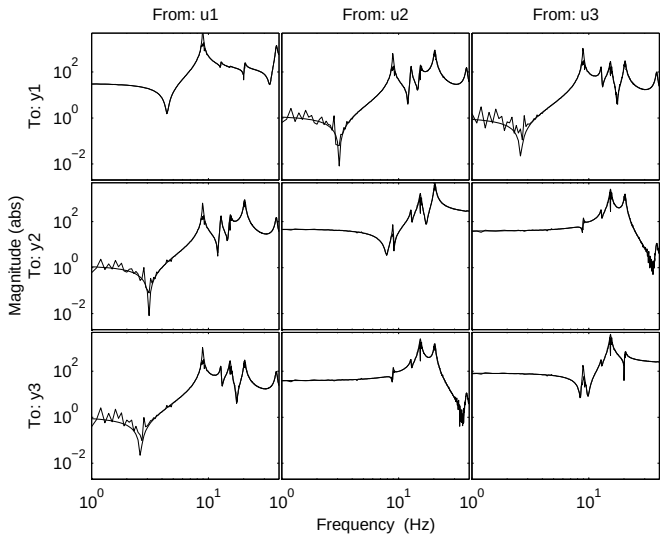

Figure 8.11 *Magnitude of the MFRF estimate averaged over 20 realizations using the arithmetic mean for $\mathcal{T} = \mathcal{T}_1$ and a smoothed square wave (thin lines). Thick lines: true system.*

- Using a single sinusoid will give improved SNR, and therefore more accurate estimates. This is crucial mainly for the low frequency part of the off-diagonal elements of the MFRF. The improvement must, however, be put into relation to the drastically increased total measurement time to cover all wanted frequencies, compared to using a multisine signal.
- Averaging over experiments using different multisines will improve the the estimates, also for the off-diagonal elements. To be noted is that averaging using the logarithmic mean is prone to give biased estimates for the off-diagonal elements. That is not the case for the arithmetic mean.

Remark: In all the simulations, a linear simulation model has been used (together with a nonlinear disturbance description). This is mainly done to reduce the simulation time, but is also a way of reducing the number of possible error sources. Simulations have also been performed using the nonlinear model for a number of cases, showing minor differences compared to the presented results for the linear model.

9

Nonlinear Gray-box Identification

System identification in robotics is a vast research area, as was discussed in Chapter 4. It can be divided into, at least, three different levels or application areas. These levels involve the estimation of the kinematic description, the dynamic model (often divided into rigid body and flexible body dynamics), and the joint model (*e.g.*, motor inertia, gearbox elasticity and backlash, motor characteristics, and friction parameters). In this chapter, the latter two areas will be covered.

In the work presented here, a three-step identification procedure is proposed in which parameters for rigid body dynamics, friction, and flexibilities can be identified only using measurements on the motor side of the flexibility. The main point is the last step, where the parameters of a nonlinear physically parameterized model (a nonlinear gray-box model) are identified directly in the time domain. The first two steps give special attention to the problem of finding good initial parameter estimates for the iterative optimization routine. The procedure is exemplified using real data from an experimental industrial robot.

The work reported here is closely related to the problems considered in, for example, Östring et al. (2003) and Isaksson et al. (2003). Östring et al. (2003) use a method where inertial parameters as well as parameters describing the flexibility can be identified directly in the time domain. This is done by utilizing a user-defined model structure in the System Identification Toolbox (SITB). However, only linear models were treated in their work. Isaksson et al. (2003) consider gray-box identification of a two-mass model with backlash, where black-box modeling is used to find initial parameter values.

The chapter is organized as follows. In Section 9.1 the nonlinear gray-box identification problem is briefly described and Section 9.2 shows the nonlinear robot

model used for identification. The three-step identification procedure is presented in Section 9.3. In Section 9.4 the data collection is described, and Section 9.5 shows the results from applying the proposed identification procedure to the experimental data. Finally, Section 9.6 contains some conclusions and notes on future work.

9.1 Nonlinear Gray-box Identification

The starting point for the nonlinear gray-box identification is the continuous-time state space model structure

$$\dot{x}(t) = f(t, x(t), \theta, u(t)) \tag{9.1a}$$

$$y(t) = h(t, x(t), \theta, u(t)) + e(t) \tag{9.1b}$$

where f and h are nonlinear functions, $x(t)$ is the state vector, $u(t)$ and $y(t)$ are input and output signals, $e(t)$ is a white measurement disturbance signal, and t denotes time. Finally θ is the vector of unknown parameters. Given a set of input/output-data the aim is to determine the parameter vector that minimizes the criterion

$$V_N(\theta) = \frac{1}{N} \sum_{t=1}^{N} \varepsilon^2(t, \theta) \tag{9.2}$$

where $\varepsilon(t)$ denotes the prediction error

$$\varepsilon(t, \theta) = y(t) - \hat{y}(t, \theta) \tag{9.3}$$

The experiments presented in this chapter will utilize the nonlinear gray-box model structure NLGREY, available in a beta version of a nonlinear extension to the System Identification Toolbox (SITB), (Ljung, 2003). The model structure NLGREY is similar to the IDGREY model structure in SITB. The model can be either a discrete-time or continuous-time state space model, and it is defined in a Matlab m-file/mex-file. In the current version of the software, only OE-models can be used, *i.e.*, only additive white noise, $e(t)$, on the output. The prediction $\hat{y}(t|\theta)$ then becomes the simulated output of the model (9.1) with the input $u(t)$ (without $e(t)$) for the current parameter vector θ. The data set, $\{y, u\}$, is put into an IDDATA object and θ is estimated by applying a prediction error method, which performs a numerical optimization of the criterion (9.2) by an iterative numerical search algorithm. This search algorithm involves simulation of the system for different values of θ. The user specifies an initial parameter vector and it is also possible to fix some components in θ. To speed up the numerical optimization, the simulation model is implemented in a mex-file (C-code).

9.2 Robot Model

The industrial robot that will be studied in this chapter is, for movements around an axis not affected by gravity, modeled by a nonlinear two-mass flexible model

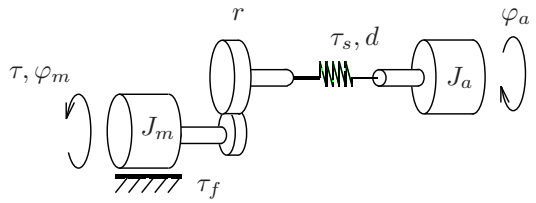

Figure 9.1 *The two-mass flexible model of the robot arm.*

which is illustrated in Figure 9.1. A two-mass model is probably too simple to describe the true system (see, for example, Östring et al. (2003) or Figure 9.3), but it can still be used as an illustration of the proposed identification procedure.

The differential equations describing the dynamics of the robot arm are

$$J_m\ddot{\varphi}_m + rd(r\dot{\varphi}_m - \dot{\varphi}_a) + \tau_f + r\tau_s = \tau \tag{9.4}$$

$$J_a\ddot{\varphi}_a - d(r\dot{\varphi}_m - \dot{\varphi}_a) - \tau_s = 0, \tag{9.5}$$

where J_m and J_a are the moments of inertia of the motor and arm respectively, r is the gear ratio, τ is the motor torque and d is the damping parameter. The spring and gear friction torques, τ_s and τ_f respectively, are often approximately modeled by linear models (see, for example Östring et al., 2003). In this work, nonlinear models will be used to capture the effect of the Coulomb friction and to get a more realistic model of the spring. The torque of the spring is modeled as

$$\tau_s = k_1(r\varphi_m - \varphi_a) + k_3(r\varphi_m - \varphi_a)^3 \tag{9.6}$$

where φ_m and φ_a are the angles of the motor and arm respectively, and k_1 and k_3 are the parameters of the spring. The torque due to friction is modeled as

$$\tau_f = F_v\dot{\varphi}_m + F_c\,\mathrm{sgn}(\dot{\varphi}_m) \tag{9.7}$$

where F_v and F_c are the viscous and Coulomb friction coefficients. A third nonlinearity of practical importance is the presence of backlash in the gearbox, but this problem is left for future work. See also Isaksson et al. (2003). Using (9.4) to (9.7), a nonlinear state space model of the system can be derived. The motor torque, τ, is used as input signal, u, and with the states defined as

$$x = \begin{pmatrix} x_1 \\ x_2 \\ x_3 \end{pmatrix} = \begin{pmatrix} r\varphi_m - \varphi_a \\ \dot{\varphi}_m \\ \dot{\varphi}_a \end{pmatrix} \tag{9.8}$$

the state space equations become

$$\dot{x}_1 = rx_2 - x_3 \tag{9.9a}$$

$$\dot{x}_2 = \frac{1}{J_m}\left(-F_v x_2 - F_c\,\mathrm{sgn}(x_2) - rd(rx_2 - x_3) - rk_1x_1 - rk_3x_1^3 + u\right) \tag{9.9b}$$

$$\dot{x}_3 = \frac{1}{J_a}\left(d(rx_2 - x_3) + k_1x_1 + k_3x_1^3\right) \tag{9.9c}$$

9.3 Identification Procedure

The aim is to identify all parameters in the robot model, described in Section 9.2, using experimental data and the nonlinear gray-box identification procedure described in Section 9.1. An inherent problem of iterative search routines is that only convergence to a local minimum can be guaranteed. In order to converge to the global minimum, a good initial parameter estimate is important. In Chapter 4, an overview of different aspects of identification in robotics has already been given. Combining some of the mentioned methods makes it possible to find good initial parameter estimates for the nonlinear gray-box identification. Therefore, a three-step identification procedure is proposed where the first two steps find initial parameter values and in the third step, the nonlinear gray-box identification procedure is applied.

9.3.1 Step 1: Initial Values for Rigid Body Dynamics and Friction

Identification of rigid body dynamics and friction has already been covered in Section 4.3. The standard procedure includes a dynamic model, linear in the parameters, that is characterized by a minimum number of parameters called base parameters. Usually a friction model with two parameters per link is used, describing viscous and Coulomb friction. The robot is moved along an (optimized) trajectory and applied torque and joint movements are recorded. The parameters are then estimated using linear regression. Since the main interest here is to find initial values, parts of this step could also be replaced by nominal values from CAD models. If, on the other hand, (some) parameters can be estimated with high accuracy in this step, they could be fixed during the third step, leading to a lower dimensional iterative search.

For the robot model in Section 9.2, the rigid body dynamics and friction is described by

$$(J_m + r^2 J_a)\ddot{\varphi}_m + F_v\dot{\varphi}_m + F_c \operatorname{sgn}\dot{\varphi}_m = \tau \tag{9.10}$$

which can be written as a linear regression

$$\begin{pmatrix}\ddot{\varphi}_m & \dot{\varphi}_m & \operatorname{sgn}\dot{\varphi}_m\end{pmatrix}\begin{pmatrix}J_m + r^2 J_a \\ F_v \\ F_c\end{pmatrix} = \tau \tag{9.11}$$

Considering N samples of data, the parameter vector can be determined as the solution to a standard least-squares problem (cf. (4.4) and (4.5)).

9.3.2 Step 2: Initial Values for Flexibilities

As was mentioned in Section 4.4 the major flexibility in an industrial robot is normally located at the joint level, due to the transmission. Weaker (more compliant) robot structures will in addition introduce significant flexibilities in the links and

their connections. Therefore higher order models are sometimes needed in order to get a sufficient description of the system. Many different methods were described in Section 4.4, differing in, for example, assumed model structure, required measurement signals, and complexity of the identification method. One interesting method was proposed by Berglund and Hovland (2000) for the identification of masses, springs and dampers, only using applied torque and joint movements. The identification was based on an estimated Frequency Response Function (FRF) in combination with the solution of an inverse eigenvalue problem. Here, a similar method will be used to obtain initial values for the flexibilities, see Section 9.5.2. One could also apply the method proposed by Isaksson et al. (2003), based on black-box identification.

9.3.3 Step 3: Nonlinear Gray-box Identification

Combining the estimates from steps 1 and 2 gives an initial parameter estimate, and the nonlinear gray-box identification method described in Section 9.1 can now be applied.

9.4 Data Collection

The data used for identification comes from the same experimental setup as in Chapter 7, *i.e.*, from an ABB IRB6600 robot with an experimental controller. The identification will therefore be carried out using closed loop data, which might lead to biased estimates (Ljung, 1999).

For the different steps in the identification procedure, different excitation signals are needed. In step 1, the rigid body dynamics and friction parameters should be excited without introducing any oscillations due to the flexibilities. Therefore a low frequency excitation is preferred. In step 2, on the other hand, the whole frequency band should be excited where notch and peak frequencies in the frequency response function are expected. The influence of static friction should also be reduced, so a broadband excitation with as few zero velocity crossings as possible is selected. Finally, for step 3 a data set (or a combination of data sets) is needed that excite all free parameters in the model.

The properties of the excitation signal will of course affect the quality of the estimated parameters. Since the system is nonlinear, not only the spectrum will matter, but also the amplitude and the actual waveforms. It is common to optimize the excitation signal according to some criterion, see Section 4.3, but that is outside the scope of this work. The following three excitation signals will be used as reference speed for the controller. They are all sampled at 2 kHz ($T = 0.5$ ms).

Data set 1: Triangle wave signal, 6.25 s of data, with amplitude 40 rad/s and period time 5 s.

Data set 2: Multisine signal (sum of sinusoids), 5 s of data, with flat amplitude spectrum in the frequency interval 1-40 Hz with a crest factor of 1.55, period

time 5 s and a peak value of 5 rad/s. The multisine signal is superimposed on a square wave with amplitude 8 rad/s and period time 5 s.

Data set 3: Similar to data set 2, but the multisine signal has a peak value of 10 rad/s and the amplitude of the square wave is 12 rad/s.

The last two data sets mainly differ in amplitude and can therefore be used to see nonlinear effects on the estimates. For details on the excitation signals, see Chapter 5.

9.5 Results

The physical parameters in the robot model from Section 9.2 will be identified by applying the proposed three-step identification procedure from Section 9.3, using the experimental data described in Section 9.4. The gear ratio $r = 1/224.3$ is known.

9.5.1 Step 1

Using data set 1 together with the linear regression (9.11) gives the following parameter estimates

$$\begin{pmatrix} J_m + r^2 J_a \\ F_v \\ F_c \end{pmatrix} = \begin{pmatrix} 0.0280 \\ 0.0136 \\ 0.642 \end{pmatrix} \tag{9.12}$$

The velocity and acceleration used in the regressor, see (9.11), are obtained from position measurements using non-causal low-pass filtering (filtfilt in Matlab) and central difference algorithms.

9.5.2 Step 2

The FRFs for data sets 2 and 3 from motor torque to motor acceleration can be seen in Figure 9.2. Note especially that the notch frequency is higher for the data set with larger amplitude. For a linear system, these estimates should be similar (except for noise). For a linear two-mass model, the approximate transfer function (ignoring the damping, d) from motor torque to motor acceleration is given by

$$\frac{s(J_a s^2 + k)}{s^3 J_a J_m + s^2 J_a F_v + s \cdot k(J_m + r^2 J_a) + k F_v} \tag{9.13}$$

with $1/J_m$ as the high frequency gain and $\omega_n = \sqrt{k/J_a}$ as the notch frequency. Using the FRFs in Figure 9.2, the following numerical values are achieved. For data set 2, $J_m^{[2]} = 0.0126$ and $\omega_n^{[2]} = 35.19$, and for data set 3, $J_m^{[3]} = 0.0120$ and $\omega_n^{[3]} = 37.70$. The estimate of J_m is taken as the average value for the two data sets, $J_m = 0.0123$. Since the gear ratio, r, is known, an estimate $J_a = 790$ is found by combining (9.12) and $J_m = 0.0123$. Knowing J_a, the spring stiffness $k^{[i]}$ for data

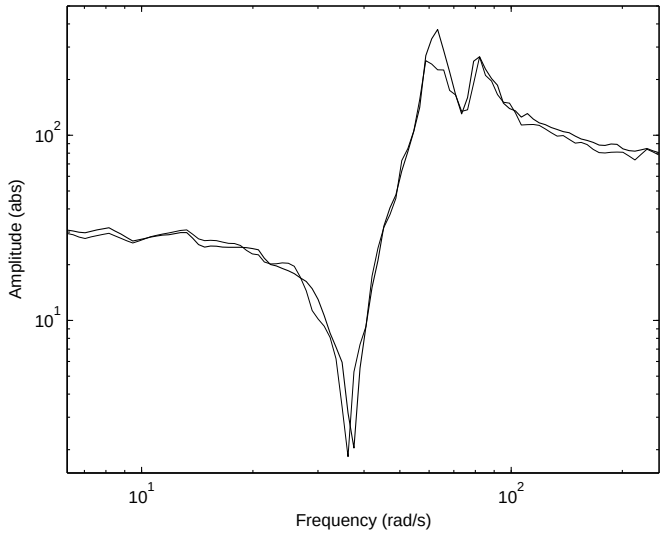

Figure 9.2 *Magnitude of the FRF for data sets 2 (thin line) and 3 (thick line) from motor torque to motor acceleration.*

set i is derived by using the approximate relation $\omega_n^{[i]} = \sqrt{k^{[i]}/J_a}$, which for the two data sets gives $k^{[2]} = 9.78 \cdot 10^5$ and $k^{[3]} = 1.12 \cdot 10^6$. Since the two amplitudes give different spring constants, it is probably fair to conclude that there is a nonlinear effect present in the experimental data. The damping is hard to estimate and its initial value is here simply set to zero. For a higher order model, the procedure described in Hovland et al. (2001) can be used in this step.

To find initial estimates for k_1 and k_3, the following ad hoc procedure is used. The spring constant k from the FRFs can, in some sense, be regarded as an "average spring constant". Reasonable estimates for k_1 and k_3 can then be found by minimizing

$$\sum_{i=2}^{3} \sum_{l=1}^{N} \left(\left(k^{[i]} x_1^{[i]}(lT) - k_1 x_1^{[i]}(lT) - k_3 (x_1^{[i]}(lT))^3 \right)^2 \right) \tag{9.14}$$

where $k^{[i]}$ and $x_1^{[i]}(t)$ are the estimated spring constants and spring deflection, respectively, for data sets $i = 2, 3$. Since the state x_1 is not measured, it is simulated using the model (9.9) with the estimated nominal parameters and a linear spring model $\tau_s = kx_1$.

9.5.3 Step 3

Combining the estimates from steps 1 and 2 gives the initial model `m0` in Table 9.1. The quality of the estimated models is assessed using the model fit (3.54), consid-

Table 9.1 *Estimated parameters, where the initial model* `m0` *comes from the first two steps and the other models are estimated in step three using the data sets denoted in the table.*

Model:	`m0`	`m1`	`m2`	`m3`	
Est. data:	Init.	1,2	1,3	1,2,3	
J_m	1.23	1.26	1.22	1.21	$(\cdot 10^{-2})$
J_a	0.79	1.07	1.11	1.13	$(\cdot 10^{3})$
k_1	0.814	1.42	1.46	1.46	$(\cdot 10^{6})$
k_3	5.4	3.77	4.69	3.72	$(\cdot 10^{10})$
d	0	2.73	3.08	2.63	$(\cdot 10^{3})$
F_v	1.36	1.18	1.36	1.3	$(\cdot 10^{-2})$
F_c	0.642	0.668	0.623	0.644	

Table 9.2 *Model fit when validating the estimated models on data sets 1,2 and 3.*

	`m0`	`m1`	`m2`	`m3`
Data set 1	84.44	97.12	97.46	96.39
Data set 2	32.8	61.54	60.59	62.33
Data set 3	49.95	74.43	74.42	74.94

ering the motor velocity as the measured output. For the estimation, data set 1 is combined with data sets 2 and/or 3 (using merge in SITB) according to Table 9.1. Including data set 1 is motivated by the fact that if only data sets 2 and/or 3 are used, the model fit is improved when validating on data sets 2 and 3, but the estimated parameters are unrealistic (*e.g.*, negative Coulomb friction) and the model fit for data set 1 is low. The optimization is carried out for 30 iterations, giving parameter estimates and models shown in Table 9.1. The estimated models are validated using the three data sets and the model fit is given in In Table 9.2.

Comparing the model fit for the different models in Table 9.2, one can notice that the model fit is substantially improved by the nonlinear gray-box identification step. However, to be fair, the initial estimates from step 1 and 2 (the `m0` model) could probably be improved by using optimal excitation. There are no major differences in model fit when validating with estimation data compared to cross validation. This is also reasonable since the signal-to-noise ratio is quite large. For the `m3` model, the relative importance of data set 1 gets lower, which also shows up in the increased model fit for data sets 2 and 3.

To analyze the relative importance on the model fit for each parameter, the estimated model `m3` is used and each parameter is perturbed $\pm 20\%$, one at a time. In Table 9.3 the difference in model fit can be seen for the three data sets. For data set 1, one can note that the parameters describing the flexibility have

Table 9.3 *Difference in model fit for the* `m3` *model, compared to Table 9.2, when each parameter is perturbed* $+20\%/-20\%$ *(one at a time).*

	Data set 1	Data set 2	Data set 3
J_m	$-4.51/-0.81$	$0.77/-8.09$	$-0.94/-10.7$
J_a	$-8.51/-5.34$	$5.03/-9.45$	$1.08/-7.36$
k_1	$0.13/\ 0.02$	$-2.73/-2.55$	$-3.93/-4.14$
k_3	$-0.01/-0.01$	$-0.05/\ 0.06$	$-0.11/\ 0.08$
d	$0.03/-0.06$	$-0.09/\ 0.02$	$0.12/-0.38$
F_v	$-5.79/-1.65$	$2.46/-4.23$	$0.70/-1.84$
F_c	$-14.7/-8.23$	$-0.11/-21.5$	$-1.25/-9.13$

a small influence, compared to the rigid body dynamics and friction parameters. The nonlinear stiffness parameter, k_3, does not significantly affect the model fit. Removing it gives almost no reduction in model fit. This is a puzzling result, since estimated FRFs (see Figure 9.2) as well as test bench measurements shows an amplitude dependent gearbox stiffness. A more detailed analysis of how the nonlinearities affect the estimate is therefore needed, including more experiments and other model structures.

In Figure 9.3 a Bode plot for the estimated model `m3`, ignoring the nonlinear model parameters (k_3 and F_c), can be seen together with the estimated FRFs for data sets 2 and 3. One can clearly see the close correspondence, which further validates the estimated model. However, to capture the two resonance peaks around 60 and 80 rad/s in the FRF, (at least) a three-mass model would be needed.

9.6 Conclusions

A three-step identification procedure has been proposed for the identification of rigid body dynamics, friction, and flexibilities, only using measurements on the motor side. The procedure has been exemplified using real data from an experimental industrial robot together with a flexible two-mass model where nonlinear spring stiffness and Coulomb friction have been added. The estimated physical parameters have realistic numerical values and give a model with high model fit and fairly good correspondence to FRF measurements. However, the nonlinear spring stiffness is not significant in the selected data sets.

There are a number of aspects of the presented results that are subjects for future work. One important problem is to find a model structure that explains the amplitude dependent properties of the system. This will probably involve higher order models as well as additional nonlinearities. A further topic could be to apply the method for a multivariable system. There are no principal problems in the proposed identification procedure, but the last step involving the iterative numerical search would be more time consuming and possibly numerically sensitive.

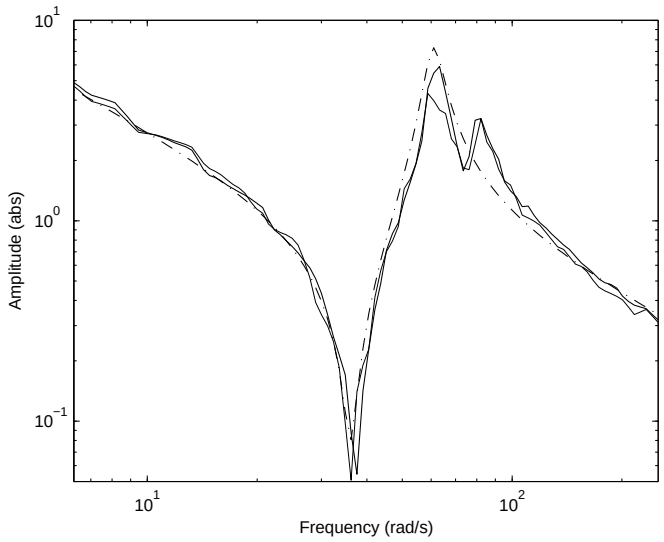

Figure 9.3 *Magnitude of the FRF for data sets 2 (thin line) and 3 (thick line) from motor torque to motor velocity together with the estimated model* `m3` *(dash-dotted line).*

10

Conclusions

In the thesis, an introduction and background to industrial robots have been given, including modeling and control. An overview of system identification methods has also been given, with a dedicated chapter on system identification in robotics. The identification problem is often simplified by considering subproblems like rigid body identification or identification of local linear flexible models. The focus of this thesis has been on identifying flexibilities and nonlinearities. In particular, a nonparametric frequency-domain estimation method for the multivariable frequency response function (MFRF) has been evaluated and analyzed for the robot application. Nonlinear gray-box identification has also been treated.

For the MFRF estimation method, an approximate expression for the estimation error has been derived. The expression describes how the estimate is affected by disturbances, the choice of excitation signal, the feedback and the properties of the system itself. Three properties of the estimation error have been pointed out; nonsymmetric estimation error, relative error larger for small elements, and dependence on the excitation signal in the different input channels (permutation matrix $\mathcal{T}$).

The MFRF estimation method has also been evaluated using both experimental data from an ABB IRB 6660 robot (Chapter 7) and simulation data (Chapter 8). A number of different aspects regarding excitation signals and averaging techniques have been studied. The most important insights are that:

- For accurate estimates, transient effects must be dealt with by a suitable waiting time until a steady state system response is reached.
- Static friction must be handled and therefore a square wave in the velocity reference is needed (or a signal with similar properties). A problem then is that the square wave will excite the repetitive disturbances in all channels.

- In simulations, the permutation matrix $\mathcal{T}_2$ gives more accurate estimates, compared to using $\mathcal{T}_1$, except for the (2,1) and (3,1) elements (cf. Table 8.2).
- The estimation error is non-symmetric. This is particularly evident in the $\mathcal{T}_2$ case where the elements (2,1) and (3,1) in general are much worse than the (1,2) and (1,3) elements (cf. Table 8.2).
- Averaging estimates from several experiments will improve the estimates on condition that random multisines with *different realizations* are used as excitation. Averaging over several periods or using experiments with identical excitation does not give any significant reduction due to the repetitive disturbances. Therefore, many short data records containing one period of data from the steady state response should be used.
- Finally, for the estimation of the coupling elements between axis one and axes two and three for low frequencies, a broadband excitation signal is not sufficient, at least not with a flat power spectrum. A single sinusoid gives remarkably better estimates. A stepped sine excitation for the low frequency part might then be a good alternative.

Nonlinear gray-box identification has also been treated. A three-step identification procedure has been proposed in which parameters for rigid body dynamics, friction, and flexibilities can be identified only using measurements on the motor side of the flexibility. Using experimental data, the estimated physical parameters have realistic numerical values and give a model with high model fit and fairly good correspondence to frequency response function measurements.

Future Work

As was mentioned in the introduction, the ultimate goal in robot modeling is to find an accurate global nonlinear flexible model. Nonlinear gray-box identification could in principle tackle this complex problem by using the proposed three-step procedure in Chapter 9 to handle the estimation of initial values. Thus, it would be interesting to extend the nonlinear two-mass flexible model example in Chapter 9 to incorporate higher order flexible models, multivariable systems, additional nonlinearities such as backlash, *etc.*

An interesting area for further research is that of identifiability. Is it possible to uniquely determine the model parameters given the measured data? Maybe additional sensors are needed, like joint angle measurements after the gearbox and accelerometers attached to the tool and links. This also relates to optimal excitation. Even if additional sensors are used, identifiability can be lost if the excitation signal is poorly chosen.

The experimental work in this thesis is carried out in one operating point with a fixed load. The robot dynamics change quite much with the operating point and load. It would be interesting to study the effects in other operating points as a step toward building the global nonlinear flexible model we are looking for.

Bibliography

ABB. Open public archive of robot images. `www.robots-imagebank.com`, 2004.

M. Abderrahim and A. R. Whittaker. Kinematic model identification of industrial manipulators. *Robotics and Computer-Integrated Manufacturing*, 16(1):1–8, Feb 2000.

M. Aberger. Effects of nonlinearities in black box identification of an industrial robot. Technical Report LiTH-ISY-R-2322, Department of Electrical Engineering, Linköping University, SE-581 83 Linköping, Sweden, Dec 2000.

A. Albu-Schäffer and G. Hirzinger. Parameter identification and passivity based joint control for a 7DOF torque controlled light weight robot. In *Proceedings of the 2001 IEEE International Conference on Robotics and Automation*, pages 2852–2858, Seoul, Korea, May 2001.

B. T. Angerer, C. Hintz, and D. Schr oder. Online identification of a nonlinear mechatronic system. *Control Engineering Practice*, 12(11):1465–1478, Nov 2004.

B. Armstrong. On finding exciting trajectories for identification experiments involving systems with nonlinear dynamics. *International journal of robotics research*, 8(6):28–48, Dec 1989.

B. Armstrong-Hélouvry, P. Dupont, and C. Canudas de Wit. A survey of models, analysis tools and compensation methods for the control of machines with friction. *Automatica*, 30(7):1083–1138, Jul 1994.

P. Avitabile. Experimental modal analysis - a simple non-mathematical presentation. *Sound and vibration*, 35(1):20–31, Jan 2001.

L. Bascetta and P. Rocco. Modelling flexible manipulators with motors at the joints. *Mathematical and Computer Modelling of Dynamical Systems*, 8(2):157–183, 2002.

F. Behi and D. Tesar. Parametric identification for industrial manipulators using experimental modal analysis. *IEEE Transactions on Robotics and Automation*, 7(5):642–652, Oct 1991.

E. Berglund and G. E. Hovland. Automatic elasticity tuning of industrial robot manipulators. In *Proceedings of the 39th IEEE Conference on Decision and Control*, pages 5091–5096, Sydney, Australia, Dec 2000.

C. Canudas de Wit, H. Olsson, K. J. Åström, and P. Lischinsky. A new model for control of systems with friction. *IEEE Transactions on Automatic Control*, 40 (3):419–425, Mar 1995.

Y.-Y. Chen, P.-Y. Huang, and J.-Y. Yen. Frequency-domain identification algorithms for servo systems with friction. *IEEE Transactions on Control Systems Technology*, 10(5):654–665, Sep 2002.

X. Chenut, J. C. Samin, J. Swevers, and C. Ganseman. Combining internal and external robot models for improved model parameter estimation. *Mechanical Systems and Signal Processing*, 14(5):691–704, Sep 2000.

J. J. Craig. *Introduction to Robotics Mechanics and Control*. Addison Wesley, 1989.

M. Enqvist. Some results on linear models of nonlinear systems. Technical Report Licentiate Thesis no. 1046, Department of Electrical Engineering, Linköping University, SE-581 83 Linköping, Sweden, Oct 2003.

G. Ferretti, C. Maffezzoni, G. Magnani, and P. Rocco. Joint stiffness estimation based on force sensor measurements in industrial manipulators. *Journal of Dynamic Systems Measurement and Control, Transactions of the ASME*, 116: 163–167, Mar 1994a.

G. Ferretti, G. Magnani, and P. Rocco. Estimation of resonant transfer functions in the joints of an industrial robot. In *2nd IFAC Symposium on Intelligent Control and Control Applications, SICICA 94*, volume 1, pages 371–376, Budapest, 1994b.

U. Forssell. *Closed-loop Identification: Methods, Theory, and Applications*. PhD thesis, Mar 1999.

U. Forssell and L. Ljung. Closed-loop identification revisited. *Automatica*, 35: 1215–1241, Jun 1999.

J. Funda, R. H. Taylor, and R. P. Paul. On homogeneous transforms, quaternions, and computational efficiency. *IEEE Transactions on Robotics and Automation*, 6(3):382–388, June 1990.

M. Gautier. Numerical calculation of the base inertial parameters of robots. In *Proceedings of the 1990 IEEE International Conference on Robotics and Automation*, volume 2, pages 1020–1025, May 1990.

M. Gautier and W. Khalil. On the identification of the inertial parameters of robots. In *Proceedings of the 27th IEEE Conference on Decision and Control*, pages 2264–2269, Austin, 1988.

M. Gautier and W. Khalil. Direct calculation of minimum set of inertial parameters of serial robots. *IEEE Transactions on Robotics and Automation*, 6(3):368–373, Jun 1990.

M. Gautier and W. Khalil. Exciting trajectories for the identification of base inertial parameters of robots. In *Proceedings of the 30th IEEE Conference on Decision and Control*, pages 494–499, Brighton, England, Dec 1991.

M. Gautier and P. Poignet. Extended kalman filtering and weighted least squares dynamic identification of robot. *Control Engineering Practice*, 9(12):1361–1372, Dec 2001.

M. Gautier, P. O. Vandanjon, and C. Presse. Identification of inertial and drive gain parameters of robots. In *Proceedings of the 33rd IEEE Conference on Decision and Control*, pages 3764–3769, Lake Buena Vista, FL, Dec 1994.

M. Grotjahn, M. Daemi, and B. Heimann. Friction and rigid body identification of robot dynamics. *International Journal of Solids and Structures*, 38:1889–1902, Mar 2001.

P. Guillaume, R. Pintelon, and J. Schoukens. Accurate estimation of multivariable frequency response functions. In *Proceedings of the 13th IFAC Triennial World Congress*, pages 423–428, San Francisco, 1996.

H.-J. Gutt, F. D. Scholl, and J. Blattner. High precision servo drives with DSP-based torque ripple reduction. In *Proceedings of IEEE AFRICON, 1996*, volume 2, pages 632–637, Sep 1996.

D. Hanselman. Resolver signal requirements for high accuracy resolver-to-digital conversion. *IEEE Transactions on Industrial Electronics*, 37(6):556–561, Dec 1990.

J. M. Hollerbach. A survey of kinematic calibration. In O. Khatib, J. J. Craig, and T. Lozano-Perez, editors, *The robotics review. Vol. 1*, pages 207–242. MIT Press, Cambridge, MA, 1989.

J. Holtz and L. Springob. Identification and compensation of torque ripple in high-precision permanent magnet motor drives. *IEEE Trans. on Industrial Electronics*, 43(2):309–320, Apr 1996.

G. E. Hovland, E. Berglund, and S. Hanssen. Identification of coupled elastic dynamics using inverse eigenvalue theory. In *Proceedings of the 32nd ISR (International Symposium on Robotics)*, pages 1392–1397, Apr 2001.

G. E. Hovland, S. Hanssen, E. Gallestey, S. Moberg, T. Brogårdh, S. Gunnarsson, and M. Isaksson. Nonlinear identification of backlash in robot transmissions. In *Proceedings of the 33rd ISR (International Symposium on Robotics)*, Oct 2002.

A. Isaksson, R. Lindkvist, X. Zhang, M. Nordin, and M. Tallfors. Identification of mechanical parameters in drive train systems. In *IFAC System Identification Symposium SYSID 2003*, 2003.

T. M. Jahns and W. L. Soong. Pulsating torque minimization techniques for permanent magnet AC motor drives – a review. *IEEE Transactions on Industrial Electronics*, 43(2):321–330, Apr 1996.

R. Johansson, A. Robertsson, K. Nilsson, and M. Verhaegen. State-space system identification of robot manipulator dynamics. *Mechatronics*, 10(3):403–418, Apr 2000.

T. Kara and I. Eker. Nonlinear modeling and identification of a DC motor for bidirectional operation with real time experiments. *Energy Conversion and Management*, 45(7-8):1087–1106, May 2004.

W. Khalil and S. Besnard. Geometric calibration of robots with flexible joints and links. *Journal of Intelligent and Robotic Systems*, 34:357–379, 2002.

W. Khalil and M. Gautier. Modeling o mechanical systems with lumped elasticity. In *Proceedings of the 2000 IEEE International Conference on Robotics and Automation*, pages 3964–3969, San Francisco, CA, Apr 2000.

F. Khorrami, S. Jain, and A. Tzes. Experimental results on adaptive nonlinear control and input preshaping for multi-link flexible manipulators. *Automatica*, 31(1):83–97, Jan 1995.

K. Kozlowski. *Modelling and identification in robotics*. Advances in Industrial Control. Springer, London, 1998.

L. Ljung. *System Identification: Theory for the User*. Prentice Hall, Upper Saddle River, New Jersey, USA, 2nd edition, 1999.

L. Ljung. *System Identification Toolbox – User's Guide*. The MathWorks Inc, Sherborn, MA, USA, 2003.

L. Ljung and S. T. Glad. *Modeling of Dynamic Systems*. Prentice-Hall, Englewood Cliffs, New Jersey, USA, 1994.

H. Mayeda, K. Yoshida, and K. Osuka. Base parameters of manipulator dynamic models. *IEEE Transactions on Robotics and Automation*, 6(3):312–321, Jun 1990.

D. Nissing and J. Polzer. Parameter identification of a substitution model for a flexible link. In *IFAC System Identification Symposium SYSID 2000*, 2000.

M. Nordin and P.-O. Gutman. Controlling mechanical systems with backlash - a survey. *Automatica*, 38(10):1633–1649, Oct 2002.

M. Nyström and M. Norrlöf. Path generation for industrial robots. Technical Report LiTH-ISY-R-2529, Department of Electrical Engineering, Linköping University, SE-581 83 Linköping, Sweden, Aug 2003.

R. Ortega and M. W. Spong. Adaptive motion control of rigid robots: A tutorial. *Automatica*, 25(6):877–888, Nov 1989.

F. Pfeiffer and J. Hölzl. Parameter identification for industrial robots. In *Proceedings of the 1995 IEEE International Conference on Robotics and Automation*, volume 2, pages 1468–1476, Nagoya, Japan, May 1995.

M. T. Pham, M. Gautier, and P. Poignet. Identification of joint stiffness with bandpass filtering. In *Proceedings of the 2001 IEEE International Conference on Robotics and Automation*, pages 2867–2872, Seoul, Korea, May 2001.

C. L. Phillips and H. T. Nagle. *Digital control system analysis and design*. Prentice-Hall, Int., London, 2nd edition, 1990.

R. Pintelon and J. Schoukens. Measurement of frequency response functions using periodic excitations, corrupted by correlated input/output errors. *IEEE Transactions on Instrumentation and Measurement*, 50(6):1753–1760, Dec 2001a.

R. Pintelon and J. Schoukens. *System identification: a frequency domain approach*. IEEE Press, New York, 2001b.

C. Presse and M. Gautier. New criteria of exciting trajectories for robot identification. In *Proceedings of the 1993 IEEE International Conference on Robotics and Automation*, volume 3, pages 907–912, Atlanta, GA, USA, May 1993.

W. J. Rugh. *Linear system theory*. Prentice Hall, Upper Saddle River, New Jersey, 2nd edition, 1996.

J. Schoukens, R. M. Pintelon, and Y. J. Rolain. Broadband versus stepped sine FRF measurements. *IEEE Transactions on Instrumentation and Measurement*, 49(2):275–278, Apr 2000.

M. Schroeder. Synthesis of low peak factor signals and binary sequences with low autocorrelation. *IEEE Transactions on Information Theory*, IT-16:85–89, 1970.

L. Sciavicco and B. Siciliano. *Modeling and Control of Robotic Manipulators*. Springer, 2000.

T. Söderström and P. Stoica. *System Identification*. Prentice-Hall Int., London, 1989.

S.-Y. Sheu and M. W. Walker. Basis sets for manipulator inertial parameters. In *Proceedings of the 1989 IEEE International Conference on Robotics and Automation*, volume 3, pages 1517–1522, May 1989.

M. W. Spong. Modeling and control of elastic joint robots. *Journal of Dynamic Systems Measurement and Control*, 109(4):310–319, Dec 1987.

M. W. Spong, F. L. Lewis, and C. T. Abdallah, editors. *Robot control : dynamics, motion planning and analysis*. IEEE Press, 1993.

M. W. Spong and M. Vidyasagar. *Robot Dynamics and Control*. Wiley, 1989.

M. Östring, S. Gunnarsson, and M. Norrlöf. Closed-loop identification of an industrial robot containing flexibilities. *Control Engineering Practice*, 11:291–300, Mar 2003.

J. Swevers, C. Ganseman, D. B. Tükel, J. De Schutter, and H. Van Brussel. Optimal robot excitation and identification. *IEEE Transactions on Robotics and Automation*, 13(5):730–740, Oct 1997.

R. J. Theodore and A. Ghosal. Comparison of the assumed modes and finite element models for flexible multilink manipulators. *International Journal of Robotics Research*, 14:91–111, 1995.

E. Uddeholt. *Identifiering och kompensering av motor- och resolverrippel*. Master thesis IR-RT-EX-9806, Dept. of Signals, Sensors & Systems, Royal Institute of Technology, SE-100 44 Stockholm, Sweden, 1998.

E. Van der Ouderaa, J. Schoukens, and J. Renneboog. Peak factor minimization using a time-frequency domain swapping algorithm. *IEEE Transactions on Instrumentation and Measurement*, 37(1):145–147, Mar 1988.

P. Van Overschee and B. DeMoor. *Subspace Identification of Linear Systems: Theory, Implementation, Applications*. Kluwer Academic Publishers, 1996.

E. Wernholt and S. Gunnarsson. Nonlinear grey-box identification of industrial robots containing flexibilities. Technical Report LiTH-ISY-R-2641, Department of Electrical Engineering, Linköping University, SE-581 83 Linköping, Sweden, Nov 2004a. Submitted to IFAC'05.

E. Wernholt and S. Gunnarsson. On the use of a multivariable frequency response estimation method for closed loop identification. In *Proc. of the 43rd IEEE Conference on Decision and Control*, Atlantis, Pardise Island, The Bahamas, Dec 2004b. To appear.

E. Wernholt and M. Östring. Modeling and control of a bending backwards industrial robot. Technical Report LiTH-ISY-R-2522, Department of Electrical Engineering, Linköping University, SE-581 83 Linköping, Sweden, May 2003.

L. Westerlund. *The Extended Arm of Man – A History of the Industrial Robot.* Informationsförlaget, Stockholm, Sweden, 2000.

X.-L. Zhong, J. M. Lewis, and F. L.N.-Nagy. Autonomous robot calibration using a trigger probe. *Robotics and Autonomous Systems*, 18(4):395–410, Oct 1996.

A

MFRF Estimation – Additional Plots

A.1 Stochastic Disturbances

The results in this section can be used as a comparison to the results in Section 8.3.1 where repetitive disturbances are treated. Here, stochastic input and output disturbances will be used, constructed as low-pass filtered Gaussian noise with a cut-off frequency of 40 Hz. The disturbances have similar power spectrum as in the repetitive disturbance case with square wave, but now the disturbances are independent of the excitation and have equal power spectrum in all channels.

As can be seen in Figures A.1 to A.4, the relative error is non-symmetric, small elements in the MFRF give higher relative error, and $\mathcal{T} = \mathcal{T}_2$ gives more accurate estimates. The square wave gives slightly improved estimates at the corresponding frequencies.

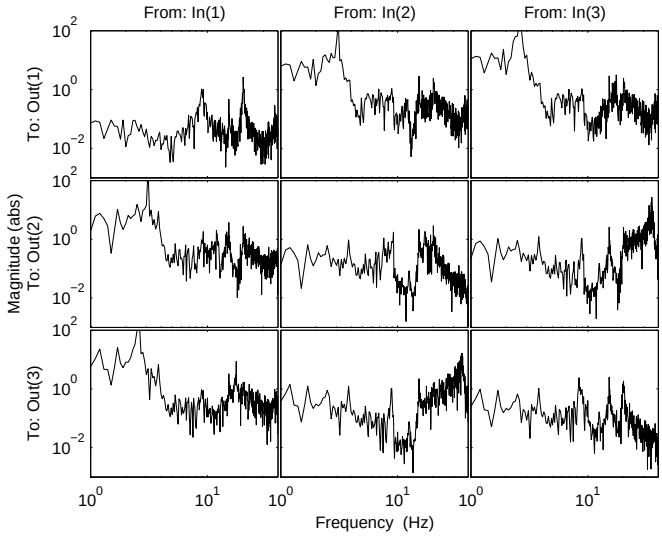

Figure A.1 *Magnitude of the relative error, $|\Delta G|$, in the MFRF estimate for $\mathcal{T} = \mathcal{T}_1$ and stochastic disturbances.*

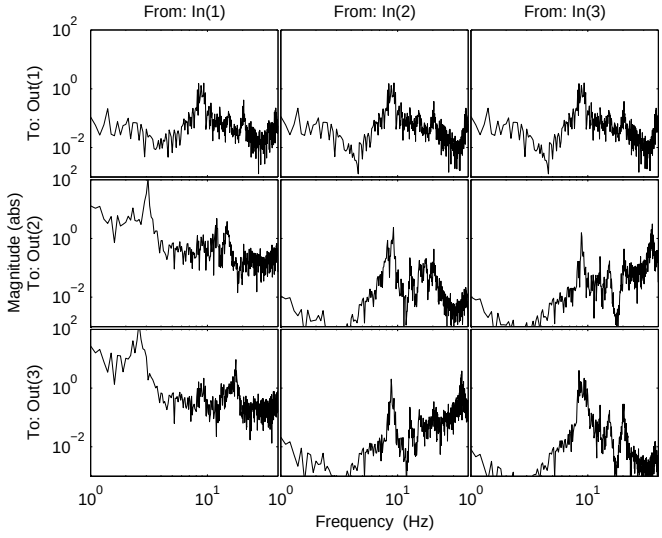

Figure A.2 *Magnitude of the relative error, $|\Delta G|$, in the MFRF estimate for $\mathcal{T} = \mathcal{T}_2$ and stochastic disturbances.*

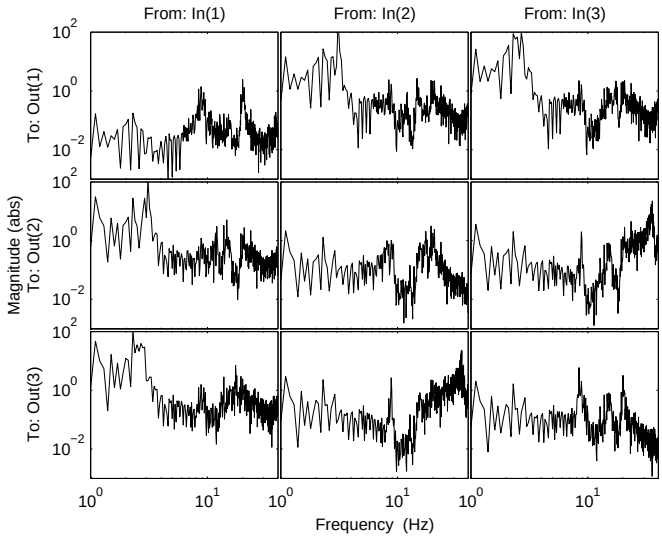

Figure A.3 *Magnitude of the relative error, $|\Delta G|$, in the MFRF estimate for $\mathcal{T} = \mathcal{T}_1$, square wave, and stochastic disturbances.*

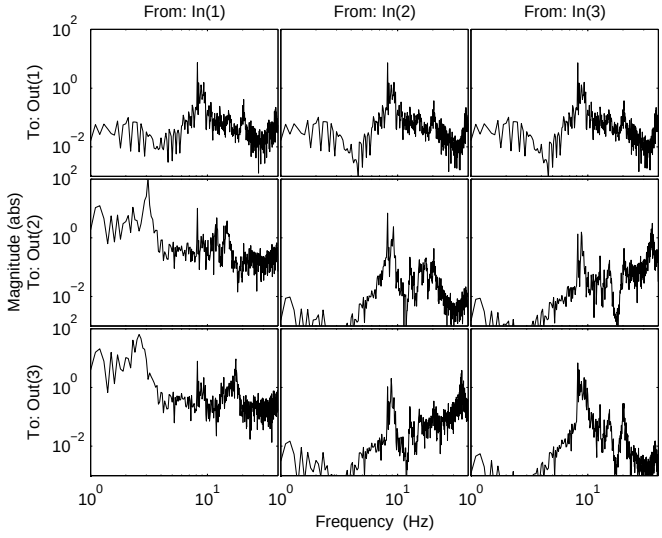

Figure A.4 *Magnitude of the relative error, $|\Delta G|$, in the MFRF estimate for $\mathcal{T} = \mathcal{T}_2$, square wave, and stochastic disturbances.*

A.2 Input and Output Spectrum for Repetitive Disturbances

Here, the spectrum (periodogram) of the input and output signals are presented together with the spectrum of the input and output disturbances. The excitation signal is a multisine signal ($\mathcal{T} = \mathcal{T}_1$) superimposed on a smoothed square wave. See Figure A.5 for the input signal and Figure A.6 for the output signal. The corresponding signal-to-noise ratio (SNR) can be seen in Figure A.7 for the input signal and Figure A.8 for the output signal. Note especially the poor SNR in the (1,2), (1,3), (2,1), and (3,1) elements for low frequencies.

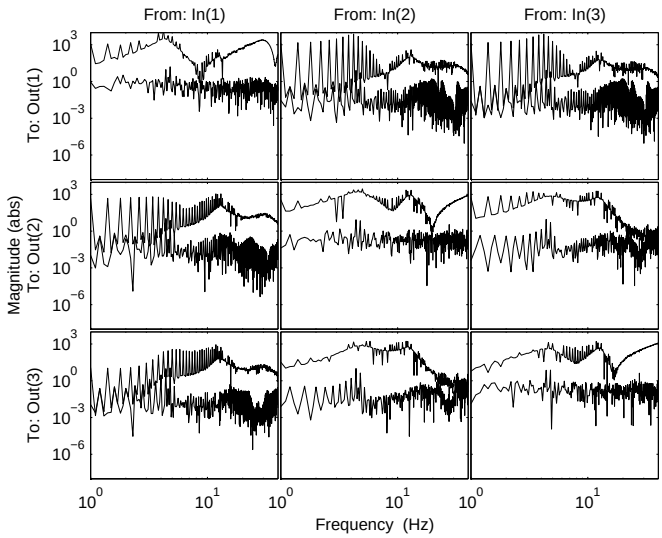

Figure A.5 *Spectrum of the input signal (thin lines) and the input disturbance /thick lines) using the multisine signal ($\mathcal{T} = \mathcal{T}_1$) superimposed on a smoothed square wave.*

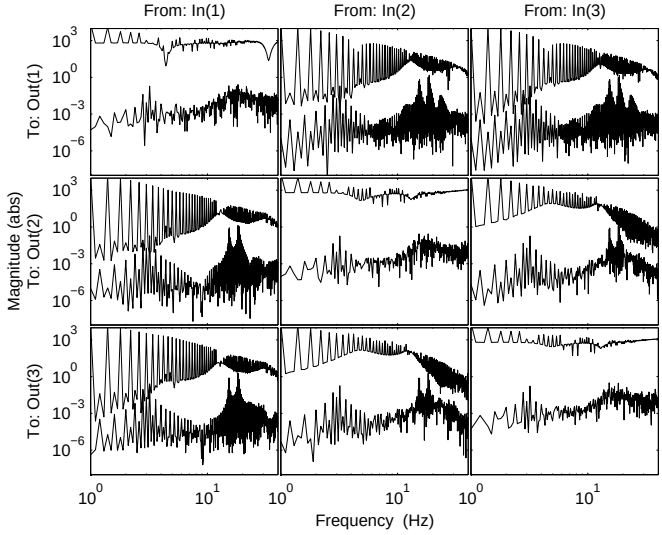

Figure A.6 *Spectrum of the output signal (thin lines) and the output disturbance (thick lines) using the multisine signal ($\mathcal{T} = \mathcal{T}_1$) superimposed on a smoothed square wave.*

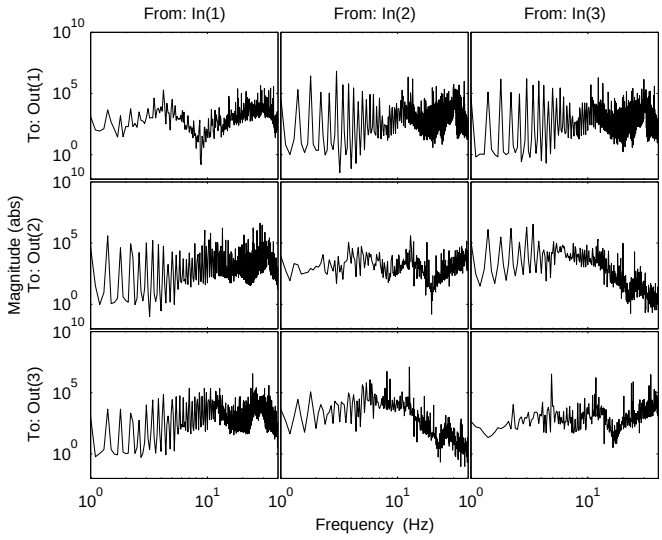

Figure A.7 *Input SNR using the multisine signal ($\mathcal{T} = \mathcal{T}_1$) superimposed on a smoothed square wave.*

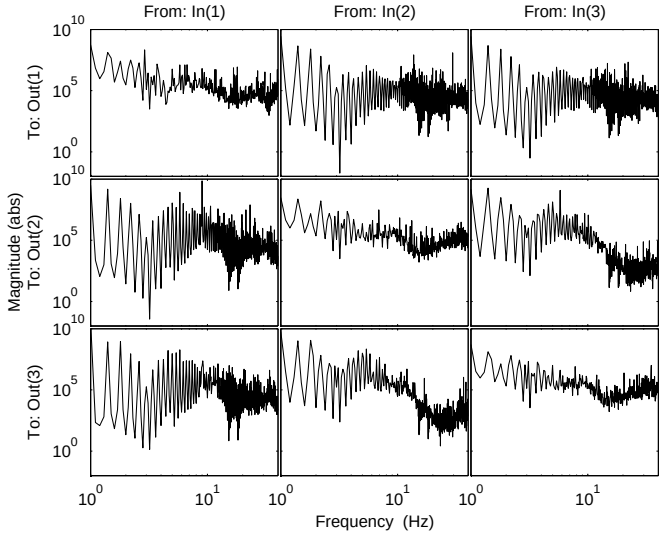

Figure A.8 *Output SNR using the multisine signal ($\mathcal{T} = \mathcal{T}_1$) superimposed on a smoothed square wave.*

Tekn. lic. Dissertations
Division of Automatic Control and Communication Systems
Linköping University

P. Andersson: Adaptive Forgetting through Multiple Models and Adaptive Control of Car Dynamics. Thesis No. 15, 1983.

B. Wahlberg: On Model Simplification in System Identification. Thesis No. 47, 1985.

A. Isaksson: Identification of Time Varying Systems and Applications of System Identification to Signal Processing. Thesis No 75, 1986.

G. Malmberg: A Study of Adaptive Control Missiles. Thesis No 76, 1986.

S. Gunnarsson: On the Mean Square Error of Transfer Function Estimates with Applications to Control. Thesis No. 90, 1986.

M. Viberg: On the Adaptive Array Problem. Thesis No. 117, 1987.

K. Ståhl: On the Frequency Domain Analysis of Nonlinear Systems. Thesis No. 137, 1988.

A. Skeppstedt: Construction of Composite Models from Large Data-Sets. Thesis No. 149, 1988.

P. A. J. Nagy: MaMiS: A Programming Environment for Numeric/Symbolic Data Processing. Thesis No. 153, 1988.

K. Forsman: Applications of Constructive Algebra to Control Problems. Thesis No. 231, 1990.

I. Klein: Planning for a Class of Sequential Control Problems. Thesis No. 234, 1990.

F. Gustafsson: Optimal Segmentation of Linear Regression Parameters. Thesis No. 246, 1990.

H. Hjalmarsson: On Estimation of Model Quality in System Identification. Thesis No. 251, 1990.

S. Andersson: Sensor Array Processing; Application to Mobile Communication Systems and Dimension Reduction. Thesis No. 255, 1990.

K. Wang Chen: Observability and Invertibility of Nonlinear Systems: A Differential Algebraic Approach. Thesis No. 282, 1991.

J. Sjöberg: Regularization Issues in Neural Network Models of Dynamical Systems. Thesis No. 366, 1993.

P. Pucar: Segmentation of Laser Range Radar Images Using Hidden Markov Field Models. Thesis No. 403, 1993.

H. Fortell: Volterra and Algebraic Approaches to the Zero Dynamics. Thesis No. 438, 1994.

T. McKelvey: On State-Space Models in System Identification. Thesis No. 447, 1994.

T. Andersson: Concepts and Algorithms for Non-Linear System Identifiability. Thesis No. 448, 1994.

P. Lindskog: Algorithms and Tools for System Identification Using Prior Knowledge. Thesis No. 456, 1994.

J. Plantin: Algebraic Methods for Verification and Control of Discrete Event Dynamic Systems. Thesis No. 501, 1995.

J. Gunnarsson: On Modeling of Discrete Event Dynamic Systems, Using Symbolic Algebraic Methods. Thesis No. 502, 1995.

A. Ericsson: Fast Power Control to Counteract Rayleigh Fading in Cellular Radio Systems. Thesis No. 527, 1995.

M. Jirstrand: Algebraic Methods for Modeling and Design in Control. Thesis No. 540, 1996.

K. Edström: Simulation of Mode Switching Systems Using Switched Bond Graphs. Thesis No. 586, 1996.

J. Palmqvist: On Integrity Monitoring of Integrated Navigation Systems. Thesis No. 600, 1997.

A. Stenman: Just-in-Time Models with Applications to Dynamical Systems. Thesis No. 601, 1997.

M. Andersson: Experimental Design and Updating of Finite Element Models. Thesis No. 611, 1997.

U. Forssell: Properties and Usage of Closed-Loop Identification Methods. Thesis No. 641, 1997.

M. Larsson: On Modeling and Diagnosis of Discrete Event Dynamic systems. Thesis No. 648, 1997.

N. Bergman: Bayesian Inference in Terrain Navigation. Thesis No. 649, 1997.

V. Einarsson: On Verification of Switched Systems Using Abstractions. Thesis No. 705, 1998.

J. Blom, F. Gunnarsson: Power Control in Cellular Radio Systems. Thesis No. 706, 1998.

P. Spångéus: Hybrid Control using LP and LMI methods – Some Applications. Thesis No. 724, 1998.

M. Norrlöf: On Analysis and Implementation of Iterative Learning Control. Thesis No. 727, 1998.

A. Hagenblad: Aspects of the Identification of Wiener Models. Thesis no 793, 1999.

F. Tjärnström: Quality Estimation of Approximate Models. Thesis no 810, 2000.

C. Carlsson: Vehicle Size and Orientation Estimation Using Geometric Fitting. Thesis no 840, 2000.

J. Löfberg: Linear Model Predictive Control: Stability and Robustness. Thesis no 866, 2001.

O. Härkegård: Flight Control Design Using Backstepping. Thesis no 875, 2001.

J. Elbornsson: Equalization of Distortion in A/D Converters. Thesis No. 883, 2001.

J. Roll: Robust Verification and Identification of Piecewise Affine Systems. Thesis No. 899, 2001.

I. Lind: Regressor Selection in System Identification using ANOVA. Thesis No. 921, 2001.

R. Karlsson: Simulation Based Methods for Target Tracking. Thesis No. 930, 2002.

P-J. Nordlund: Sequential Monte Carlo Filters and Integrated Navigation. Thesis No. 945, 2002.

M. Östring: Identification, Diagnosis, and Control of a Flexible Robot Arm. Thesis No. 948, 2002.

C. Olsson: Active Engine Vibration Isolation using Feedback Control. Thesis No. 968, 2002.

J. Jansson: Tracking and Decision Making for Automotive Collision Avoidance. Thesis No. 965, 2002.

N. Persson: Event Based Sampling with Application to Spectral Estimation. Thesis No. 981, 2002.

D. Lindgren: Subspace Selection Techniques for Classification Problems. Thesis No. 995, 2002.

E. Geijer Lundin: Uplink Load in CDMA Cellular Systems. Thesis No. 1045, 2003.

M. Enqvist: Some Results on Linear Models of Nonlinear Systems. Thesis No. 1046, 2003.

T. Schön: On Computational Methods for Nonlinear Estimation. Thesis No. 1047, 2003.

F. Gunnarsson: On Modeling and Control of Network Queue Dynamics. Thesis No. 1048, 2003.

S. Björklund: A Survey and Comparison of Time-Delay Estimation Methods in Linear Systems. Thesis No. 1061, 2003.

M. Gerdin: Parameter Estimation in Linear Descriptor Systems. Thesis No. 1085, 2004.

A. Eidehall: An Automotive Lane Guidance System. Thesis No. 1122, 2004.